Study on Design and Performance Evaluation of Free Space Optical Communication System for Radio Signal Transmission

Kyung-Hwan Kim

Graduate School of Engineering
Osaka University
2011

To my loving grandparents, parents, sister,
and Eun-Young

Preface

This thesis presents the study on design and performance evaluation of free space optical communication system for radio signal transmission. The outcomes summarized in the research have been carried out during the Ph.D course pursued at Division of Electrical, Electronic and Information Engineering, Graduate School of Engineering, Osaka University.

This thesis is organized in five chapters as follows:

Chapter 1 addresses the background of the research on free space optical communication system for radio signal transmission. The object of the research, radio on free space optical (RoFSO) communication system, is introduced, and its basic configuration, characteristics, merits, and differences with conventional free space optical (FSO) communication systems are discussed. From the discussion, the necessity of a research on design and performance evaluation of RoFSO system is explained. Also, the objective and value of the thesis are described.

Chapter 2 proposes RoFSO channel models for design and performance evaluation of RoFSO link and describes about the difference with conventional FSO link models. Firstly, a spectral model of optical scintillation applicable to RoFSO system is proposed, which enables us to estimate the spectral parameters of cutoff frequency and spectral slope in power spectral density (PSD) of optical scintillation from a given combined condition of time-zones, temperature, and rainfall intensity. Dependencies of the spectral parameters on the weather parameters including difference between daytime and night are discussed. Secondly, dependency of the scintillation index on the weather parameters is investigated for conventional FSO system, and the results are extended to RoFSO system. Thirdly, a new optical transmission loss model is proposed on the basis of measured data in a long-term experiment of RoFSO transmission. The proposed model is applicable to the design of the link margin of RoFSO system operating wavelength of 1550nm band.

Chapter 3 evaluates the effect of optical scintillation on the system performance, especially on the throughput of RF signal transmitted over RoFSO system. We assume WLAN signal as RF signal because WLAN signal is susceptible to the effect of optical scintillation due to its high bit rates, spectrum efficient modulation format, and required high signal to noise ratio. In this analysis, both speed and strength of optical intensity fluctuation are considered. The normalized Gamma distribution is introduced as a statistical model of the intensity fluctuation caused by optical scintillation.

Time-correlated optical scintillation model is proposed for the expression of the time correlation characteristic and the probability density function of optical intensity fluctuation. The evaluation is performed for the worst case of largest scintillation index. The results show the changes in throughput performance caused by optical scintillation. Next, assuming radio communication environments like office and corridor, the effects of optical scintillation in RoFSO channel and shadowing in radio channel are evaluated with some discussion.

Chapter 4 proposes WDM optical power allocation method as an optimal design method for RoFSO system. The proposed method can effectively guarantee each radio regulation of heterogeneous radio signals at a remote station of RoFSO downlink under the condition that the total optical transmission power is limited due to Eye-safety regulation. Theoretical analysis derives a ratio of WDM optical power allocation to effectively guarantee different requirement for each radio signal for two cases of fixed optical modulation indexes (OMI) and optimum OMIs. The results of numerical calculation of CNDR show that the proposed method can improve the tolerance in the optical transmission loss and the RoFSO link distance, compared with the conventional system in which the optical transmission power is equally allocated in each WDM channel.

Chapter 5 summarizes the results obtained in the original works mentioned previous chapters and gives the important role of originally proposed methods in the design and performance evaluations of the RoFSO system.

Acknowledgments

This thesis presents the study on design and performance evaluation of free space optical This study has been carried out during my Ph.D course pursued at the Division of Electrical, Electronic and Information Engineering, Graduate School of Engineering, Osaka University.

I would like to express my sincere gratitude to my supervisor, Prof. Shozo Komaki of the Division of Electrical, Electronic and Information Engineering, Graduate School of Engineering, Osaka University, for continuing encouragement, valuable discussions, academic advice, and various supports throughout this research.

I am much indebted to Prof. Seiichi Sampei of the Division of Electrical, Electronic and Information Engineering, Graduate School of Engineering, Osaka University, for his insightful suggestion, careful review, and valuable criticism on the whole contents of this thesis.

I would like to express my deep sense of appreciation to Associate Prof. Katsutoshi Tsukamoto of the Division of Electrical, Electronic and Information Engineering, Graduate School of Engineering, Osaka University, for his helpful discussions, various academic comments, untiring efforts in guidance, and continuing encouragement from the beginning to the end of this research.

I am deeply grateful to Prof. Tetsuya Takine, Prof. Ken-ichi Kitayama, Prof. Noboru Babaguchi, Prof. Kyo Inoue, and Prof. Zen Kawasaki of the Division of Electrical, Electronic and Information Engineering, Prof. Takashi Washio and Prof. Riichiro Mizoguchi of the Institute of Science and Industrial Research of Osaka University, and all other academic lectures of the Division of Electrical, Electronic and Information Engineering, for their enlightening guidance, discussions, and creative comments for this research.

I also would like to express my sincere appreciation to Assistant Prof. Takeshi Higashino for his academic guidance, valuable discussions and comments on the whole of this research.

I appreciate Dr. Yozo Shoji of National Institute of Information and Communications Technology (NICT), Prof. Mitsuji Matsumoto of Global Information and Telecommunication Institute (GITI), Waseda University, Dr. Kamugisha Kazaura and Dr. Pham Tien Dat who were members of GITI, Waseda University, Dr. Kazuhiko Wakamori of Hamamatsu Photonics K. K., and Assistant Prof.

Kazuo Kumamoto of Osaka Institute of Technology, for their valuable discussions and comments for this research.

I am deeply indebted to Prof. Chun-Woo Shin, Prof. Kwang-Ho Shin, Prof. Jinwoo Kim, and Prof. Jong-Sung Kim of Kyungsung University, Korea, for their kind instruction of basic backgrounds for writing this thesis.

Without the financial support from NICT, this research could not carried out. I would like to give my appreciation to NICT for its special helps as well as financial supports.

I would like to acknowledge ICOM Incorporated for granting me the scholarship to pursue the Ph.D. course.

I also appreciate all members of Komaki Laboratory for their useful discussions for this research, especially, Mr. Satoru Okumura, Mr. Keisuke Hayasaka, and Mr. Tatsuhiko Iwakuni for their helpful assistance.

I am heartily thankful to my family, including grandfather, grandmother, father, mother, and sister, for their love, concern, enabling me to conduct the research without worry.

Last, but by no means least, I am also heartily thankful to my beloved Eun-Young Kim for her love, concern, praying for me, always.

Kyung-Hwan Kim

Osaka, Japan
February 2012

Contents

List of figures

Acronyms

ACLR	adjacent channel leakage ratio
AGC	automatic gain control
AFD	average fade duration
AOA	angle-of-arrival
AP	access point
ASE	amplified spontaneous emission
BER	bit error rate
CBR	constant bit rate
CCS	central control station
CDF	cumulative distribution function
CNDR	carrier to noise-plus-distortion ratio
CNR	carrier-to-noise ratio
CW	continuous wave
DD	direct detection
DEMUX	demultiplexer
DTV	digital terrestrial television
DWDM	dense wavelength division multiplexing
EA	equal allocation
EDFA	erbium-doped fiber amplifier
E/O	electrical-to-optical
FPM	fine pointing mirror
FSO	free space optics
IF	interface
IM	intensity modulation
IMD	intermodulation distortion
IMD3	third order intermodulation distortion
LCR	level crossing rate
LD	laser diode

LTE	long term evolution
MSE	mean square error
MUX	multiplexer
NF	noise figure
OMI	optical modulation index
O/E	optical-to-electrical
PD	photodiode
PDF	probability density function
PSD	power spectral density
PSI	power scintillation index
QPD	quadrant photodiode
RIN	relative intensity noise
RBS	radio base station
RoF	radio on fiber
RoFSO	radio on free space optics
Rx	receiver
SMF	single-mode fiber
SNR	signal-to-noise ratio
Tx	transmitter
WCDMA	wideband code division multiple access
WDM	wavelength division multiplexing
WiMAX	worldwide interoperability for microwave access
WLAN	wireless local area network
WOPA	WDM optical power allocation
3G	third generation

Chapter 1

Introduction

Recently, various types of wireless services such as cellular, wireless local area network (WLAN), and digital terrestrial broadcasting services are widely spread in our society. The advance in electronics technology rapidly progresses high performance, miniaturization and price reduction of communication device, and a variety of mobile communication terminals such as smart phone and tablet PC become widely used. In this situation, users want to promptly access any communication services as they wish at any time, any place and any situation, and such demands are increasing without intermission. This is called ubiquitous networks and/or wireless cloud services.

In current wireless networks, such wireless services are offered independently by their own radio stations and networks, and many wireless networks have been deployed to meet the increasing demand. This leads redundant equipments and the increase of their maintenance cost, and also prevents the quick start of new wireless services such as worldwide interoperability for microwave access (WiMAX), long term evolution (LTE), and 4G [1, 2]. Especially, in rural areas, these problems are conspicuous since broadband fiber-infrastructures have not yet been constructed due to their low investment efficiency. Consequently, a huge gap for investment in broadband communication infrastructures between urban and rural areas still remains to date in Japan. For example, in urban areas with optical fiber network, broadband internet services over wire and wireless access are abundant, and there are few fringe areas for digital terrestrial broadcasting service. In rural areas, however, there are awfully few cellular base stations.

Radios on fiber (RoF) technologies have become one of the strong candidates realizing a cost effective universal platform for wireless access networks. Fig. 1.1 shows a basic configuration of the RoF links. The RoF is totally an analog transmission system since it transmits radio signals to remote stations with keeping their radio formats, such as carrier frequency and modulation format, unlike conventional optical networks transmitting digital signal. Since all signal processing is performed in the central control station (CCS), a radio base station (RBS) needs to equip only optical-to-electrical (O/E) and electrical-to-optical (E/O) converters to receive/transmit radio signals in each radio zone,

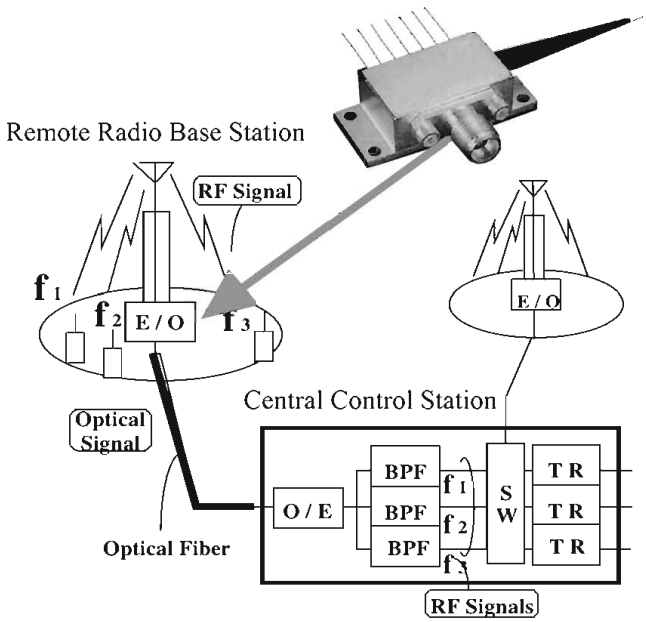

Fig. 1.1: Basic configuration of RoF link.

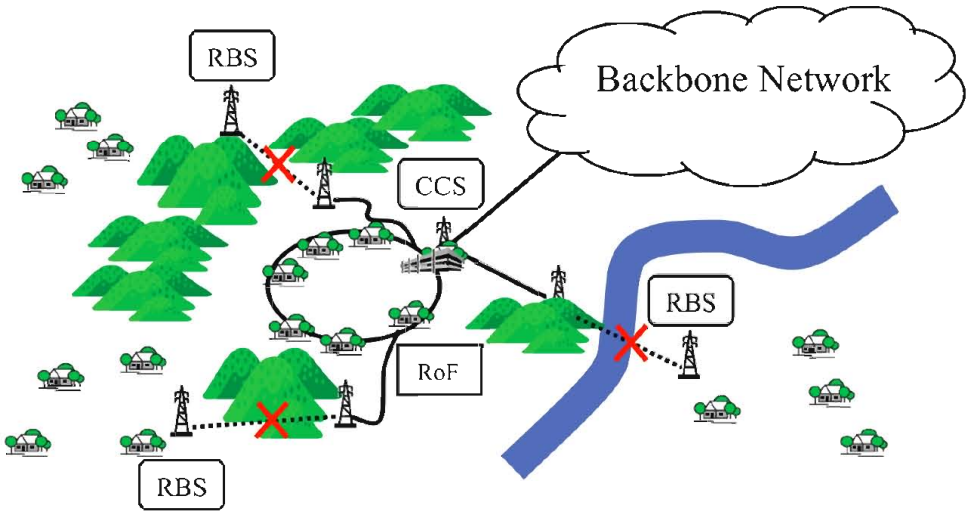

Fig. 1.2: Geographical restrictions in RoF link.

and the RBS requires neither modulation functions nor demodulation functions of radio signals [3-6]. The radio signals are converted into optical signals by the intensity modulation (IM) at a laser diode (LD), and then, transmitted through a RoF link with its low transmission loss (0.2 dB/km for 1550 nm, and 0.5 dB/km for 1310 nm optical wavelengths) and wide optical bandwidth. At the receiver, the

optical signals are converted into the radio signals by the direct detection at a photo diode (PD). Therefore, a RoF link can transmit various types of radio services regardless of their radio and baseband formats. Recently, it has been introduced to reduce the dead-zones like tunnel, in-building, and underground at urban areas [3].

A radio wave is transmitted to other spaces such dead zones through a RoF link. In practice, however, degradation in quality of radio signal occurs due to the nonlinearity of the LD and the dispersion in fiber. Furthermore, it is difficult to deploy fiber networks fundamentally in any place. As shown in Fig 1.2, when constructing RoF networks, there are difficulties in respects of the investment efficiency to construct RoF links on some areas with geographical obstacles, such as river, road, and so on. Also, when a RoF link is destroyed by a natural disaster such as a strong earthquake, big flood, or so on, it is expected to spend a long time and high cost in the restoration.

Fortunately, free space optics (FSO) technology can be an alternative method for RoF link constructions, because fundamentally an optical wireless technology transmits modulated optical signals over free space just like atmosphere to implement point-to-point link without optical fiber medium. When compared with optical fiber systems such as RoF, free space optics (FSO) systems have a variety of advantages. It can be deployed much faster and easily without the need of laying optical fiber and without any geographical limitation. When compared with wireless systems using radio wave, the license for operation is not required in FSO system [7-11]. Therefore, FSO system has been developed as a promising technology for realizing optical wireless link providing the same capacity with optical fiber system in carrying radio signals. Recently, thanks to its attractive advantage of high-capacity communication without geographical restriction, its use is being extended to a short-range wireless connectivity such as among buildings and a mobile entrance link for mobile phone base station in urban areas and disadvantageous areas with difficulties in optical fiber construction [10, 11]. However, FSO link performance is largely affected by weather conditions such as rain, fog, snow, and atmospheric turbulence.

Fig. 1.3 (a) and (b) show the concepts of conventional FSO system, and radio on free space optical (RoFSO) system that is focused in the thesis, respectively. Conventional FSO system needs to perform O/E conversion of optical digital signal transmitted over optical fiber at the FSO transmitter, and E/O conversion before emission of optical signal to atmosphere. The O/E and E/O conversions are also necessary to be performed before the FSO receiver transmits the optical signal received from the atmosphere to optical fiber. In order to transmit multiple wireless service signals, optical fibers, FSO transmitters and receivers were necessary to be installed as many as the number of transmitted wireless service signals. Conventional FSO system generally operates 800 nm optical wavelength band. Unfortunately, because of limitations in output optical power and modulation bandwidth of the LD in this wavelength band, it is difficult to operate at the data rate of more than 2.5 Gbits/s [9, 12,

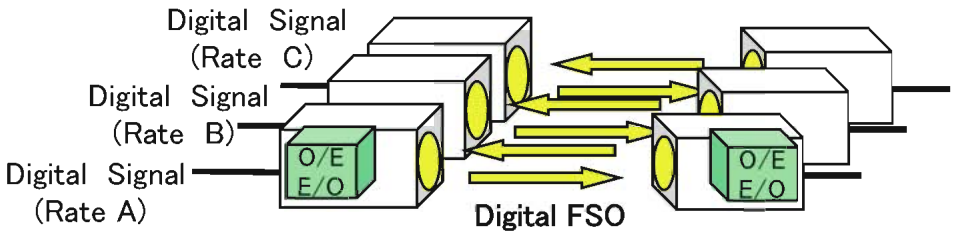

Conventional FSO System

(a)

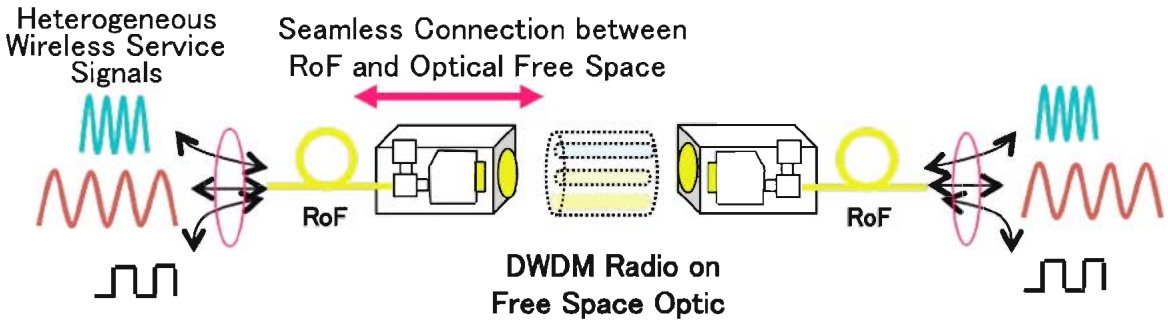

RoFSO System

(b)

Fig. 1.3: Concepts of (a) conventional FSO system and (b) RoFSO system.

13].

FSO systems have been used for digital data transmission for a long time [14]. Recently, there is a new trend that an interest to use FSO systems for radio signal transmission increases [15-17]. Radio on free space optical (RoFSO) communication systems shown in Fig. 1.3 (b) have been developed for radio signal transmissions [18-20]. The RoFSO system is based on RoF technologies, utilizes seamless connection between free space and optical fiber, and uses wavelength division multiplexing (WDM) technologies. It directly radiates dense WDM (DWDM) optical signals from a core of optical fiber to free space, and directly couples the optical signals into a core of optical fiber at the optical receiver. In RoFSO systems, therefore, O/E and E/O conversions at the parts of transmitter and receiver in conventional FSO systems are unnecessary, and it enables us to transmit and receive WDM optical signals with only a couple of optical transmitter and receiver. In short, the RoFSO system realizes a seamless transmission of heterogeneous wireless services between optical fiber and free space with

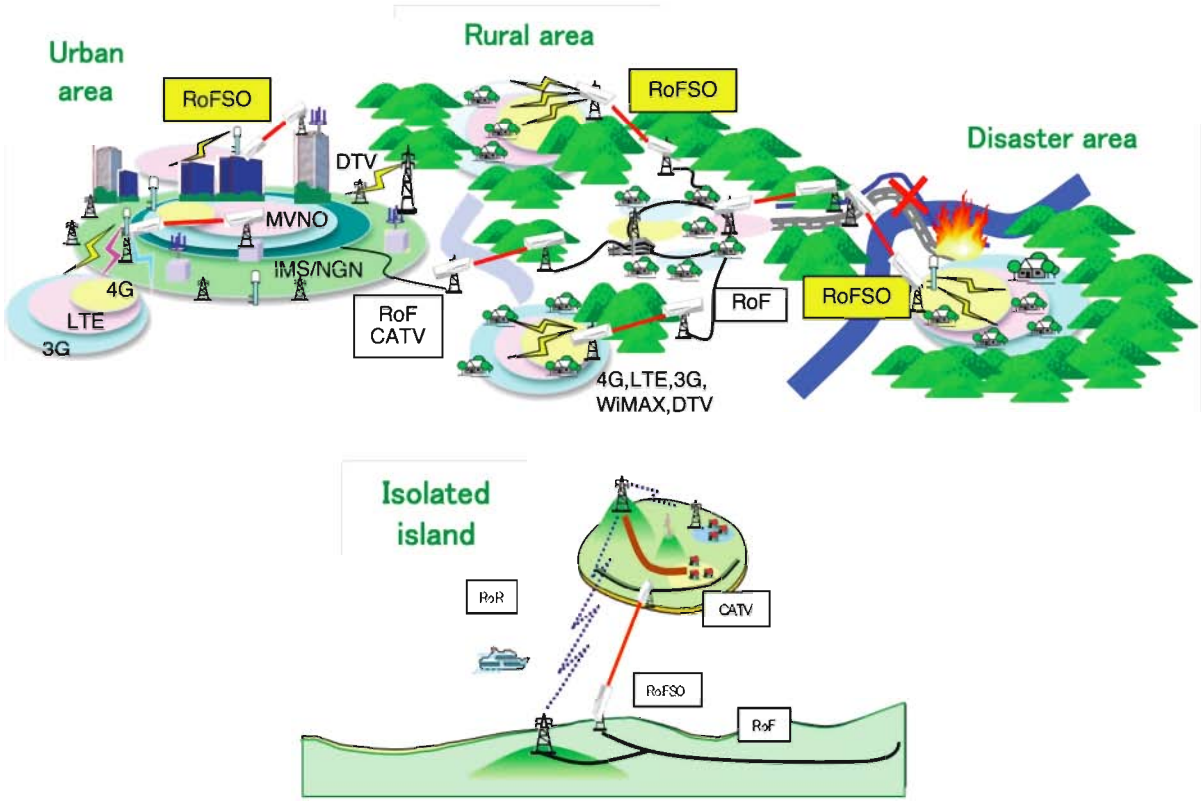

Fig. 1.4: Application scenarios of RoFSO system for providing broadband wireless connectivity to underserved areas.

keeping their radio signal formats, by combination of three technologies of RoF, WDM, and FSO. Moreover, the transmission capacity of RoFSO system can be also outstandingly enhanced by using the erbium-doped fiber amplifier (EDFA), which is developed for long haul optical fiber communication. These are the fundamental differences between the conventional FSO system and RoFSO system.

Fig. 1.4 shows several application scenarios of RoFSO system for providing broadband wireless connectivity in urban, rural and isolated island, and fiber backup when fiber network is broken by a devastating disaster. The RoFSO system can provide entrance links that can simultaneously transmit various types of radio services such as cellular phone, WLAN, and digital terrestrial broadcasting. Moreover, even though any future radio service is newly released, the RoFSO enables us to easily add entrance link for the service by allocating an optical wavelength. Thanks to the valuable features of RoFSO systems, it is considered as a promising solution that can easily, cost-effectively, quickly extend broadband connectivity to underserved area.

While RoFSO systems have several merits, the transmission performance is largely affected by atmospheric conditions on optical propagation path unlike optical fiber system. Therefore,

atmospheric conditions have to be considered in designing a RoFSO system. Many pioneering works of design and performance evaluation on FSO systems have been almost based on the statistical analysis of atmospheric attenuation. Optical power loss due to atmospheric attenuation was calculated by using the visibility collected during several years at a few airports in Japan [11], America [21], and Europe [22]. The FSO link availability and the link margin were estimated on the basis of the results. In addition, a laser beam propagating through the free space like the atmosphere undergoes the cumulative effect of a large number of refractive inhomogeneities. It may lead to fluctuation in received optical intensity, referred as optical scintillation. Optical power loss due to optical scintillation is modeled by using the Rytov's theory [23]. Actually, margins of most FSO systems were estimated to compensate for atmospheric attenuation, because the links of more than 99.9% availability typically have enough margin to compensate for large atmospheric attenuation, and it was more than enough margin to compensate for optical scintillation [24].

The seamless connection is one of most attractive characteristics in RoFSO system, but it naturally brings out a demerit that RoFSO link performance is considerably degraded by the fluctuation in received optical intensity, referred as optical scintillation. While the conventional FSO systems focus the received optical beam on a PD with its detection area of 0.2 ~ 0.5 mm diameter, RoFSO system has to directly couple the received optical beam into a single-mode fiber (SMF) core with its diameter of 8 ~ 10 μm. Since optical beam focusing area is extremely smaller than that of conventional FSO system, the fluctuation in received optical intensity may be enhanced by angle-of-arrival (AOA) due to atmospheric turbulence. Consequently, RoFSO link performance is more sensitive to optical scintillation than conventional FSO system. Because of these differences in configurations and characteristics between conventional FSO system and RoFSO system, the results obtained in previous works for the conventional FSO systems cannot be directly applicable to RoFSO system. Therefore, design and performance evaluation of RoFSO system are newly required.

Based on the background, the objective of this thesis is to study design and performance evaluation of RoFSO communication system for radio signal transmission. The rest of the thesis is organized as the following four chapters:

Chapter 2 proposes models of optical scintillation and optical transmission loss for design and performance evaluation of RoFSO system. Firstly, a spectral model of optical scintillation [25] applicable to RoFSO system is proposed, which enables us to estimate the spectral parameters of cutoff frequency and spectral slope in the power spectral density (PSD) of optical scintillation from a given conditions of time-zones, temperature, and rainfall intensity. Dependencies of the spectral parameters on the weather parameters, and the difference between daytime and night are investigated [25-28]. Secondly, dependency of scintillation index on the weather parameters is investigated for FSO system, and the results are extended to estimate the scintillation index for RoFSO system [26-28].

Thirdly, a new optical transmission loss model [29] applicable to RoFSO system is proposed on the basis of measured data in a long-term experiment of RoFSO transmission. Estimation of RoFSO link margin is conducted by the use of the model.

Chapter 3 evaluates the effect of optical scintillation on the system performance, especially on the throughput of WLAN signal transmitted over RoFSO system [30-33], because it is expected that WLAN system is susceptible to the effect of optical scintillation due to its high bit rates and modulation level. In this analysis, both optical intensity fluctuation speed and strength are considered. The normalized Gamma distribution is introduced as a statistical model of optical scintillation in the analysis [34]. Time-correlated optical scintillation model [30-33] is proposed, which can express the time correlation characteristic and the probability density function of optical scintillation. The evaluation is performed for the worst case that the scintillation index is largest. Changes of throughput performance caused by optical scintillation are quantitatively evaluated [30-32]. Moreover, the evaluations under the radio communication environments like office and corridor are also conducted [33], and the effects of optical scintillation in RoFSO channel and shadowing in radio channel are compared and discussed.

Chapter 4 proposes WDM optical power allocation method [29, 35, 36] as a design method for RoFSO system. The proposed method can effectively guarantee the regulation for each of heterogeneous radio signals at a remote station of RoFSO downlink under the condition that total optical transmitted power is limited by Eye-safety regulation. To effectively guarantee different requirement on each wireless service signal, a ratio of WDM optical power allocation is theoretically derived for the fixed optical modulation indexes (OMI) and the optimum OMIs. The results show that the proposed method can improve the tolerable optical transmission loss and the achievable RoFSO link distance, compared with the equal WDM power allocation method, for the cases of the fixed OMIs and the optimum OMIs.

And, finally chapter 5 summarizes obtained in the original works mentioned previous chapters and gives the important role of originally proposed methods in the RoFSO system study, and the thesis is concluded.

Chapter 2

RoFSO channel model for design and performance evaluation

2.1 Introduction

Firstly, this chapter proposes a Butterworth type spectral model of optical scintillation for design of RoFSO systems. The proposed power spectral density (PSD) model is determined by simple two parameters, cutoff frequency and spectral slope. Cutoff frequency and spectral slope are estimated from the data of the intensity fluctuation measured in the experiment, and then their dependencies on time zone, temperature, and rainfall intensity are examined. The goal of this analysis is to find influences of temperature, rainfall intensity, and time zone on the PSD of optical scintillation.

Secondly, dependencies of the scintillation index on such weather parameters are investigated, based on the measured data in the long-term experiment of FSO transmission, and extended to an estimation of the scintillation index for RoFSO system.

Finally, this chapter also proposes an optical transmission loss model for RoFSO systems, based on scintillation loss data measured in the long-term experiment of RoFSO transmission, and examines the scintillation loss data and its theoretical model. The proposed model is valid for design of DWDM RoFSO system operated at 1.5 μm WDM band, which has the 100 GHz grid spacing standardized by the ITU-T Recommendation G.694.1.

2.2 Spectral model of optical scintillation

In designing a terrestrial FSO system, the frequency characteristic of optical scintillation is one of the most important factors. For example, in a terrestrial FSO link transmitting digital data at high speed of up to several Gbps, a deep and long-term fading in optical intensity results in considerable

burst errors in the received data. In compensating for the intensity fluctuations by using an automatic gain control (AGC) function of an optical amplifier at an optical receiver side, the slower response speed of the AGC causes degradation in the link performance. Many previous works on such terrestrial FSO systems have focused on its design or performance evaluation [23, 37, 38]. Ref. [23] analyzes the FSO link availability considering the atmospheric effects, and Ref. [37] examines FSO link performance related parameters through a field experiment. Ref. [38] experimentally evaluates performances of simultaneous transmissions of multiple RF signals over a RoFSO link.

For the system evaluation or design in these researches, although the intensity fluctuations represented by the scintillation index or the refractive index structure constant C_n^2 has been considered, frequency characteristics of optical scintillation have not been considered.

Recent terrestrial FSO links such as RoFSO link directly focus a received optical beam into a core of single-mode fiber (SMF) [18-20, 37-43] that is much smaller than the detection area of PDs. Therefore, a higher ability to track beam's angle-of-arrival (AOA) is strongly needed in FSO link. Refs. [42] and [43] present some samples of power spectra of the optical scintillation in a conventional FSO system operating at 800 nm wavelength and a FSO system with the seamless connection operating at 1550 nm wavelength, and describe the correlation between them. They focus on effective tracking and beam steering to the SMF for frequency above 100 Hz. However, cutoff frequency has not been studied in the pioneering works on RoFSO systems. An estimation model of optical scintillation's spectrum, especially its cutoff frequency is necessary to achieve an adequate capacity of AGC and the beam tracking.

Many studies focused on the power spectral density (PSD) of optical scintillation have been carried out. Ref. [44] considers the temporal frequency spectrum of the amplitude of a plane wave propagating through atmosphere, and the asymptotic forms for the temporal frequency spectra for plane and spherical waves are developed in Refs. [45-47]. From the formulas, it is found that the spectra for both waves depend on the wind velocity. Refs. [45] and [46] also characterize a spectrum of optical scintillation by cutoff frequency, and figure out the ratio of the cutoff frequency value to wind velocity component vertical to the directions of optical propagations length of 1 km and 2 km. In Ref. [48], dependency of optical scintillation frequency characteristics on the wind velocity is also described. It quantitatively evaluates the relationship between the cutoff frequency of optical scintillation and the wind velocity component vertical to the direction of an optical propagation in cases of some different path lengths and heights. Refs. [49] and [50] derive general formulas for the temporal frequency spectra of amplitude fluctuations for plane and spherical waves, and extend them to beam wave case. Ref. [50] also presents a spectral model using the average and the fluctuation of wind velocity and obtains the frequency spectral slope proportional to $f^{-8/3}$ for a plane wave.

The PSD of the optical scintillation varies directly with wind velocity. Variation period of the wind

velocity is relatively shorter than those of the other parameters such as temperature and rainfall intensity. On the other hand, for the design of the link budget and the beam tracking of RoFSO system, it is also important to model and figure out the changes of the cutoff frequency and the spectral slope in the PSD of optical scintillation which are also depend on the weather condition, such as temperature or rainfall intensity. However, the dependencies on such weather conditions have not been considered to date.

Based on the background, the objective of this section is to clarify the influences of temperature, rainfall intensity, and time zone on the PSD of optical scintillation.

2.2.1 Experimental setup for measuring optical scintillation

Fig. 2.1 shows PSDs of optical scintillation measured in two systems, FSO system operating at 785 nm wavelength where the received optical beam is focused on a PD and RoFSO system operating at 1550 nm wavelength where the received optical beam is directly coupled into a SMF. They were measured at the same location and time, that is, under the same propagation path and atmospheric turbulence conditions. It is found that two different systems have almost the same PSD of optical scintillation caused by the atmospheric turbulence. In other words, for modeling the PSD of optical scintillation for RoFSO system, there is no problem to use measured data obtained in the experiments of FSO transmissions. In this chapter, the PSD of optical scintillation is modeled based on the data measured in the long-term experiments of FSO transmissions.

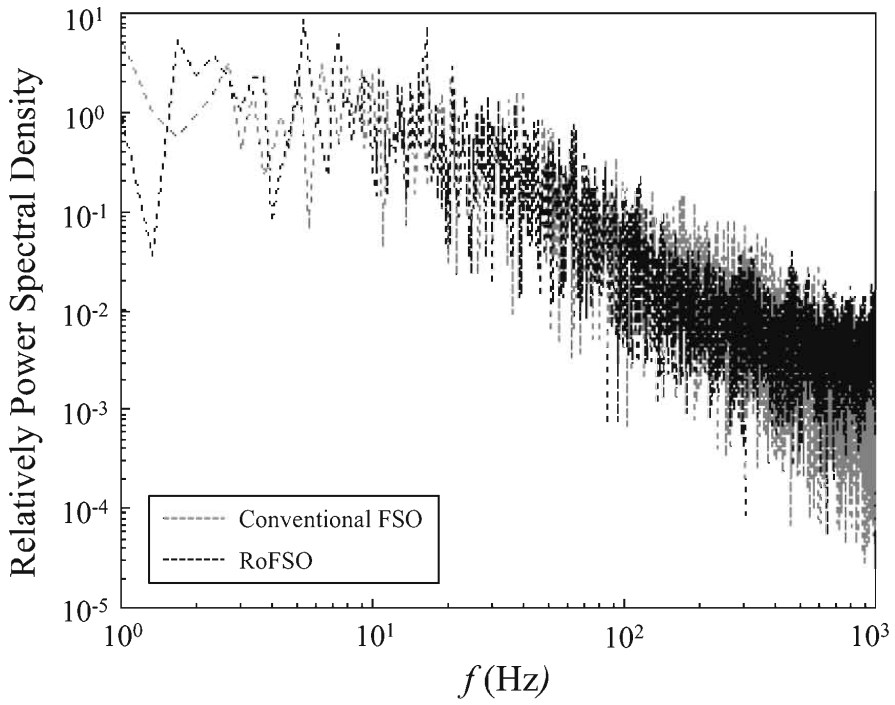

Fig. 2.1: PSDs of optical scintillation measured in conventional FSO system and RoFSO system at the same location and time.

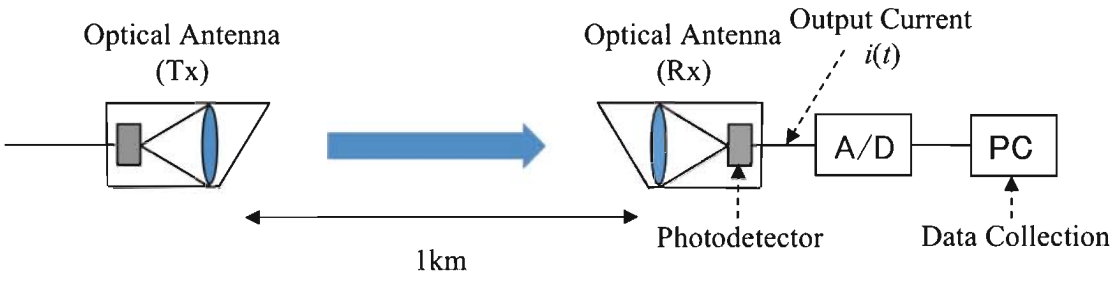

Fig. 2.2: Experimental setup.

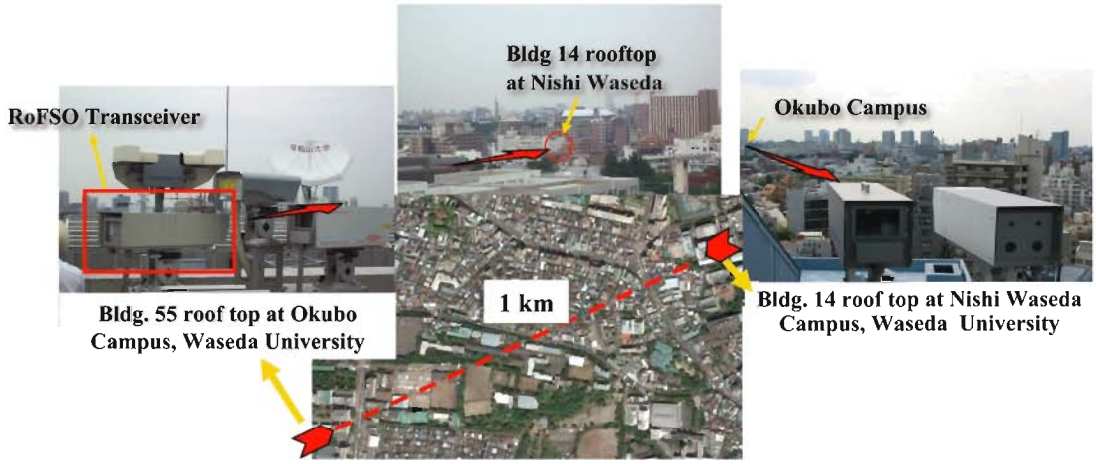

Fig. 2.3: Experimental field.

Fig. 2.2 shows a FSO experimental setup at the Waseda University in Tokyo. The distance between the optical Tx and Rx antennas is 1 km. Their apertures were 10 cm, and the beam divergence angle was 5 mrad. Both of Tx and Rx antennas are located on the rooftop of 10 floor buildings. The optical beam with its wavelength of 785 nm is radiated from the optical Tx antenna, and received at the photodiode (PD). The output current, $i(t)$, is sampled with its sampling rate of 10 kHz during a period of 3 seconds, and recorded in the PC every 5 minutes. A weather meter to measure temperature and rainfall intensity is also installed on the rooftop of one of the buildings. Fig. 2.3 shows the experimental field at the Waseda University located in Tokyo, Japan.

2.2.2 Approximated PSD of optical scintillation with Butterworth type transfer function

2.2.2.1 Butterworth-type PSD as a spectral model of optical scintillation

Spectral model of optical scintillation was modeled using a Butterworth type PSD, which is characterized by two spectral parameters, cutoff frequency and spectral slope. We estimate the cutoff

frequencies and spectral slopes of optical scintillation for different weather conditions through fitting the autocorrelation of the impulse response of Butterworth filter to the measured autocorrelation $\phi_{ii}(\tau)$. The $\phi_{ii}(\tau)$ is derived by $\phi_{ii}(\tau)=\phi'_{ii}(\tau)/\phi'_{ii}(0)$, where $\phi'_{ii}(\tau)$ is the measured autocovariance of $i(t)$.

The power transfer function of Butterworth filter is given by

$$\left|B(f)\right|^2=\frac{1}{1+\left(f/f_c\right)^{2N}}, \tag{2.1}$$

where f_c is the cut-off frequency, and N is the slope order.

The impulse response of first, second, and third order Butterworth filter, $b(t)$, is respectively given by

$$b(t)=\begin{cases}2\pi f_c e^{-2\pi f_c t} & ;N=1\\ 2\sqrt{2}\pi f_c \sin\left(\sqrt{2}\pi f_c t\right)e^{-\sqrt{2}\pi f_c t} & ;N=2\\ 2\pi f_c\left[e^{-2\pi f_c t}+\left\{\sin\left(\sqrt{3}\pi f_c t\right)/\sqrt{3}-\cos\left(\sqrt{3}\pi f_c t\right)\right\}e^{-\pi f_c t}\right] & ;N=3\end{cases}, \tag{2.2}$$

where N is the slope order in higher frequency region. Furthermore, each normalized autocorrelation of $b(t)$, $\phi_{bb}(\tau)$, is obtained as

$$\begin{aligned}\phi_{bb}(\tau)&=\frac{\int_{-\infty}^{\infty}b(t)b(t+\tau)dt}{\int_{-\infty}^{\infty}b^2(t)dt}\\ &=\begin{cases}e^{-2\pi f_c\tau} & ;N=1\\ \sqrt{2}e^{-\sqrt{2}\pi f_c\tau}\sin\left(\sqrt{2}\pi f_c\tau+\pi/4\right) & ;N=2\\ e^{-2\pi f_c\tau}/2+\sin\left(\sqrt{3}\pi f_c\tau+\pi/6\right)e^{-\pi f_c\tau} & ;N=3\end{cases}.\end{aligned} \tag{2.3}$$

We define $A_i(\tau)$ and $A_b(\tau)$ as the area under the curve of $\phi_{ii}(\tau)$ and $\phi_{bb}(\tau)$ respectively,

$$\begin{aligned}A_i(\tau)&=\int_0^{\tau}\phi_{ii}(\tau)d\tau\\ A_b(\tau)&=\int_0^{\tau}\phi_{bb}(\tau)d\tau\end{aligned}. \tag{2.4}$$

We derive a pair of approximated N and f_c satisfying the following equation,

$$A_i(\tau_0)=A_b(\tau_0), \tag{2.5}$$

in the sense of $\int_0^{\tau_0}\left\{\phi_{ii}(\tau)-\phi_{bb}(\tau)\right\}^2 d\tau=0$, where τ_0 is the first zero-crossing time of $\phi_{ii}(\tau)$. Eq. (2.5) means that the areas of the two waveforms of $\phi_{ii}(\tau)$ and $\phi_{bb}(\tau)$ are identical. In general, $\phi_{ii}(\tau)$ is small enough to disregard for a large τ.

Fig. 2.4 (a), (c), and (d) show some examples of measured $\phi_{ii}(\tau)$, and $\phi_{bb}(\tau)$ satisfying Eq. (2.5). The approximated $\phi_{bb}(\tau)$ is obtained as follows. It is seen from these figures that the value of $\phi_{ii}(\tau)$

in $\tau > \tau_0$ becomes negligibly small. Therefore, we focus on high frequency components at a small τ, and find $\phi_{bb}(\tau)$ which fits to $\phi_{ii}(\tau)$ by making their areas identical within the integral range of $0 \le \tau < \tau_0$. Each f_c for N = 1, 2, and 3 is respectively derived. Then, we select one of autocorrelations to minimize the time averaged squared error, Δ, between the two waveforms of $\phi_{ii}(\tau)$ and $\phi_{bb}(\tau)$, where the Δ is calculated by,

$$\Delta = \frac{1}{\tau_0}\int_0^{\tau_0}\left\{\phi_{ii}(\tau)-\phi_{bb}(\tau)\right\}^2 d\tau . \tag{2.6}$$

2.2.2.2 Evaluation of approximation

Fig. 2.4 (a), (c), and (e) depict some examples of measured $\phi_{ii}(\tau)$ derived from experimental data and their approximations $\phi_{bb}(\tau)$. In the fitting, firstly, we calculate autocorrelation of normalized $i(t)$ by its mean value, $\phi_{ii}(\tau)$, from data obtained in the experiment as shown in Fig. 2.2. Next, we estimate cutoff frequency f_c and spectral slope N in the PSD by fitting $\phi_{bb}(\tau)$ to $\phi_{ii}(\tau)$ through the process as described previously. It is observed that $\phi_{bb}(\tau)$ is well matched with $\phi_{ii}(\tau)$. Therefore, the power density spectra of $b(t)$, $S_b(f)$, are naturally matched with those of $i(t)$, $S_i(f)$, as plotted in Fig. 2.4 (b), (d), and (f), respectively. For these samples, f_c of 9.164 Hz, 18.765 Hz, and 37.215 Hz are found respectively, and N of 1 is found in all the cases. For these samples, Δ was 0.0004, 0.0004, and 0.0002, respectively. It is found that the Butterworth-type PSD shows good approximation for the PSD of optical scintillation.

Fig. 2.5 (a) and (b) show examples of variations of measured temperature θ(°C), rainfall intensity R(mm/h), and f_c(Hz) measured from 31 January 2006, 12:00 to 1 February 2006, 18:00, and from 4 August 2006, 6:00 to 5 August 2006, 6:00, respectively. Each value of f_c plotted in the figures denotes the value obtained from each period of experimental data through the approximating process of the PSD of optical scintillation described in Sec. 2.2.2.1. We estimated spectral parameters of f_c and N corresponding to each period of FSO experimental data.

Now, the performance of the approximating process is evaluated in terms of Δ by the weather conditions. We summarize the average value of Δ, $\langle\Delta\rangle$, by combined weather conditions of θ and R in all day, daytime, and night in Table 2.2. The $\langle\Delta\rangle$ is defined by

$$\langle\Delta\rangle = \frac{1}{D}\sum_{j=1}^{D}\Delta_j , \tag{2.7}$$

where D denotes the total number of periods corresponding to combined weather parameters. We summarize each number of periods under several combined weather conditions of θ and R in Table 2.1. Δ_j is one of D number of Δs. For example, there are D = 4176 periods of experimental data measured under the combined condition of $\theta < 10$ and $R = 0$ for the case of all

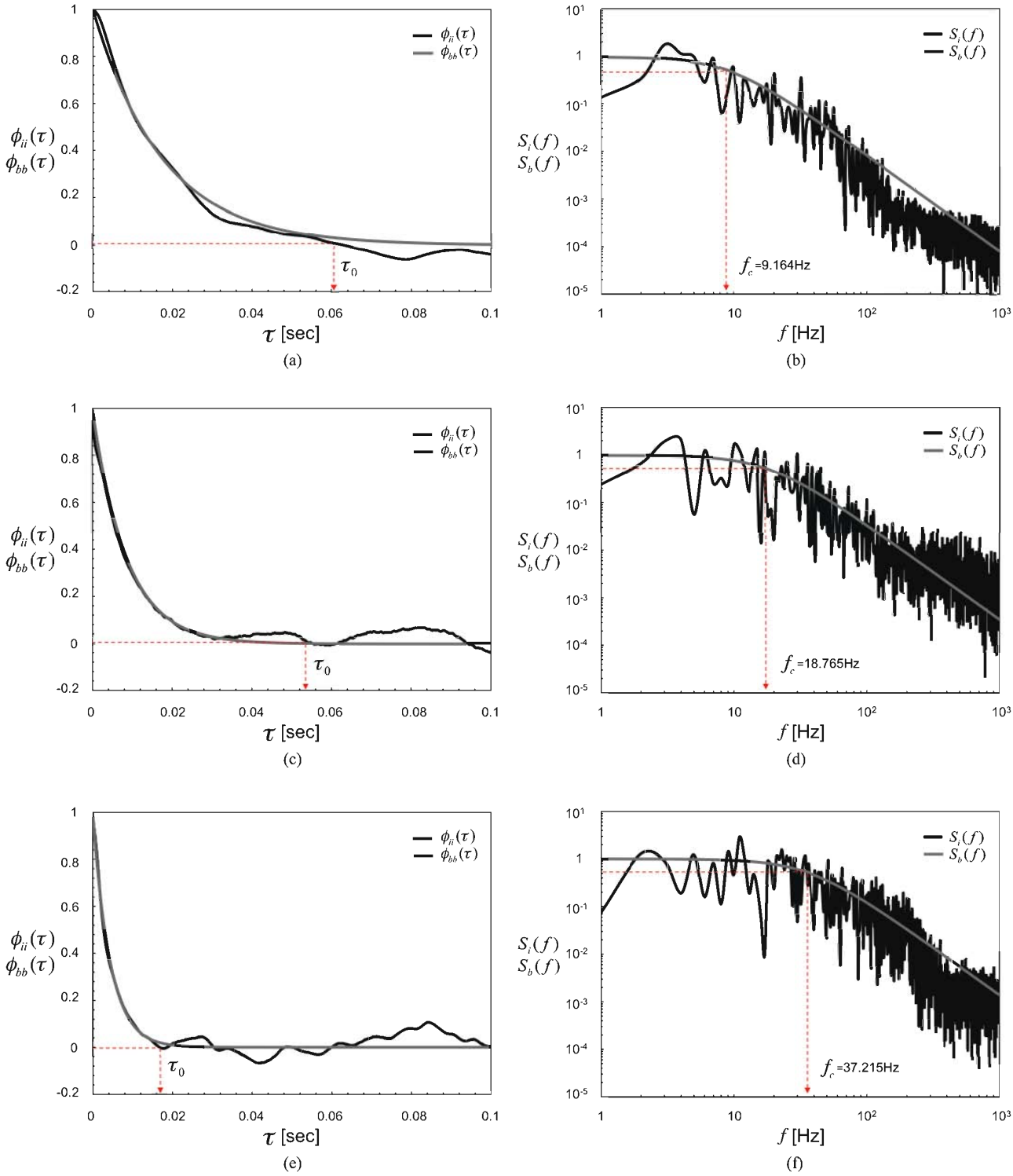

Fig. 2.4: (a) (c) (e) $\phi_{bb}(\tau)$ matched with $\phi_{ii}(\tau)$, and (b) (d) (f) $S_b(f)$ matched with $S_i(f)$.

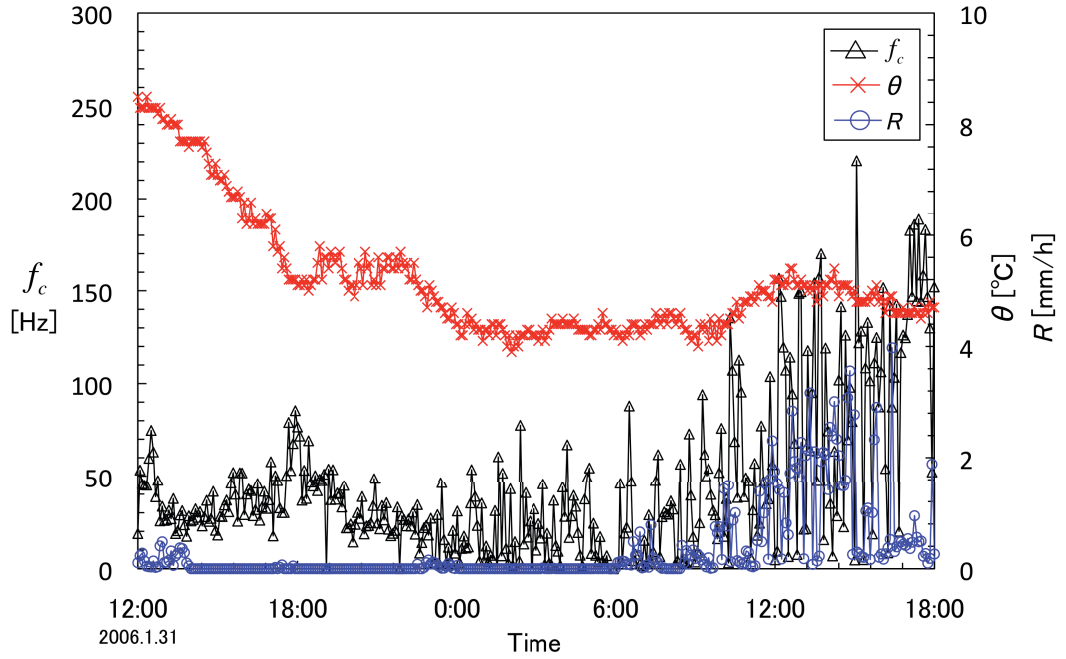

(a)

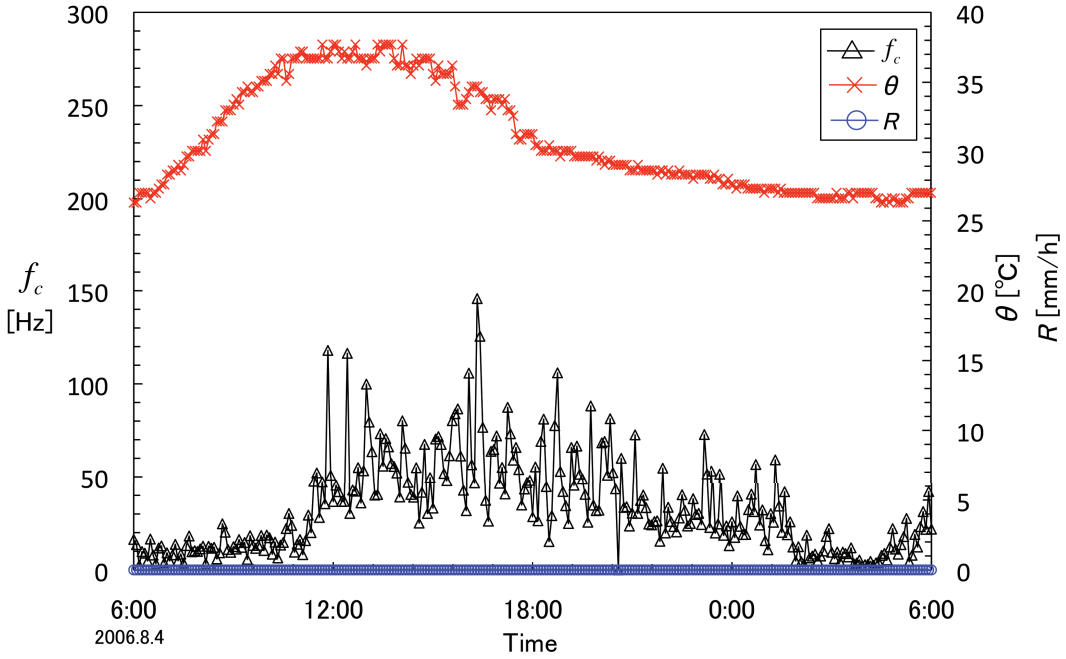

(b)

Fig. 2.5: Examples of variations of temperature, rainfall intensity, and f_c over (a) from 31 January 2006, 12:00 to 1 February 2006, 18:00, and (b) from 4 August 2006, 6:00 to 5 August 2006, 6:00.

Table 2.1: Each number of periods measured under combined weather conditions of θ and R

Number of Data	θ<10			10≤θ<20			20≤θ<30			30<θ		
	All day	*Daytime*	*Night*	*All day*	*Daytime*	*Night*	*All day*	*Daytime*	*Night*	*All day*	*Daytime*	*Night*
R=0	4176	1036	1675	1192	270	567	13545	3247	5494	2332	1682	181
0<R≤3	2372	837	758	735	154	324	3490	944	1377	18	10	0
3<R≤6	29	8	9	73	16	37	323	68	159	1	1	0
6<R≤9	2	0	0	13	3	8	137	25	71	0	0	0
9<R	0	0	0	17	3	12	115	35	60	1	1	0

Table 2.2: $<\Delta>$ yielded under combined weather conditions of θ and R

<Δ>	θ<10			10≤θ<20			20≤θ<30			30<θ		
	All day	*Daytime*	*Night*	*All day*	*Daytime*	*Night*	*All day*	*Daytime*	*Night*	*All day*	*Daytime*	*Night*
R=0	0.0049	0.0046	0.0048	0.0038	0.0041	0.0038	0.0034	0.0036	0.0032	0.0033	0.0032	0.0032
0<R≤3	0.0071	0.0058	0.0072	0.0057	0.0064	0.0056	0.0059	0.0043	0.0067	0.0037	0.0047	
3<R≤6	0.0082	0.0031	0.0134	0.0065	0.0071	0.0063	0.0099	0.0061	0.0117	0.0031	0.0031	
6<R≤9	0.0028			0.0103	0.0155	0.0100	0.0091	0.0066	0.0115			
9<R				0.0131	0.0079	0.0146	0.0074	0.0056	0.0091	0.0022	0.0022	

day. Δ_j for each period of data measured under the condition is calculated by Eq. (2.6), and then their sum divided by 4176 is 0.0049. It is found that $\langle\Delta\rangle$ between $\phi_{ii}(\tau)$ and $\phi_{bb}(\tau)$ yielded has the values from 0.0022 to 0.0155. The $\langle\Delta\rangle$ over all periods is 0.0044.

2.2.3 Dependency of f_c and N on weather parameters

If f_c and N can be estimated from some sort of conditions of a FSO link, we are able to estimate the PSD of optical scintillation with the Butterworth-type PSD. The characteristics of f_c and N depend on weather conditions, so their relationship among them is important.

In Fig. 2.5 (a) and (b), it is found that f_c changes according to each variation of θ and R on a long time scale. In this section, we estimate f_c and N under a same weather condition such as temperature θ and rainfall intensity R as $\langle f_c\rangle$ and $\langle N\rangle$, respectively. $\langle f_c\rangle$ and $\langle N\rangle$ denote averages of f_c and N, respectively. Differences of their values between daytimes (9:00 ~ 16:00) and night (0:00 ~ 4:00, 19:00 ~ 24:00), and their stats also are presented. On the basis of the results, we model the spectrum of optical scintillation.

Since there are a number of data in each identical condition of θ and R as shown in Table 2.1, averaging period for measured data is enough long for the change of wind velocity. Therefore, it should be noted that the effect of wind is eliminated in the results presented in this section.

2.2.3.1 Dependency of f_c and N on temperature

Fig. 2.6 (a), (b), (c), and (d) shows cumulative distribution functions of f_c, $P(f_c)$, for temperature conditions of $\theta < 10$, $10 \le \theta < 20$, $20 \le \theta < 30$, and $30 \le \theta$ in cases of daytime, night and all day, respectively. We summarized each value of X for those conditions in Fig. 2.7, where $P(f_c < X) = 0.8$. While values of X for $\theta < 10$ and $30 \le \theta$ are relatively larger than those for the other range of θ at daytime, the value of X decreases as θ increases at night. The values of X at daytime are similar or more than those at night. Especially, the difference between the two cases is 29.5 Hz which is the largest when $30 \le \theta$. If $\theta < 10$ or $30 \le \theta$ during the daytime, optical scintillation fluctuation is faster than in the other ranges of θ. However, optical scintillation has the slowest fluctuation when $30 \le \theta$ at night.

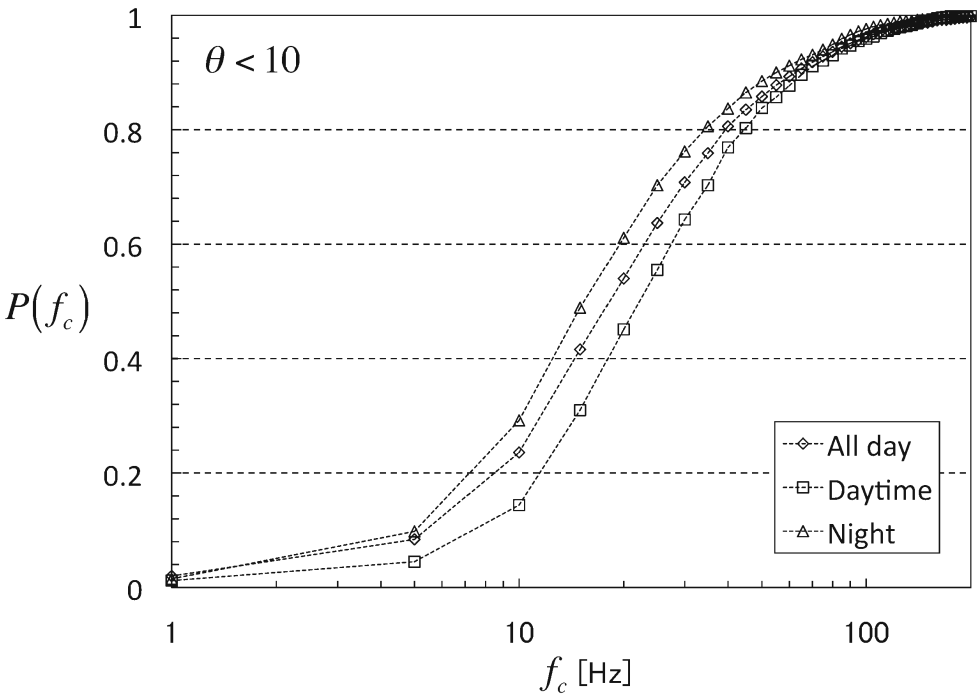
θ < 10
P(f_c)
f_c [Hz]
All day
Daytime
Night
1
0.8
0.6
0.4
0.2
0
1
10
100

(a)

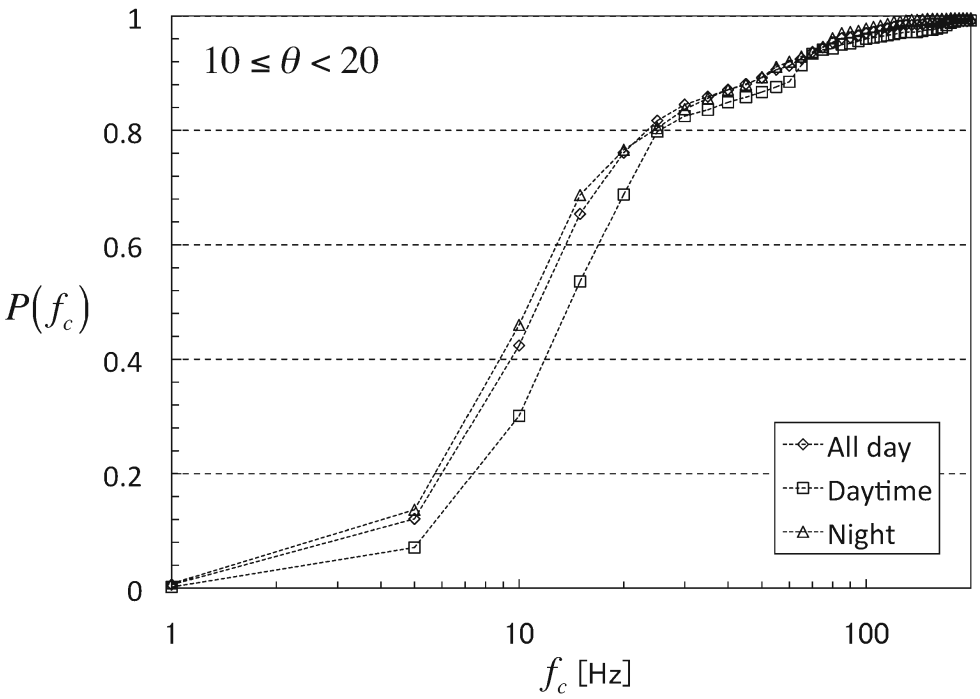
10 ≤ θ < 20
P(f_c)
f_c [Hz]
All day
Daytime
Night
1
0.8
0.6
0.4
0.2
0
1
10
100

(b)

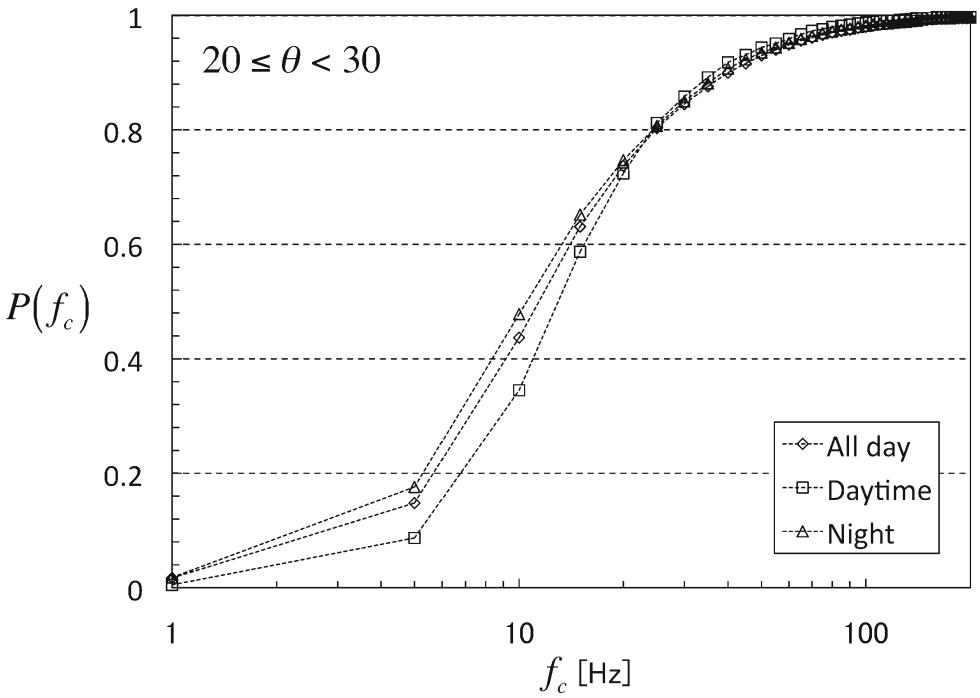

(c)

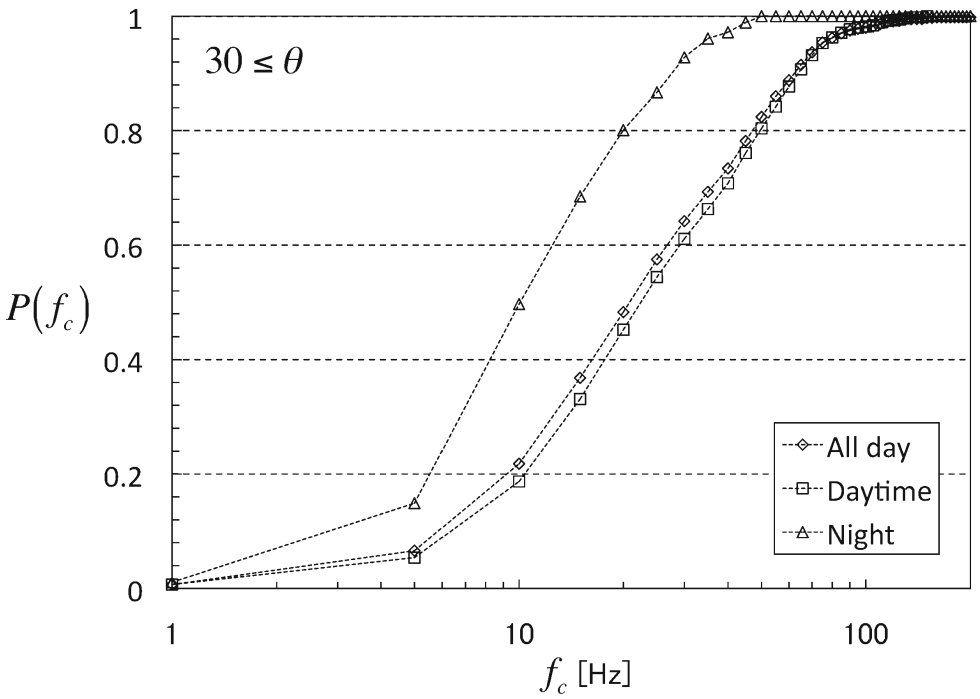

(d)

Fig. 2.6: $P(f_c)$ in each time zone for (a) $\theta \leq 10$, (b)$10 \leq \theta < 20$, (c) $20 \leq \theta < 30$, and (d) $30 \leq \theta$.

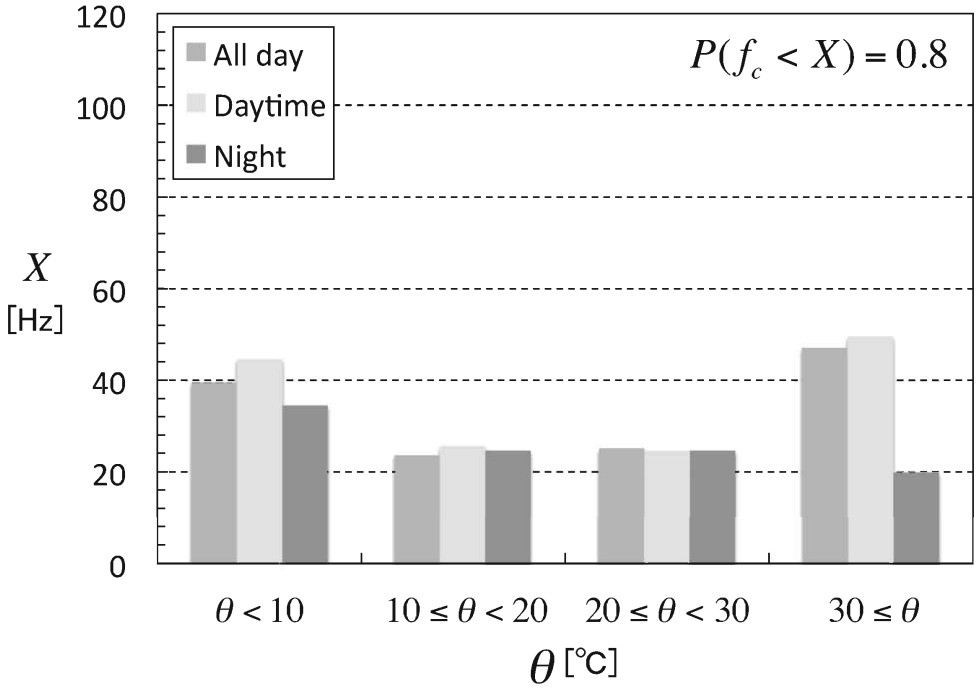

Fig. 2.7: X for θ in each time zone, where $P(f_c < X) = 0.8$.

The tendency described above is also observed in Fig. 2.8 (a). For the case of daytime, the values of $\langle f_c(\theta) \rangle$ for $\theta < 10$ and $30 \le \theta$ are about 33 Hz, which is the largest. At night, $\langle f_c \rangle$ decreases as temperature increases, and eventually, $\langle f_c \rangle$ for $30 \le \theta$ is 15 Hz which is the smallest among all cases shown in the graph. As described in Ref. [51], spectrum of the refractive index fluctuations is proportional to the structure constant of the temperature fluctuations, C_T , and C_T is directly linked to the structure constant of the refractive index fluctuation, C_n^2. From this, we expect smaller amplitude and slower speed of scintillation as temperature fluctuations become lower. Although there are some pioneering studies on C_n^2 or C_T [51-54], any discussion about their night behaviors have not been clarified. Meanwhile, Ref. [55] shows C_n^2 measured in summer and winter seasons, and we can observe that at night C_n^2 in summer is smaller than that in winter. From the result, we may estimate that C_T is relatively smaller in higher temperature at night, and thus $\langle f_c \rangle$ will be relatively small. For $30 \le \theta$, while $\langle f_c \rangle$ for the case of all day is very similar to that in case of daytime, there is a striking difference between two values of $\langle f_c \rangle$ for the cases of all day and night. It results from difference between total number of periods for $30 \le \theta$ measured during the daytime and those at night, as the same reason mentioned above. For $30 \le \theta$, thus the tendency during the daytime dominates.

Fig. 2.8 (b) shows $\langle N \rangle$ for θ in cases of daytime, night, and all day. The value of $\langle N \rangle$ is almost constant as $\langle N \rangle \approx 1$ for all θ of any time zone. When $N = 1$ in Eq. (2.1), the spectral slope of optical scintillation is f^{-2} for high frequencies of $f >> f_c$, and this result matches the conventional

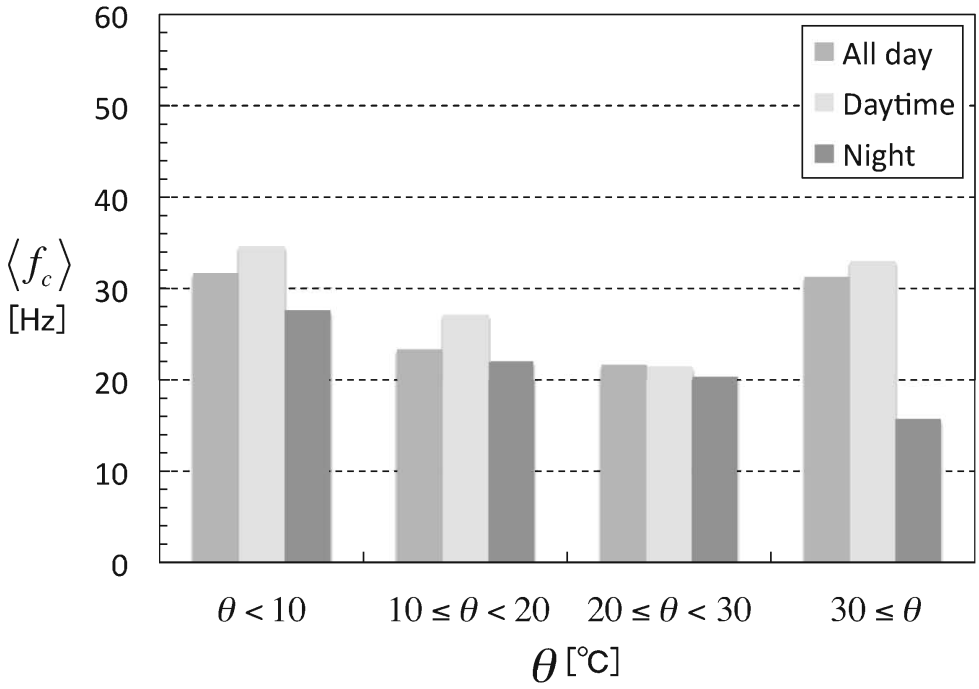

(a)

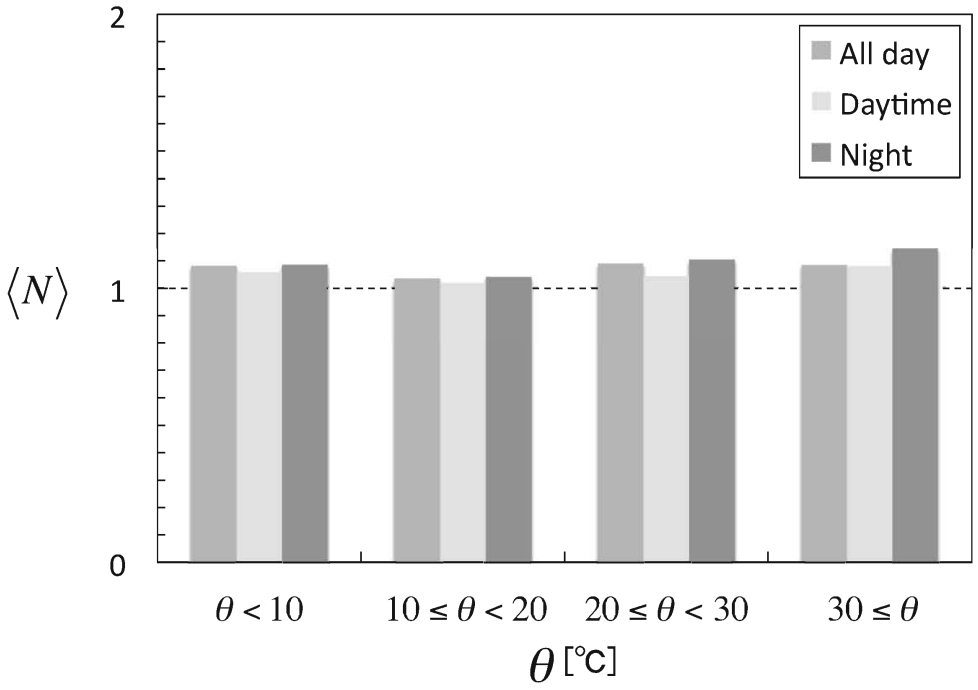

(b)

Fig. 2.8: (a) Each $\langle f_c \rangle$ and (b) $\langle N \rangle$ for θ in each time zone.

spectral model of $f^{-8/3}$ [50].

2.2.3.2 Dependency of f_c and N on rainfall intensity

Fig. 2.9 (a), (b), (c), (d), and (e) show $P(f_c)$ for rainfall intensity conditions of $R = 0$, $0 < R \leq 3$, $3 < R \leq 6$, $6 < R \leq 9$, and $9 < R$ for the cases of daytime, night and all day, respectively. We summarized each value of X for those conditions in Fig. 2.10, where $P(f_c < X) = 0.8$. It is found that for any time zone, probability of higher f_c increases as R increases up to a certain level of R, and then probability of higher f_c decreases as R increases when R exceeds that level. For the case of daytime, X increases up to 100.0 Hz as R increases by $3 < R \leq 6$, it then begins decreasing when R exceeds that range of R and reaches 65.0 Hz when $9 < R$. For the case of night, X increases up to 76.0 Hz as R increases by $6 < R \leq 9$, and it seems that even though $9 < R$, without no more outstanding increase or decrease, it becomes saturated as its value of 72.5 Hz, which is similar value to that for $6 < R \leq 9$.

Each value of X in case of daytime is larger than that in case of night by $3 < R \leq 6$, where the difference between them is 37.0 Hz which is largest when $3 < R \leq 6$. For $6 < R$, X at night becomes larger than that at daytime, there is difference of 5.0 ~ 7.5 Hz between them. X during rainy period is larger than that during no rainy period for any time zone, differences between them are 17.5 ~ 53.5 Hz at daytime, 12.5 ~ 68.0 Hz at night, and 16.0 ~ 64.5 Hz for the case of all day, respectively. In short, optical scintillation during no rainy period more slowly fluctuates than rainy period.

For $0 < R \leq 3$, $P(f_c)$s in all cases of time zone almost conforms to each other and there is also little difference among the values of X in three cases. Therefore, when $0 < R \leq 3$, the value of X can be expected as that value in case of all day regardless of time zone. For example, if rainfall intensity condition of $0 < R \leq 3$ is given only, we can expect the X of 42.5 Hz regardless of current time. In contrast, it is necessary to consider time zone for $R = 0$ and $3 < R$.

The tendency described above is also observed in Fig. 2.11 (a). In case of daytime, $\langle f_c \rangle$ increases up to about 57.8 Hz as R increases by $3 < R \leq 6$, it then begins to decreases when R exceeds that level, and it becomes about 39.2 Hz when $9 < R$. For the case of all day, $\langle f_c \rangle$ increases up to about 49.8 Hz as R increases by $6 < R \leq 9$, it decreases up to 43.8 Hz when $9 < R$. For the case of night, however, $\langle f_c \rangle$ increases up to 43.8 Hz as R increases by $9 < R$ without decrease, unlike two cases of time zone.

Fig. 2.11 (b) shows $\langle N \rangle$ for R for the cases of daytime, night, and all day. The value of $\langle N \rangle$ is almost constant as $\langle N \rangle \approx 1$ for all R of any time zone, as the result shown in Fig. 2.8 (b). It is found that our result approximates to the conventional spectral slope of $f^{-8/3}$ also in the graph.

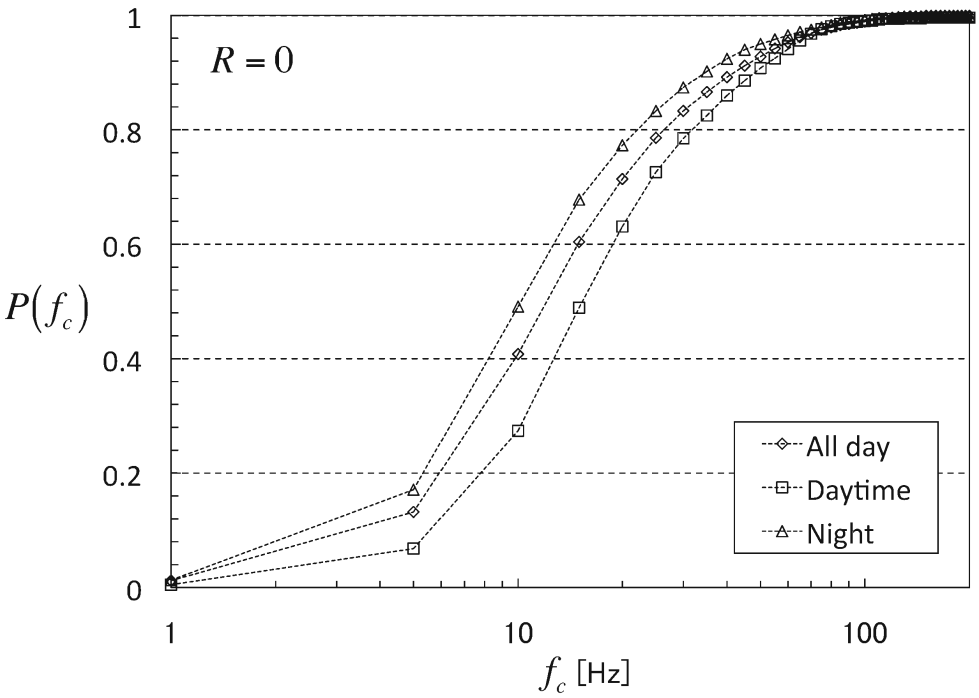
R = 0
P(f_c)
f_c [Hz]
All day
Daytime
Night
1
0.8
0.6
0.4
0.2
0
1
10
100

(a)

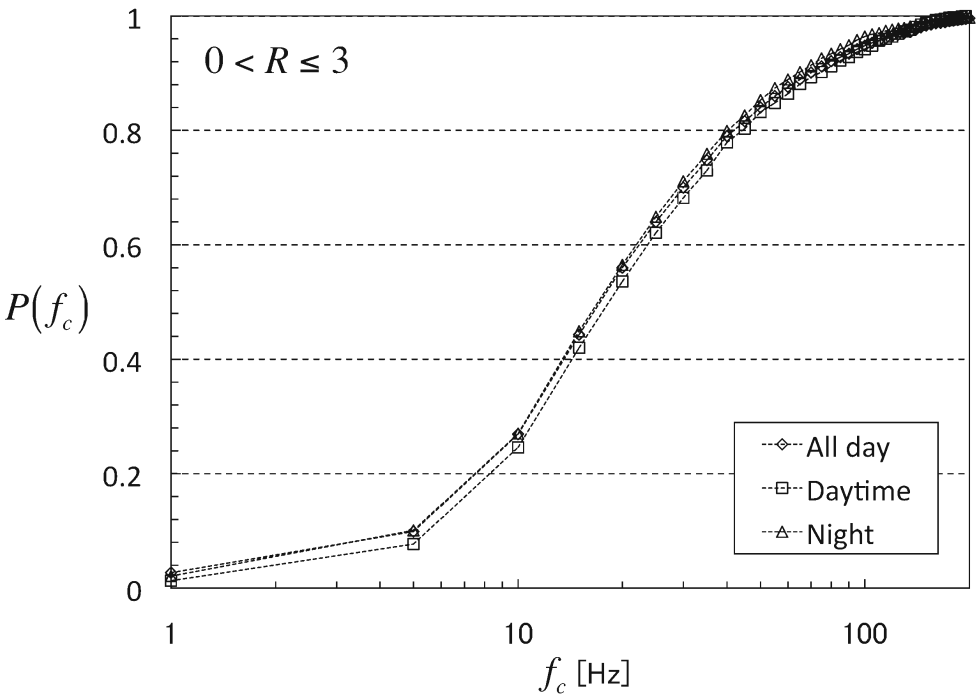
0 < R ≤ 3
P(f_c)
f_c [Hz]
All day
Daytime
Night
1
0.8
0.6
0.4
0.2
0
1
10
100

(b)

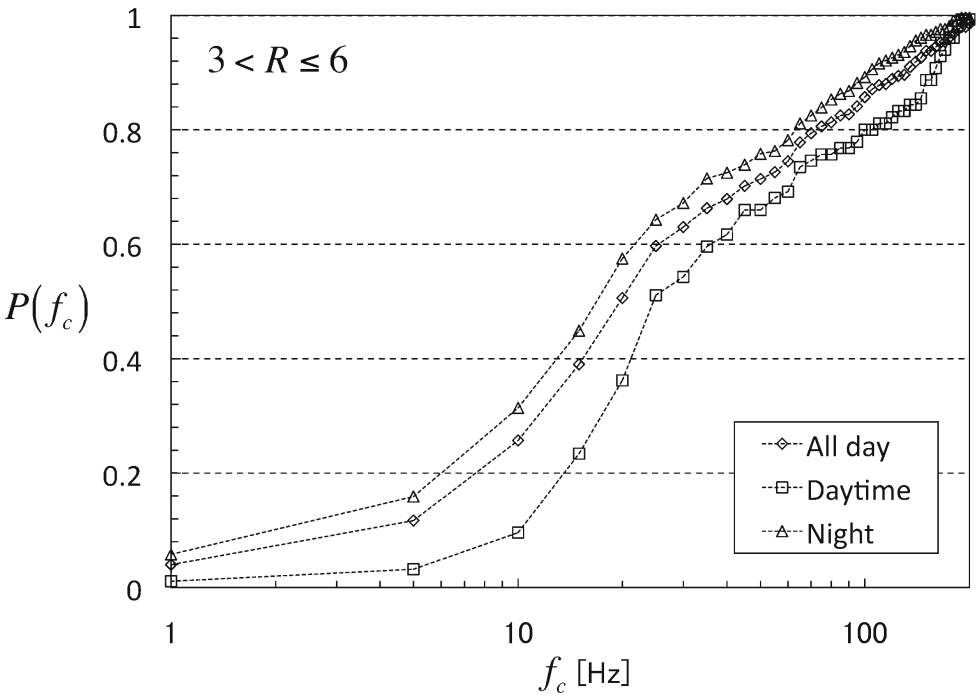
3 < R ≤ 6
1
0.8
0.6
0.4
0.2
0
P(f_c)
All day
Daytime
Night
1
10
100
f_c [Hz]

(c)

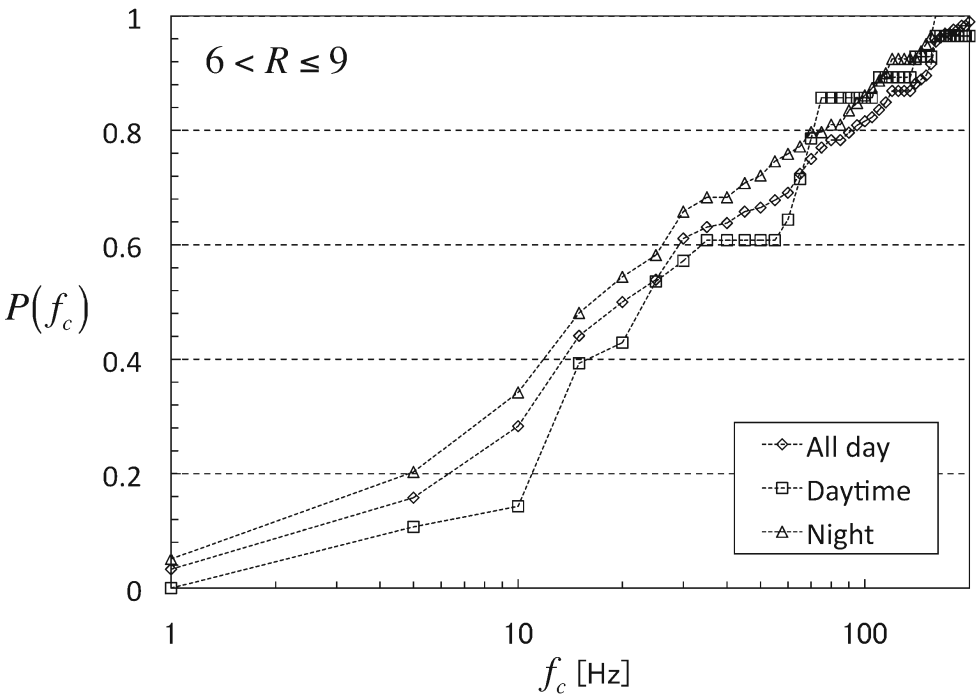
6 < R ≤ 9
1
0.8
0.6
0.4
0.2
0
P(f_c)
All day
Daytime
Night
1
10
100
f_c [Hz]

(d)

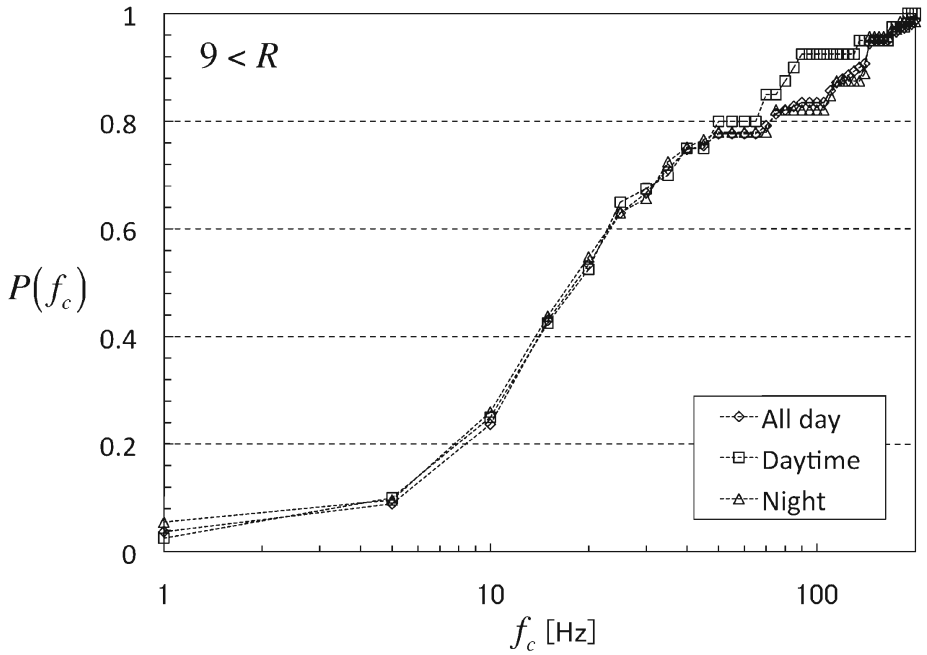

(e)

Fig. 2.9: $P(f_c)$ in each time zone for (a) $R = 0$, (b) $0 < R \leq 3$, (c) $3 < R \leq 6$, (d) $6 < R \leq 9$, and (e) $9 < R$.

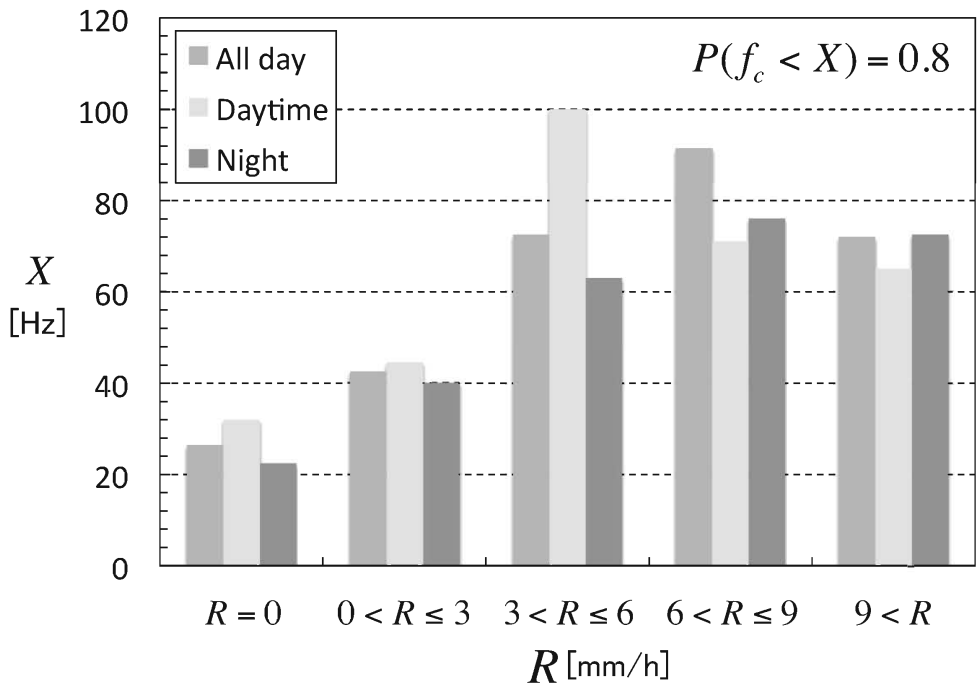

Fig. 2.10: X for R in each time zone, where $P(f_c < X) = 0.8$.

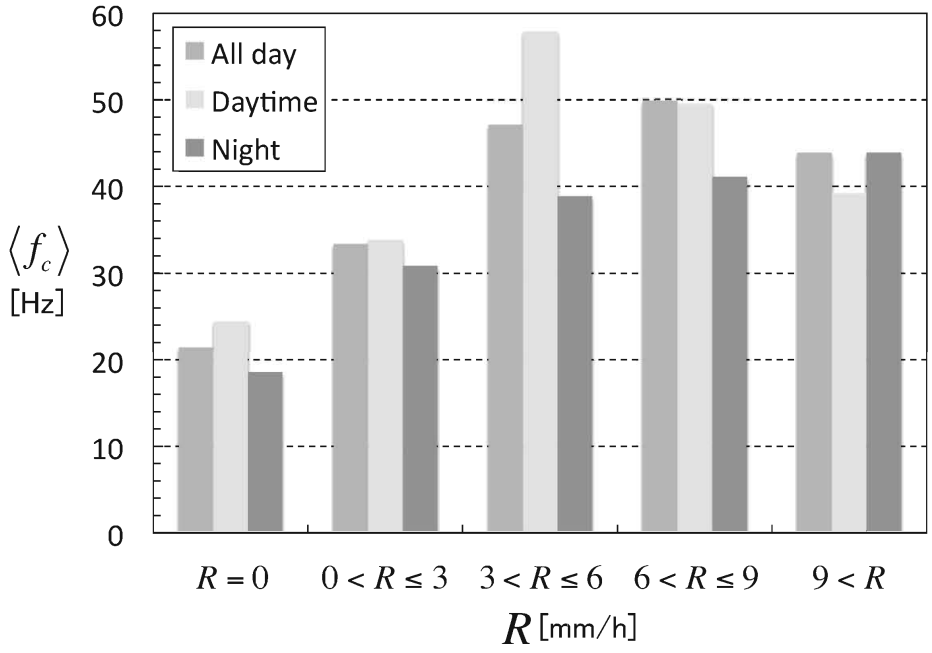

(a)

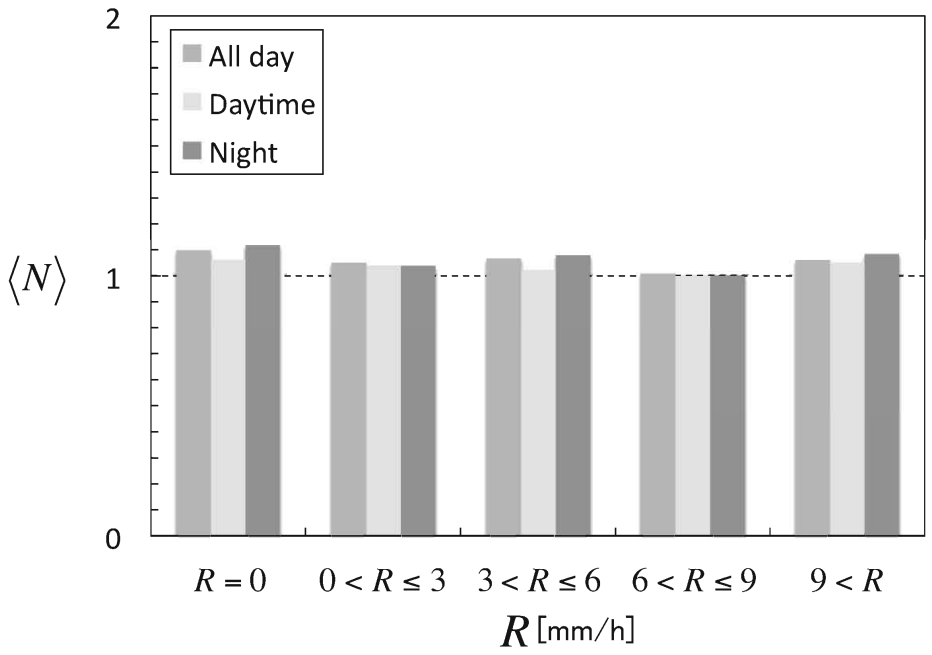

(b)

Fig. 2.11: (a) Each $\langle f_c \rangle$ and (b) $\langle N \rangle$ for R in each time zone.

2.2.3.3 Estimated values of f_c and N under combined conditions of temperature and rainfall intensity

We summarized the estimated value of cutoff frequency in the PSD of optical scintillation, $\hat{f}_c(\theta,R)$, under given combined weather conditions of θ and R for the cases of daytime, night, and all day in Fig. 2.12 and Table 2.3, where $\hat{f}_c(\theta,R)$ is defined as the average value of f_c under each combined condition, that is, $\hat{f}_c(\theta,R)=\langle f_c(\theta,R)\rangle$ in this thesis. It should be noted that several blanks in the figure and table denote not zero, but that there is no data under the corresponding condition. The tendency of $\hat{f}_c$ corresponding to θ under condition of $R=0$ agrees with results shown in Fig. 6, Fig. 7, and Fig. 8 (a) in Sec. 2.2.3.1. However, there are some cases that disagree with such tendency under condition of $R\neq 0$. For example, for $3 < R \leq 6$ for the case of all day, it is observed that $\hat{f}_c$ decreases as θ increases. When θ is only considered, the tendency of $\hat{f}_c$ corresponding to θ agrees with such tendency, because that the number of data measured for each range of θ under condition of $R=0$ is much more than under the condition of $R\neq 0$. Especially, it was extremely rare for it to be $30 \leq \theta$ while $R\neq 0$. Except for the cases of $10 < R \leq 20$ at night and $30 \leq \theta$, tendency of $\hat{f}_c$ according to R agrees with results shown in Fig. 9, Fig. 10, and Fig. 11 (a) in Sec. 2.2.3.2.

With regard to spectral slope, estimated value of N is 1 which is denoted as $\hat{N}=1$, regardless of θ and R, where $\hat{N}$ is defined as $\hat{N}=\langle N(\theta,R)\rangle$. In Secs. 2.2.3.1 and 2.2.3.2, we have observed that $\langle N\rangle$ is almost constant as $\langle N\rangle\approx 1$ in any ranges of θ and R of any time zone, and the result approximates to the conventional spectral slope of optical scintillation.

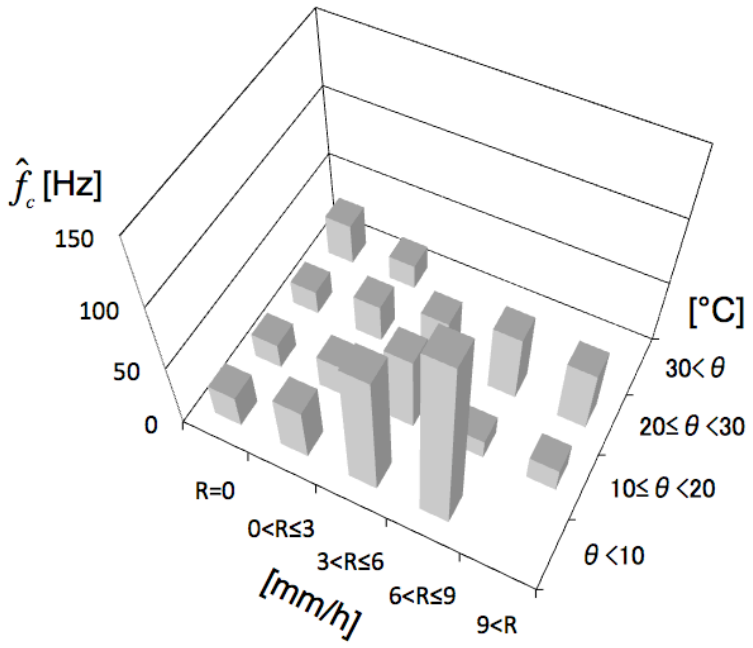

(a)

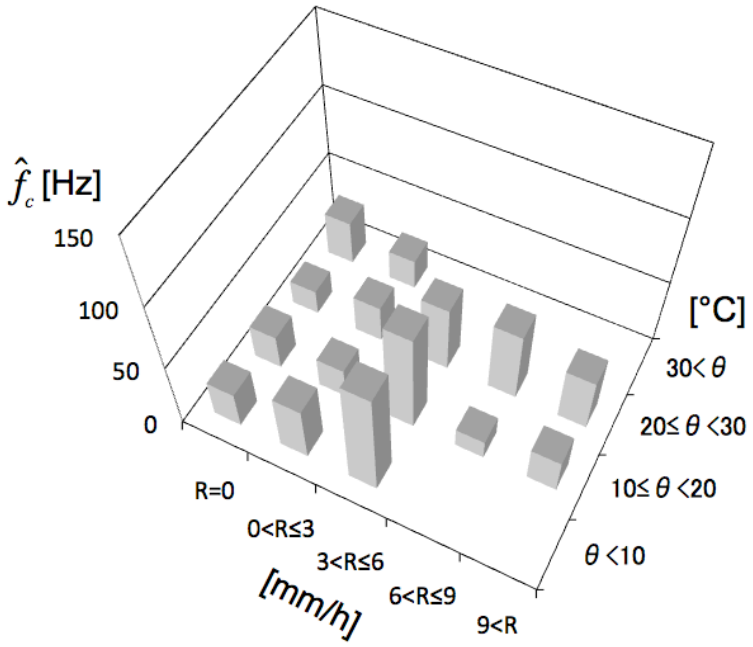

(b)

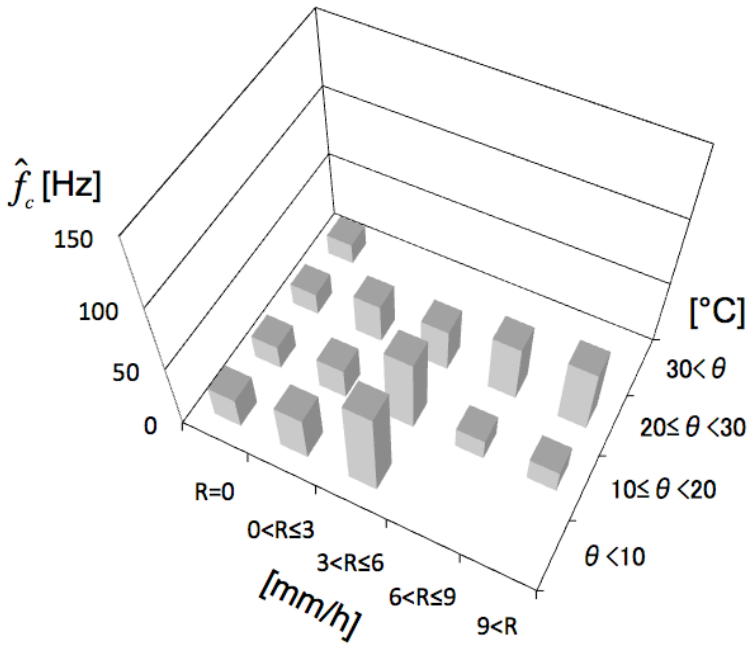

(c)

Fig. 2.12: Estimated values of f_c, $\hat{f}_c(\theta,R)$, under combined weather conditions of θ and R for the cases of (a) all day, (b) daytime, and (c) night.

Table 2.3: Estimated values of f_c under combined weather conditions of θ and R

$\hat{f}_c(\theta,R)$ [Hz]	θ<10			10≤θ<20			20≤θ<30			30<θ		
	All day	*Daytime*	*Night*	*All day*	*Daytime*	*Night*	*All day*	*Daytime*	*Night*	*All day*	*Daytime*	*Night*
R=0	25.6	28.2	24.1	19.9	26.6	18.8	18.6	18.5	17.0	31.4	33.1	15.7
0<R≤3	41.4	42.1	35.0	25.7	23.0	23.9	29.4	28.2	30.2	18.9	22.6	
3<R≤6	97.1	82.5	66.9	58.8	76.9	56.9	40.1	50.8	33.1			
6<R≤9	137.6			15.2	14.6	16.4	51.8	53.7	43.9			
9<R				18.9	26.3	17.7	47.7	40.7	49.1			

Table 2.4: MSE when the proposed model is applied to the design of a RoFSO link

MSE	θ<10			10≤θ<20			20≤θ<30			30<θ		
	All day	*Daytime*	*Night*	*All day*	*Daytime*	*Night*	*All day*	*Daytime*	*Night*	*All day*	*Daytime*	*Night*
R=0	0.0238	0.0159	0.0282	0.0294	0.0250	0.0308	0.0242	0.0156	0.0236	0.0236	0.0217	0.0151
0<R≤3	0.0238	0.0200	0.0238	0.0262	0.0203	0.0238	0.0275	0.0269	0.0256	0.0142	0.0089	
3<R≤6	0.0156	0.0108	0.0156	0.0235	0.0223	0.0187	0.0275	0.0239	0.0270			
6<R≤9	0.0034			0.0178	0.0169	0.0191	0.0256	0.0209	0.0209			
9<R				0.0148	0.0103	0.0156	0.0258	0.0272	0.0236			

2.2.3.4 Estimating performance of the proposed model

From our preceding discussion, we approximated PSD of optical scintillation by the proposed model of Butterworth type PSD, and have extracted the spectral parameters f_c and N from the experimental data. We then classified the obtained parameters by time zone and weather parameters such as temperature and rainfall intensity, and model estimated values of f_c and N as their average value under the given weather parameters and time zone. Therefore, if temperature and rainfall intensity are given, we are able to estimate PSD of optical scintillation in a current RoFSO channel.

In this section, estimating performance of the proposed model of optical scintillation's PSD is evaluated in terms of the mean square error (MSE) defined as following equation,

$$MSE_{\hat{\phi}_{ii}} = \frac{1}{D}\sum_{k=1}^{D}\frac{1}{\tau_0^{(k)}}\int_0^{\tau_0^{(k)}}\left\{\hat{\phi}_{ii}(\tau;\hat{f}_c;\hat{N}) - \phi_{ii}^{(k)}(\tau;\theta;R)\right\}^2 d\tau, \tag{2.8}$$

where $\phi_{ii}^{(k)}(\tau;\theta;R)$ is one of D-$\phi_{ii}(\tau)$s in a same weather condition of θ and R, and $\tau_0^{(k)}$ is a zero-crossing time of $\phi_{ii}^{(k)}(\tau;\theta;R)$ at first. $\hat{\phi}_{ii}(\tau;\hat{f}_c;\hat{N})$ is an estimated autocorrelation for the given conditions, where $\hat{f}_c$ and $\hat{N}$ are determined by given θ and R. For example, when θ < 10 and R=0 in the daytime, $\hat{f}_c$ of 28.2 Hz and $\hat{N}$ of 1 are determined by Table 2.3, they are then substituted in Eq. (2.3), thus, $\hat{\phi}_{ii}(\tau;\hat{f}_c;\hat{N}) = e^{-56.4\pi\tau}$ in the condition. The $\phi_{ii}^{(k)}(\tau;\theta;R)$ may change randomly due to variations of other weather parameters even in the same weather conditions of θ and R. Through calculating Eq. (2.8), we investigate estimation error of $\hat{\phi}_{ii}(\tau;\hat{f}_c;\hat{N})$, a representative autocorrelation under a given condition θ and R, for variation of $\phi_{ii}(\tau;\theta;R)$.

We summarized value of MSE for each combined weather parameters of θ and R in Table 2.4. It is found that MSE has a value between 0.01 and 0.03 on the whole. This table is one of references when the estimation error is restricted to be below a certain value in applying the proposed model to design a RoFSO link.

2.3 Estimation of scintillation index

With regard to the scintillation index or the refractive index structure constant C_n^2, there is a well-known model referred as Rytov variance [22]. Refs. [22] and [56] developed a model expressing the scintillation index as a function of Rytov variance and the ratio of the aperture radius to the Fresnel zone size. We need to know the C_n^2 value in the current atmospheric channel for the scintillation index calculation. Various macrometeorological parameters are required to estimate C_n^2, furthermore, there are the limitations to estimate C_n^2 in the present situation [51-54]. Consequently, we cannot help measuring for a terrestrial FSO system through its transmission experiment.

This section investigates dependencies of the scintillation index on such weather parameters are investigated, based on measured data in long-term experiment of FSO transmission, and extends it to estimated scintillation index for RoFSO system.

2.3.1 Dependency of scintillation index on weather conditions

Based on measured data in the experiment as shown in Fig. 2.2, we summarized the estimated value of the scintillation index $\sigma_i'^2$, $\hat{\sigma}_i'^2(\theta,R)$, under given combined weather conditions of temperature θ and R for the cases of daytime, night, and all day in Fig. 2.13 and Table 2.5. The scintillation index is defined as

$$\sigma_i'^2 = \frac{\langle i^2(t) \rangle}{\langle i(t) \rangle^2} - 1, \tag{2.9}$$

and $\hat{\sigma}_i^2(\theta,R)$ is defined as the average value of $\sigma_i'^2$ under each combined condition, that is, $\hat{\sigma}_i'^2(\theta,R) = \langle \sigma_i'^2(\theta,R) \rangle$.

In Fig. 2.13, we found as follows: The values of $\hat{\sigma}_i'^2(\theta,R)$ at daytime are larger than those at night on the whole. It means that during daytime, the atmospheric turbulence is stronger than night. We expect that it is because at night, temperature difference between the air and ground is smaller than daytime. When R = 0, the difference between them is the largest, and when R > 0, both $\hat{\sigma}_i'^2(\theta,R)$ values become very similar. It means that for a rainy day, the atmospheric turbulence become weak daytime and night. While at daytime, $\hat{\sigma}_i'^2(\theta,R)$ value increases as θ increases on the whole, $\hat{\sigma}_i'^2(\theta,R)$ value decreases as θ increases for the case of R = 0 and night. It is very similar to the case of f_c. We expect that amplitude of optical scintillation is smaller as temperature fluctuations become lower, and C_T is relatively smaller for higher θ at night, like the tropical night, thus $\langle \sigma_i'^2 \rangle$ will be relatively small.

2.3.2 Estimated scintillation index for RoFSO system

It should be noted that Fig. 2.13 and Table 2.5 are valid for FSO system shown in Fig. 2.2. Ref. [57] compares the power scintillation indexes (PSI) for FSO and RoFSO systems. Under moderate to strong turbulence conditions, the PSI of RoFSO system σ_P^2 can be derived as $\sigma_P^2 = \sigma_P'^2 + \beta$, where $\sigma_P'^2$ is the PSI for FSO system and β is an additional fading factor due to direct coupling. From the experimental results given in Ref. [57], it is found that β of 0.25 is presumed to the RoFSO system. Assuming that β is constant as its value of 0.25, and a statistical model of optical scintillation as the normalized Gamma distribution [58, 59], the scintillation index for RoFSO system σ_i^2 can be estimated from that for FSO system $\sigma_i'^2$ using the characteristics function [60] of the normalized

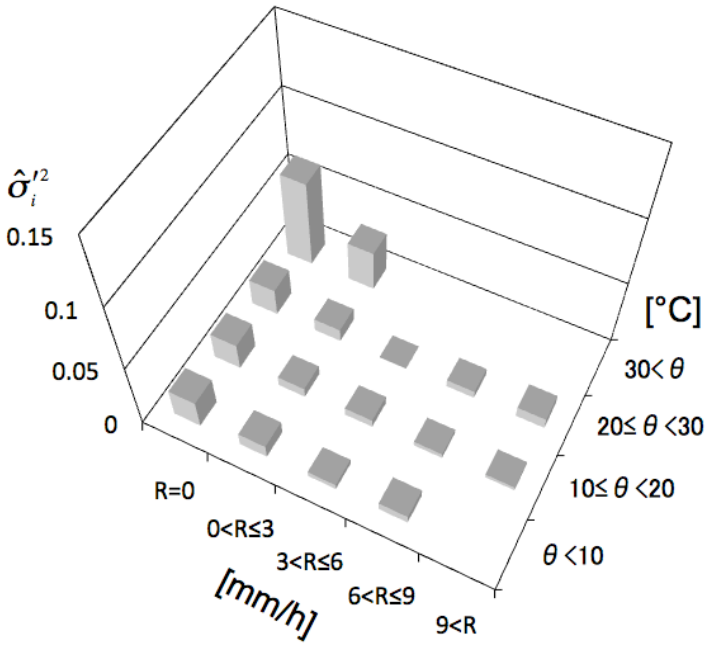
$\hat{\sigma}_i'^2$
0.15
0.1
0.05
0
R=0
0<R≤3
3<R≤6
6<R≤9
9<R
[mm/h]
[°C]
30< θ
20≤ θ <30
10≤ θ <20
θ <10

(a)

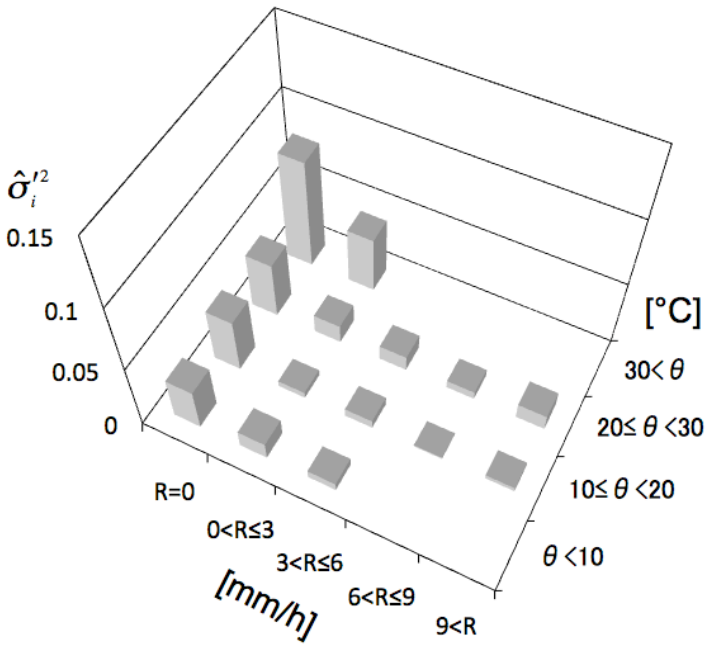
$\hat{\sigma}_i'^2$
0.15
0.1
0.05
0
R=0
0<R≤3
3<R≤6
6<R≤9
9<R
[mm/h]
[°C]
30< θ
20≤ θ <30
10≤ θ <20
θ <10

(b)

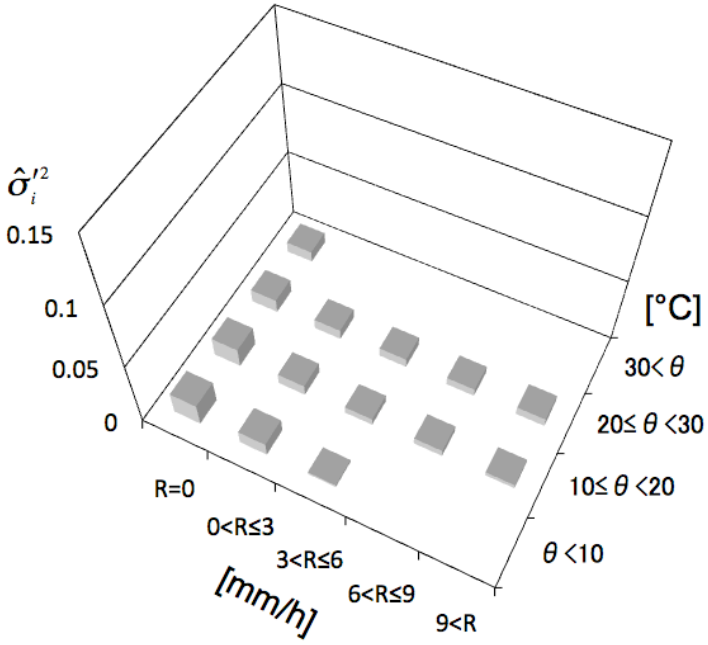

(c)

Fig. 2.13: Estimated values of $\sigma_i'^2$, $\hat{\sigma}_i'^2(\theta,R)$, under combined weather conditions of θ and R for the cases of (a) all day, (b) daytime, and (c) night.

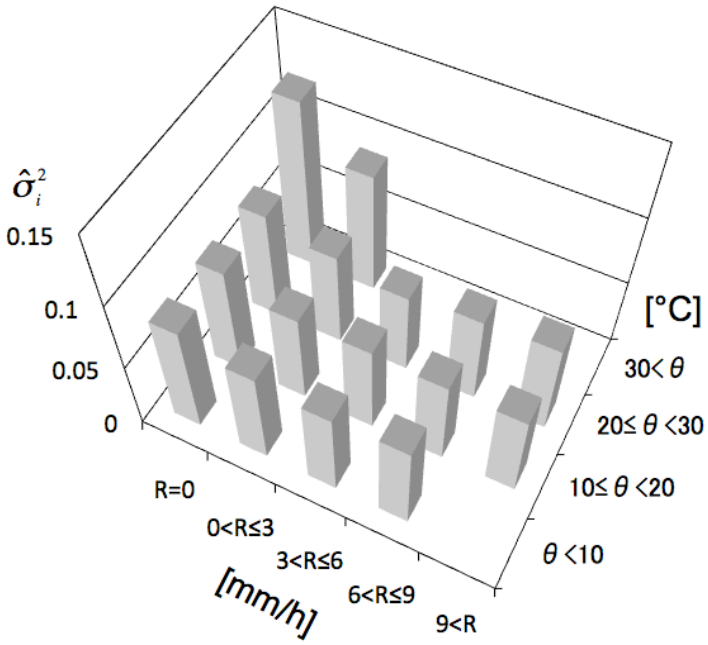

(a)

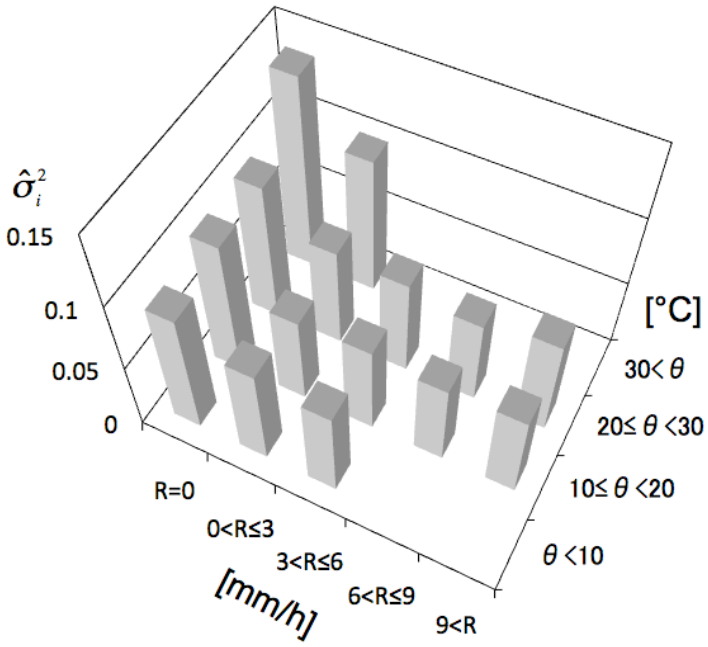

(b)

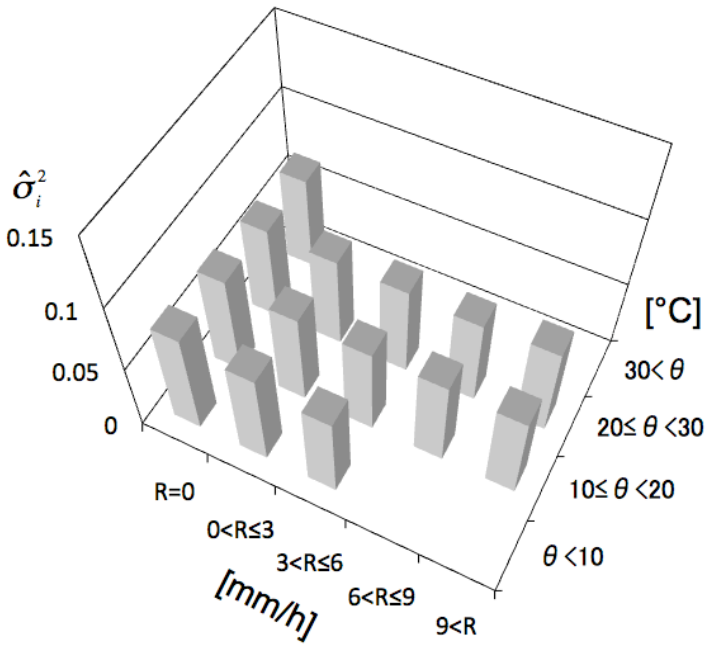

(c)

Fig. 2.14: Estimated values of σ_i^2, $\hat{\sigma}_i^2(\theta,R)$, under combined weather conditions of θ and R for the cases of (a) all day, (b) daytime, and (c) night.

Table 2.5: Estimated values of scintillation index combined weather conditions of θ and R for FSO system

$\hat{\sigma}_i'^2(\theta,R)$	θ<10			10≤θ<20			20≤θ<30			30<θ		
	All day	*Daytime*	*Night*	*All day*	*Daytime*	*Night*	*All day*	*Daytime*	*Night*	*All day*	*Daytime*	*Night*
R=0	0.0213	0.0317	0.0167	0.0203	0.0412	0.0145	0.0206	0.0426	0.0101	0.0656	0.0824	0.0080
0<R≤3	0.0099	0.0128	0.0100	0.0073	0.0045	0.0080	0.0097	0.0139	0.0075	0.0306	0.0422	
3<R≤6	0.0039	0.0058	0.0016	0.0060	0.0062	0.0052	0.0003	0.0113	0.0067			
6<R≤9	0.0060			0.0035	0.0010	0.0049	0.0056	0.0058	0.0059			
9<R				0.0027	0.0030	0.0030	0.0080	0.0116	0.0062			

Table 2.6: Estimated values of scintillation index combined weather conditions of θ and R for RoFSO system

$\hat{\sigma}_i^2(\theta,R)$	θ<10			10≤θ<20			20≤θ<30			30<θ		
	All day	*Daytime*	*Night*	*All day*	*Daytime*	*Night*	*All day*	*Daytime*	*Night*	*All day*	*Daytime*	*Night*
R=0	0.0810	0.0909	0.0766	0.0800	0.1000	0.0745	0.0803	0.1013	0.0703	0.1233	0.1395	0.0683
0<R≤3	0.0701	0.0729	0.0702	0.0667	0.0650	0.0683	0.0700	0.0739	0.0679	0.0899	0.1009	
3<R≤6	0.0645	0.0663	0.0623	0.0664	0.0666	0.0657	0.0610	0.0715	0.0671			
6<R≤9	0.0664			0.0641	0.0617	0.0654	0.0661	0.0663	0.0664			
9<R				0.0633	0.0636	0.0636	0.0683	0.0718	0.0666			

Gamma distribution, as following equation,

$$\sigma_i^2 = \frac{1}{12}\left(\varphi - 5 + \sqrt{\varphi^2 + 14\varphi + 1}\right), \tag{2.10}$$

where φ is derived as

$$\varphi = \frac{1 + 6\sigma_i'^2 + 11\sigma_i'^4 + 6\sigma_i'^6}{(\sigma_i'^2 + 1)^2} + 0.25. \tag{2.11}$$

We then can derive the estimated scintillation index for RoFSO system $\hat{\sigma}_i^2(\theta, R)$ by substituting $\hat{\sigma}_i'^2(\theta, R)$ given in Fig. 2.13 and Table 2.5 into Eqs. (2.10) and (2.11), under the assumption. It should be noted that $\sigma_i^2 = \sigma_i'^2$ in Eq. (2.10) when $\beta = 0$. We summarize the estimated scintillation index for RoFSO system in Fig. 2.14 and Table 2.6.

2.4 Optical transmission loss model

In this section, we propose a new optical transmission loss model for RoFSO system L_{opt}, which is represented by

$$L_{opt}(d) = L_{atm}(V, d) + L_{geo}(d) + L_{scin}(d) + L_{tra}(d) \ \text{[dB]}, \tag{2.12}$$

where $L_{opt}(V,d)$, V, d represent the atmospheric attenuation loss caused by absorption or scattering, the visibility, and RoFSO link length, respectively. $L_{geo}(d)$ is the optical geometric loss due to broadening of the laser beam. $L_{scin}(d)$ and $L_{tra}(d)$ respectively represent the scintillation loss and the tracking error loss, and both are caused by the atmospheric turbulence.

2.4.1 Atmospheric attenuation loss and optical geometric loss

2.4.1.1 Atmospheric attenuation loss

In conventional FSO systems, the performance is typically dominated by the atmospheric attenuation, which is primarily caused under a low visibility condition like fog, snow weather [24]. The atmospheric attenuation loss is inversely proportional to the transmittance, which is described by the Beers-Lambert law represented as [11, 13, 61]

$$\begin{aligned} L_{atm}(V, d) &= 10\log_{10}\left(\frac{P(d)}{P(0)}\right) \ \text{[dB]}. \\ &= 10\log_{10}(e^{-\alpha d}) \end{aligned} \tag{2.13}$$

In Eq. (2.13), $P(0)$ and $P(d)$ are the optical intensities at the source and at a distance d, respectively. V and d respectively represent the visibility given in kilometer and RoFSO link length, and α is the

atmospheric attenuation coefficient given by

$$\alpha = \frac{3.91}{V}\left(\frac{\lambda}{550nm}\right)^{-q}, \tag{2.14}$$

where q is the particle size distribution coefficient. The latest investigations indicate no wavelength dependence of the atmospheric attenuation coefficient under foggy conditions, where the visibility is V < 500m. A new method for evaluating the particle size distribution coefficient that considers this fact was proposed by Kim et al., [13]

$$q(V) = \begin{cases} 1.6 & : V > 50 \\ 1.3 & : 6 < V \le 50 \\ 0.16V + 0.34 & : 1 < V \le 6 \\ V - 0.5 & : 0.5 < V \le 1 \\ 0 & : V \le 0.5 \end{cases}. \tag{2.15}$$

Further studies of atmospheric attenuation loss caused by scattering were conducted by a number of other authors. Naboulsi proposed relationships for atmospheric attenuation loss caused by radiation and advection fog for wavelengths from 690 nm to 1550 nm and for visibilities from 50 m to 1000 m [62, 63].

Since the phenomena like absorption and scattering occur independing on the small beam focusing area of RoFSO system, Eq. (2.13) is directly applicable to the optical transmission loss model for RoFSO system given in Eq. (2.12).

2.4.1.2 Optical geometric loss

The optical geometric loss occurs due to the spreading of the transmitted beam between the FSO transmitter and the FSO receiver. Typically, the optical beam spreads to a larger size than the receive aperture, and then this overfill energy is lost. In general, larger receive apertures or smaller transmit divergences reduce the optical geometric loss for a give link distance, that is, the optical geometric loss depends on the optical antenna structure. For a uniform transmit power distribution with specific transmitter and receiver, the optical geometric loss can be approximated by the following equation [11, 64],

$$L_{geo}(d) = 20\log_{10}\left(\frac{D_{RX}}{D_{TX} + d \cdot \theta_{div}}\right) \text{ [dB]}, \tag{2.16}$$

where D_{RX} and D_{TX} are diameters of the optical transmitter and optical receiver, respectively, and θ_{div} represents the divergence angle of the transmitter laser beam.

It should be noted that Eq. (2.16) is appropriate for only FSO systems, and is not typically used in

microwave system design where geometric loss is based on assumptions for transmit beam diffraction as limited by the antenna.

Since the optical geometric loss depends on the apertures of optical antennas and the phenomenon like beam broadening is independent on the small beam focusing area of RoFSO system, Eq. (2.16) can be directly substituted into Eq. (2.12).

2.4.2 Scintillation loss and tracking error loss

Besides the effects of optical scintillation in conventional FSO systems, RoFSO system using seamless connection between SMF and free space is also affected by the fluctuations of the angle of arrival (AOA). Because of this, the location of the optical images on the focal plane of receiver antenna changes randomly. Therefore, conventional model on optical losses caused by atmospheric turbulence is not directly applicable to RoFSO system. In this section, we drive an appropriate scintillation loss model for RoFSO system based on a long-term experiment of RoFSO transmission.

2.4.2.1 Examination of scintillation loss models

There is the well-known scintillation loss model using the refractive index structure constant C_n^2 as its parameter, and it is given by the following equation [65],

$$L_{scin}(d) = 2\sqrt{23.17k^{7/6}C_n^2 d^{11/6}} \quad \text{[dB]}. \tag{2.17}$$

In Eq. (2.17), $k = 2\pi/\lambda$ represents the wave number. Eq. (2.17) will be referred to “Old Model” in the thesis.

Old model is only applicable for the case of weak turbulence and it has not taken the saturation phenomenon of scintillation into consideration. It is known that the scintillation index increases with the increasing of Rytov variance $\sigma_R^2 = 1.23C_n^2k^{7/6}d^{11/6}$ [65, 66], until it reaches a maximum value greater than unity in the regime characterized by random focusing, so called because the focusing caused by large scale inhomogeneities achieves its strongest effect. With increasing path length or inhomogeneity strength, the focusing effect is weakened by multiple scattering, and the fluctuations slowly begin to decrease, saturation at a level for which the scintillation index approaches unity from above. Qualitatively, saturation occurs because multiple scattering causes the optical wave to become increasingly less coherent as it propagates, eventually appearing like extended multiple sources, each scintillating with a distinct random phase. This phenomenon is referred as aperture averaging effect [65, 67-70].

Recently, Giggenbach et. al., developed a scintillation loss model for FSO systems using the power scintillation index as its parameter, it is given by the following equation [71],

$$L_{scin}(d) = 4.343\left\{\text{erf}^{-1}(2P_{thr}-1)\cdot[2\ln(\sigma_P^2+1)]^{1/2} - \frac{1}{2}\ln(\sigma_P^2+1)\right\} \text{ [dB]}. \quad (2.18)$$

In Eq. (2.18), P_{thr} is the fraction of outage time and equals the probability that the actual power fall below the threshold minimum received optical power, and erf^{-1} is inverse error function. σ_P^2 is the power scintillation index, and this parameter depends on the other system parameters and atmospheric turbulence as,

$$\sigma_P^2 = \exp\left\{\frac{0.20\sigma_R^2}{[1+0.81D^2+0.20(\sigma_R^2)^{6/5}]^{7/6}} + \frac{0.21\sigma_R^2[1+0.24(\sigma_R^2)^{6/5}]^{-5/6}}{1+0.90D^2+0.21D^2(\sigma_R^2)^{6/5}}\right\} - 1. \quad (2.19)$$

In Eq. (2.19), $D = D_{RX}(\pi/2\lambda d)^{1/2}$ is the ratio of the aperture radius to the Fresnel zone size, $\sigma_R^2 = 1.23C_n^2k^{7/6}d^{11/6}$ is Rytov variance, D_{RX} is aperture diameter of the receiving antenna. Eq. (2.18) will be referred to "New Model" in the thesis. Unlike Old Model, New Model takes the saturation of scintillation caused by aperture averaging effect into consideration [71].

2.4.2.2 Experimental setup for measuring scintillation loss and tracking error loss

We have conducted an experimental demonstration of RoFSO transmission for a long-term from April 2008 to February 2009 at Waseda University in Tokyo. Fig. 2.15 illustrates the experimental set up for DWDM RoFSO transmission. Two RoFSO antennas are installed on the rooftop of two buildings at Waseda University campus. The transmission distance is 1km. The system consists of two interface units, an optical interface unit (Optical IF unit) and a RF interface unit (RF IF unit). RF interface unit consists of a RoF module to perform E/O conversion for RF signals and other control circuits. The transmitted optical signals from the RF interface units are matched with the ITU grid wavelength of a 100 GHz space [72]. The optical interface unit consists of a DWDM multi/de-multiplexer, booster/post EDFA and optical circulator to separate transmitting/receiving optical signals. In the experiment, multiple RF signals including 3G cellular, WLAN (802.11g and 802.11a), and digital terrestrial television broadcasting (DTV) are simultaneously transmitted over the link. The specifications of RoFSO equipment and optical antenna are summarized in Table 2.7. Its detailed design features and operation of the DWDM RoFSO system have been reported in Ref. [73, 74].

At the same time, we have performed an experiment of continuous wave (CW) optical beam transmission over the RoFSO link. The scintillation loss caused by atmospheric turbulence is estimated on the basis of measured fluctuation in received optical intensity inside the SMF.

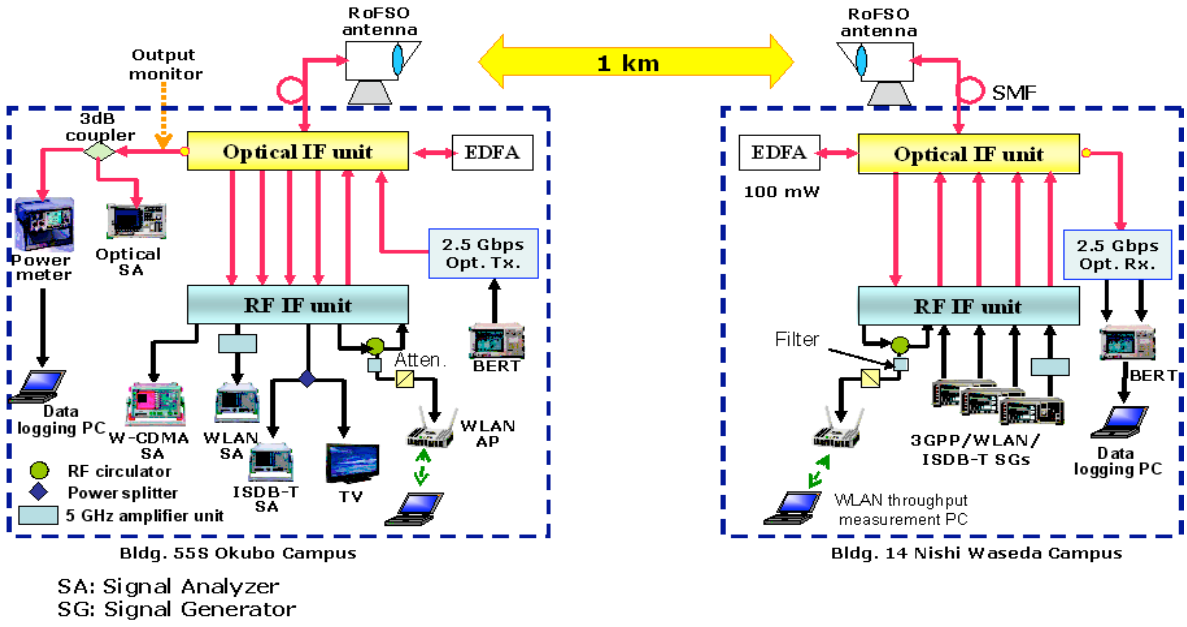

Fig. 2.15: Experimental setup for RoFSO transmission.

Table 2.7: Specification of RoFSO equipment and optical antenna

Operating optical wavelength	1550 nm (ITU-T C band)
WDM	4 wavelengths
Optical transmission power	20 dBm per wavelength
Antenna aperture diameter	80 mm
Fiber-air coupling loss	5 dB
Beam divergence	47.3 μrad
Fiber coupling technique	Direct coupling using FPM*
Beam tracking method	Automatic using QPD Course tracking using beacon at 850 nm Fine tracking using signal at 1550 nm

*FPM (Fine Pointing Mirror) used for control and steering the optical beam to single mode fiber (SMF) core.

2.4.2.3 Comparison of measured scintillation loss and its theoretical models

Fig. 2.16 shows the scintillation loss of the RoFSO system compared with the theoretical models, Old Model and New Model, as mentioned above in Eq. (2.17) and (2.18). There are two kinds of measured scintillation loss shown in Fig. 2.16. The black points are for scintillation loss estimated from the minimum received optical power measured in every minute, while the gray points are for scintillation loss estimated from the average optical power measured in every minute with the sampling rate of 10KHz.

As described in Sec. 2.4.2.1, Old Model is only applicable for weak turbulence and has not taken the saturation phenomenon of scintillation into consideration. As shown in Fig. 2.16, therefore, it is found that around $C_n^2 = 10^{-13}$ large scintillation loss is estimated by Old model, and thus under strong turbulence condition of $C_n^2 > 10^{-13}$, its estimation errors for measured scintillation loss from the average optical power become larger.

On the other hand, New Model has taken the saturation phenomenon of scintillation into consideration, as described in Sec. 2.4.2.1. In Fig. 2.16, it is found that New Model well reflects saturation of measured scintillation loss from the average optical power at $C_n^2 > 10^{-13}$. Furthermore, New model enable us to better approximate measured scintillation loss from the average optical power by controlling the parameter of P_{thr}. Three types of curves for New Model with $P_{thr} = 10^{-5}$, 10^{-7}, and 10^{-9} are shown in Fig. 2.16. Among them, New Model for the case of $P_{thr} = 10^{-7}$ shows best approximation to the measured scintillation loss, and thus we adopted $P_{thr} = 10^{-7}$ when the proposed

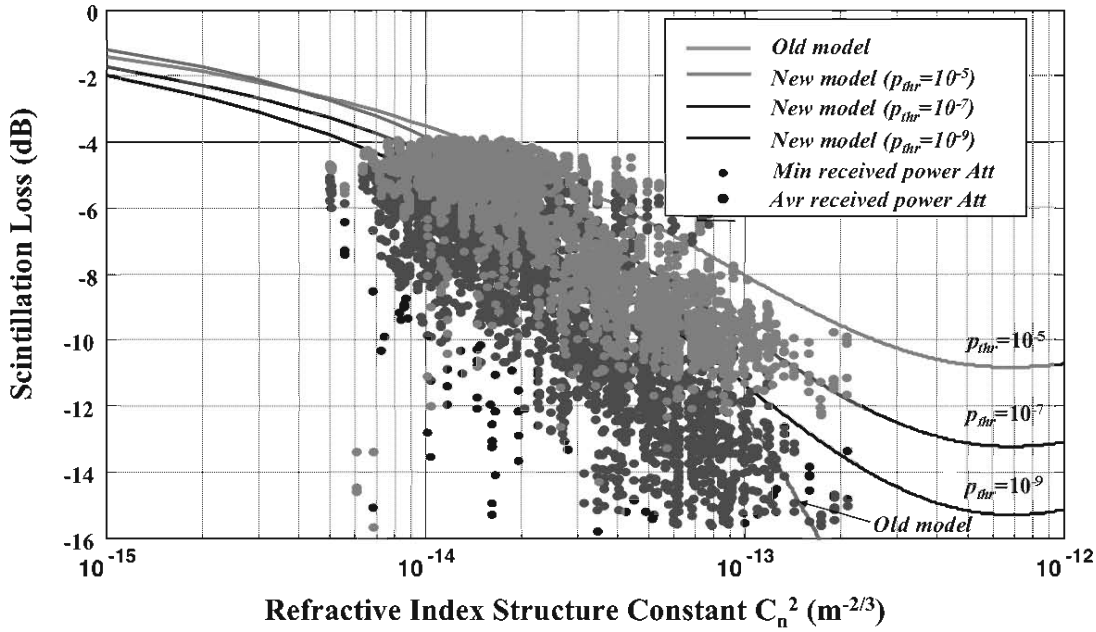

Fig. 2.16: Scintillation loss versus refractive index structure constant C_n^2.

optical transmission loss model in given in Eq. (2.12) is applied to the RoFSO link shown in Fig. 2.15.

It should be noted that scintillation loss in the RoFSO system is larger than that in the conventional FSO system due to the effect of AOA fluctuations. The tracking scheme is expected to compensate for this fluctuation, however, in the practice it is impossible to avoid the tracking loss error because the moving of the tracking mirror is not completely matched with the change of incoming beam point. It is known that the tracking error loss considerably depends on a capacity of a tracking device [24, 75]. We have measured the tracking error loss by comparing fading losses measured in the conventional FSO system and the RoFSO system, which are co-located on the rooftop. In the experiment, it is found that the tracking error can increase up to 8 dB at the time of noon when the atmospheric turbulence is strongest, and thus we assumed 8 dB of tracking error loss when the proposed optical transmission loss model in given in Eq. (2.12) is applied to the RoFSO link shown in Fig. 2.15.

2.4.3 Estimation of RoFSO link margin

In this section, RoFSO link margin is estimated on the basis of the proposed optical transmission loss model.

Fig. 2.17 shows the required link margin for scintillation loss, optical geometric loss, and tracking error loss, $-\{L_{scin}(d)+L_{geo}(d)+L_{tra}(d)\}$. The scintillation loss is based on New model given in Eq. (2.18), and three types of curves for the refractive index structure constant of $C_n^2 = 5\times10^{-13}$, 1×10^{-13}, 5×10^{-14} are plotted in Fig. 2.17. The tracking error loss is added on the basis of the following observation: The link margin of 8 dB to compensate for the tracking error in the case of the link distance is 1 km under strong turbulence condition. Tracking error loss will depends on the link distance. However, the scintillation will saturate after 1 km transmission under strong turbulence by aperture averaging effect. When the scintillation is saturated, the tracking error is considered to be also saturated. This means that for the link distance of more than 1 km, the margin of 8 dB is enough for the tracking error loss. When the transmission is less than 1 km, the tracking error increases together with the scintillation loss.

The required link margin for atmospheric attenuation loss $-L_{atm}(V,d)$ is also plotted in Fig. 2.17, where the margin for V = 0.85km is assumed to design conventional FSO link with availability of 99.9 % [76].

Under strong turbulence condition of $C_n^2 > 5\times10^{-14}$, $L_{scin}(d)+L_{geo}(d)+L_{tra}(d)$ becomes larger than $L_{atm}(V,d)$ at the link distance of around 1 km, and thus $L_{scin}(d)+L_{geo}(d)+L_{tra}(d)$ dominates the total optical transmission loss $L_{opt}(d)$, as shown in Fig. 2.17. Strong turbulence of $C_n^2 > 5\times10^{-14}$ occurs in daytime of clear sunny days [77]. At the same time, the visibility V has a large value, and thus the atmospheric attenuation loss $L_{atm}(V,d)$ is small. On the other hand, under low visibility

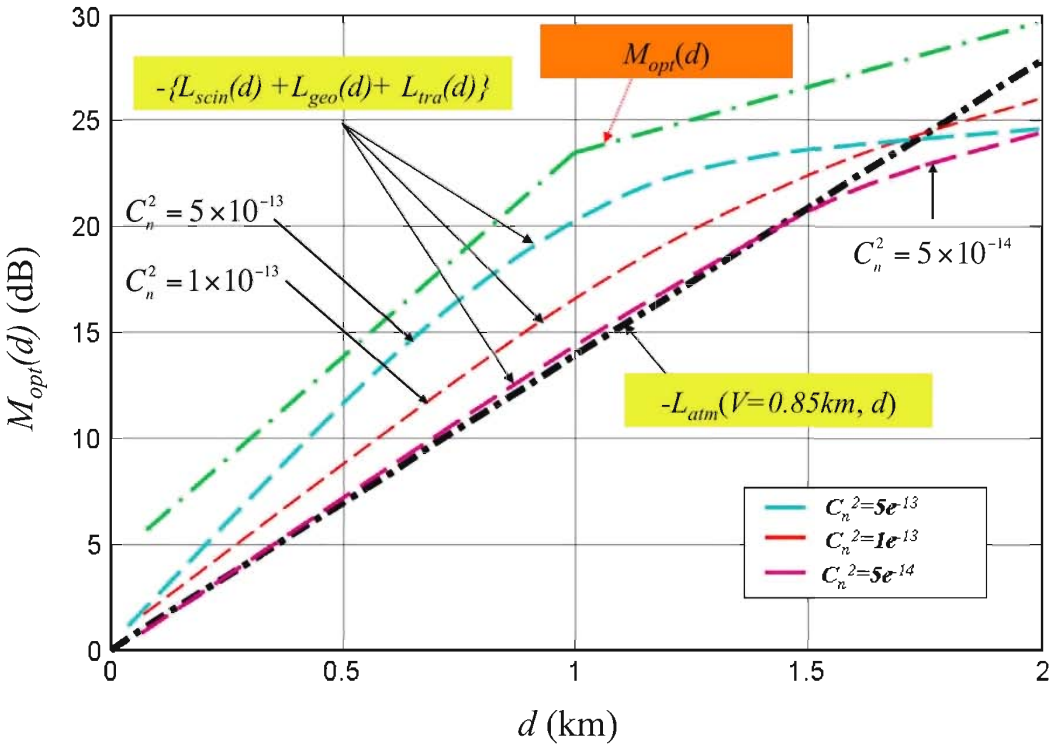

Fig. 2.17: Estimated RoFSO link margin $M_{opt}(d)$ versus RoFSO link distance d.

condition like rain, turbulence strength is very weak, and then scintillation loss and tracking error loss are not significant. Therefore, it is found that $L_{scin}(d)+L_{geo}(d)+L_{tra}(d)$ is larger than $L_{atm}(V,d)$ for the link distance of around 1 km.

However, for the link distance of more than 2 km, $L_{scin}(d)$ begins saturating by the aperture averaging effect, and then $L_{atm}(V,d)$ becomes dominant in the total optical transmission loss $L_{opt}(d)$. Consequently, difference between $L_{atm}(V,d)$ and $L_{scin}(d)+L_{geo}(d)+L_{tra}(d)$ increases with the increasing of the link distance.

According to Ref. [77], under a clear sunny weather with strong turbulence condition of $C_n^2 > 5\times 10^{-14}$, the atmospheric attenuation loss is typically about mere 3 dB/km. Therefore, for a RoFSO system with link distance d of less than 2 km, sufficient margin for scintillation loss taking very strong turbulence into consideration should be designed, and it is enough for the atmospheric attenuation loss. On the other hand, for a RoFSO system with relatively long link distance d of more than 2 km, it is enough to consider margin design for atmospheric attenuation loss. This is fundamental difference in design of link margin with the conventional FSO systems in which atmospheric attenuation is typically dominated. From the above observation, we can estimate the link margin for RoFSO system

$M_{opt}(d)$ as shown in Fig. 2.17.

Furthermore, the link margin for RoFSO system shown in Fig. 2.17 can be approximately expressed as

$$M_{opt}(d) = -L_{opt}(d) = \begin{cases} 19d + 4 & : 0 \le d < 1 \\ 7d + 16 & : 1 \le d < 2.667 \\ 13d & : 2.667 \le d \end{cases} \text{ [dB]}. \tag{2.20}$$

Eq. (2.20) is valid for the RoFSO system shown in Fig. 2.15 with the specifications summarized in Table 2.7, but the similar modeling with Eqs. (2.12), (2.18), and (2.19) can be applicable to other RoFSO system with different specifications or different beam tracking capacity.

2.5 Concluding remarks

We have proposed the Butterworth-type PSD model as the PSD of optical scintillation in RoFSO channel. Using the model, we have investigated the dependency of the cutoff frequency f_c and the spectral slope N on time zone and weather parameters of the temperature θ and the rainfall intensity R, based on analysis of optical scintillation data measured in a long-term experiment of FSO transmission. We derived estimated f_c, $\hat{f}_c(\theta,R)$, and estimated N, $\hat{N}(\theta,R)$, as their time average value under a given combined conditions of time zone, θ, and R. From the results, it is newly found followings:

- In general, optical scintillation with higher fluctuation speed occurs for the case of $R > 0$ than that of $R = 0$.
- When $R = 0$ at night, higher the temperature θ, slower the optical scintillation is.
- In general, $\hat{N}(\theta,R) = 1$ regardless of time zone, θ, and R.

We have also investigated the dependency of the scintillation index $\sigma_i'^2$ on time zone, θ, and R, based on the analysis of optical scintillation data measured in a long-term experiment of FSO transmission. We derived estimation value of $\sigma_i'^2$ for FSO system, $\hat{\sigma}_i'^2(\theta,R)$, as its time average value under a given combined conditions of time zone, θ, and R. From the results, it is newly found that the value of $\sigma_i'^2$ decreases as θ increases for the case of $R = 0$ and night. On the other hand, at daytime, the value of $\sigma_i'^2$ increases as θ increases on the whole. Furthermore, we extended $\hat{\sigma}_i'^2(\theta,R)$ to the estimation value of σ_i^2 for RoFSO system $\hat{\sigma}_i^2(\theta,R)$ under that assumption that the additional fading factor β is constant.

We have proposed a new optical transmission loss model for RoFSO system based on measured data in a long-term experiment of RoFSO transmission. Using the proposed model, we estimated

RoFSO link margin. It enables us to easily estimate the transmission quality of radio signal as a function of RoFSO link distance. The estimated RoFSO link margin is valid for the RoFSO system operated at 1.5 μm WDM band with the specifications shown in Table 2.7. Also, the similar modeling with the proposed model can be applicable for other RoFSO with different specifications like beam tracking capacity.

Chapter 3

Effect of optical scintillation on throughput of WLAN signal transmitted over RoFSO system

3.1 Introduction

As described in Chapter 2, the intensity fluctuation referred as optical scintillation occurs in the RoFSO channel, when an optical beam propagates through a turbulent atmosphere. When wireless services are extended to some outdoor spot areas or indoor areas over a RoFSO link, the fluctuations in the received optical signal intensity due to atmospheric turbulence result in power fluctuation of the RF signal transmitted from a remote antenna of RoFSO link. It may degrade quality of the RF signal transmitted over a RoFSO link. In evaluating the link budget of a radio communication link, fade duration in which the received RF power falls below a required RF power level is important, and this is directly related to the fluctuation speed of received RF power.

The previous researches mostly focused on the effects of atmospheric attenuation caused by fog, rain, and snow, on wireless optical communication link, because the atmospheric attenuation most dominates in the transmission performance of conventional FSO systems. However, few works have evaluated the effect of optical scintillation. For example, Refs. [78] and [79] evaluate the effect of optical scintillation on digital FSO systems in terms of signal-to-noise ratio (SNR) and bit error rate (BER). In evaluating the effect of optical scintillation, these works considered only the strength of optical scintillation by using statistical models of optical scintillation, for example, lognormal distribution or Gamma distribution, but they have not considered optical scintillation speed. Moreover, these works for FSO link cannot be applied to RoFSO link.

In this chapter, we propose a two-dimensional statistical model of optical scintillation, to evaluate the effect of optical scintillation on transmission performance of RF signals over RoFSO link. The proposed model can treat a time correlation of optical scintillation. In the proposed model, the optical

scintillation is modeled as a Gamma random process, and its probability density function (PDF) is determined by the PSD and the variance estimated in Chapter 2. Next, we evaluate the effect of optical scintillation on the system performance, especially on the throughput of WLAN signal transmitted over RoFSO system, because WLAN system is susceptible to the effect of optical scintillation due to its high bit rates and modulation level. In this analysis, both strength and speed of optical scintillation are taken into consideration.

3.2 Statistical model of time correlated optical scintillation

In this section, in order to investigate an effect of optical scintillation on WLAN signal transmission over RoFSO system, we propose a statistical model, which can express time correlation characteristic of optical scintillation.

Fig. 3.1 shows an analysis model of RoFSO channel. Free space optical channel can be generally modeled that transmitted optical intensity $I_0(t)$ is multiplied by the random gain $y(t)$ in turbulent atmosphere. Therefore, the received optical intensity $I_R(t)$ is expressed as [80],

$$I_R(t) = I_0(t) \cdot y(t). \tag{3.1}$$

There are some statistical models of $y(t)$. The lognormal distribution, normalized Gamma distribution, or Gamma-Gamma distribution are widely used [22, 58, 59, 81]. Recently, Ref. [57] compared the three PDFs with data measured in a RoFSO experiment. From their fitting test, it is found that the normalized Gamma distribution presents the closest property to RoFSO system. In the thesis, we introduce the normalized Gamma distribution as a PDF of optical scintillation, which is closely related to the Nakagami-m distribution and describes intensity fluctuations for rapid fading in long distance propagation [59]. The normalized Gamma distribution is given by

$$P_z(y;1;\sigma_i^2) = \frac{m_i^{m_i}}{\Gamma(m_i)} y^{m_i-1} e^{-m_i y}, \tag{3.2}$$

where m_i is the scintillation extent parameter given as $1/\sigma_i^2$, the number "1" denotes the mean value of intensity scintillation, and $\Gamma(x)$ is Gamma function given by

$$\Gamma(x) = \int_0^\infty t^{x-1} e^{-t} dt. \tag{3.3}$$

As shown in Sec. 2.2, the PSD of the optical scintillation shows the band-limited characteristic of optical scintillation channel. This means that optical scintillation has a time correlation in the time domain.

Fig. 3.2 shows the proposed statistical model of time correlated optical scintillation. Inputting a white Gamma process $z(t)$, to a filter with its impulse response $h(t)$, an output random process $y(t)$ is

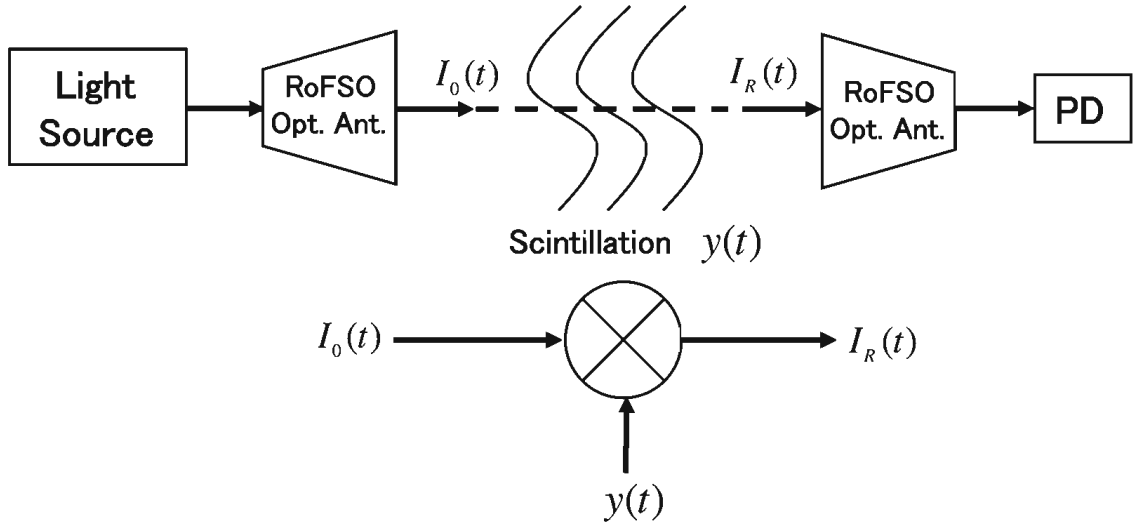

Fig. 3.1: An analysis model of RoFSO channel.

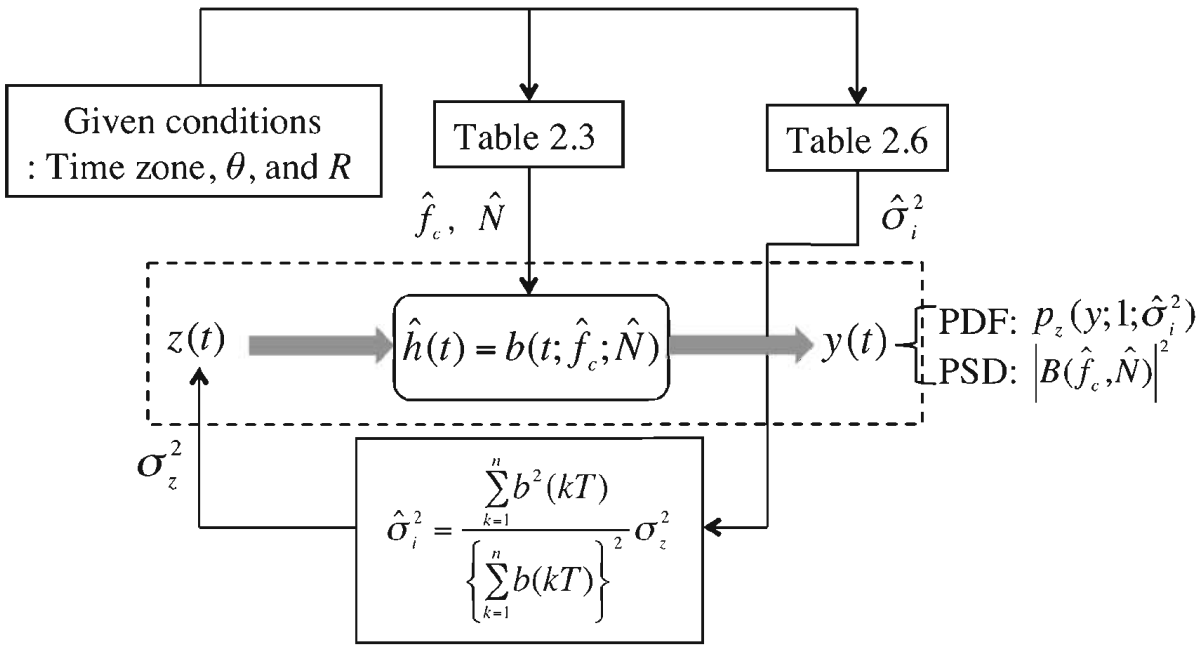

Fig. 3.2: Proposed statistical model of time correlated optical scintillation.

then expressed as

$$y(t) = \int_{-\infty}^{\infty} z(t)b(t-\tau)d\tau . \tag{3.4}$$

If the response time of the filter is longer than an interval of $z(t)$, then $y(t)$ becomes time correlated and its PSD is equivalent to that of the filter because the PSD of $z(t)$ is unity at whole frequency domain. At that time, inputting uncorrelated Gamma random process as $z(t)$, to the Butterworth filter with estimated impulse response $\hat{h}(t) = b(t;\hat{f}_c;\hat{N})$ as $h(t)$, then an output random process $y(t)$ has estimated PSD from a given RoFSO channel condition.

The variance of output random process $y(t)$, σ_y^2 can be derived as following equation,

$$\sigma_y^2 = \frac{\sum_{k=1}^{n} b^2(kT)}{\left\{\sum_{k=1}^{n} b(kT)\right\}^2}\sigma_z^2. \tag{3.5}$$

In Eq. (3.5), $b(kT)$, k = 1, 2,..., n, is the discrete impulse response value of Butterworth filter. In order to evaluate PDF of $y(t)$, $P_y(y;1;\sigma_y^2)$, a variance of uncorrelated Gamma random process $z(t)$, σ_z^2, should be set to a value that makes $\sigma_y^2 = \sigma_i^2$. It can be done by using the relationship given in Eq. (3.5).

Fig. 3.3 shows two examples of PDFs, PDF of measured scintillation data $i(t)$, $p_i(y;1;\sigma_i^2)$, PDF of the output random process $y(t)$, $p_y(y;1;\sigma_y^2)$, and Gamma distribution $p_z(y;1;\sigma_i^2)$ fitted to $p_i(y;1;\sigma_i^2)$, for the cases of σ_i^2 = 0.012, and σ_i^2 = 0.03. $y(t)$ has a frequency characteristic estimated under a given RoFSO channel condition. It is found that these three PDFs are very similar each other, especially, $p_y(y;1;\sigma_y^2)$ has a conformity with $p_z(y;1;\sigma_i^2)$ of curve in shape. Consequently, $p_y(y;1;\sigma_y^2)$ is Gamma distribution, and it is found that the PDF of a sum of statistically independent Gamma random variables is also Gamma distribution. Therefore, by substituting $\sigma_y^2 = \hat{\sigma}_i^2$ into Eq. (3.5), we can generate $y(t)$ which has an estimated PDF from a given RoFSO channel condition, because the normalized Gamma distribution is determined by only one parameter of variance as shown in Eq. (3.2). It should be noted that $p_y(y;1;\sigma_y^2)$ well agrees with $p_z(y;1;\sigma_i^2)$ measured under various weather conditions shown in Chapter 2.

In the next section, we investigate the effects of optical scintillation on throughput performance of WLAN signal transmitted over RoFSO system by using the time correlated Gamma random process $y(t)$.

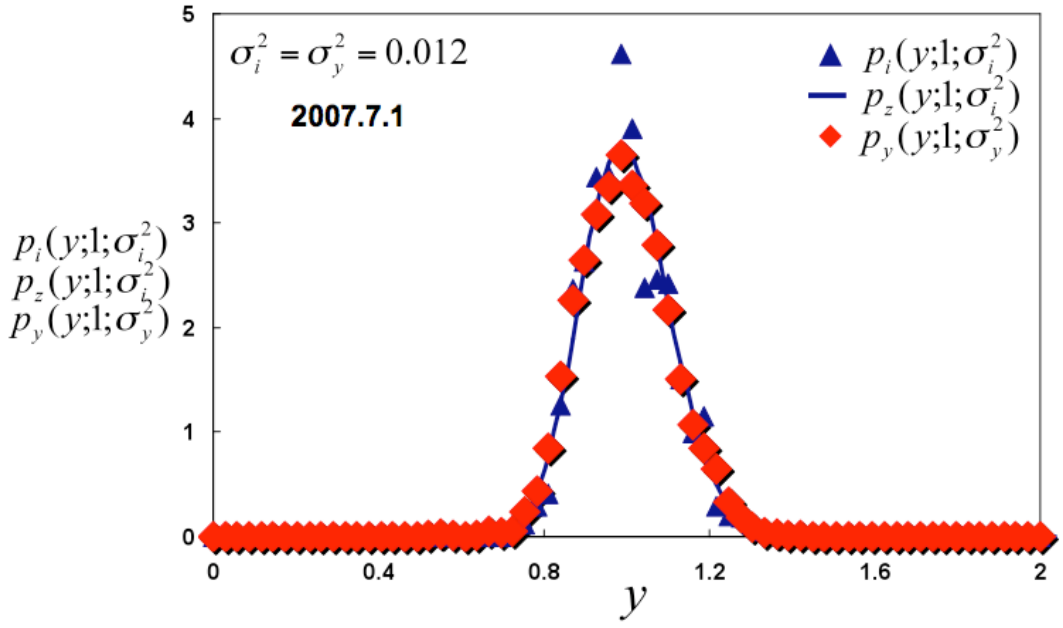

(a)

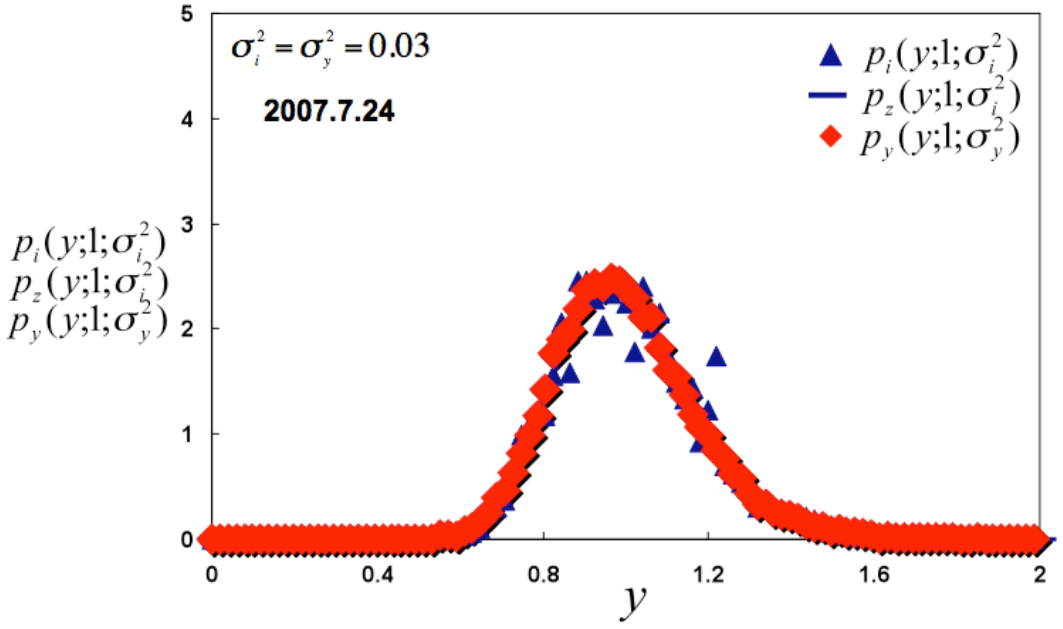

(b)

Fig. 3.3: $p_i(y;1;\sigma_i^2)$, and fitted $p_y(y;1;\sigma_y^2)$, $p_z(y;1;\sigma_i^2)$ for the cases of (a) $\sigma_i^2 = 0.012$, and (b) $\sigma_i^2 = 0.03$.

3.3 Effect of optical scintillation on throughput of WLAN signal transmitted over RoFSO link

In this section, we evaluate the effect of optical scintillation on throughput performance of IEEE 802.11a signal transmitted over RoFSO link by executing computational simulations. Qualnet [82] is used as a simulator.

3.3.1 Effects of strength and speed of optical scintillation

In Sec. 3.3.1, effects of two parameters of optical scintillation, its strength σ_i^2 and speed f_c, on throughput performance are evaluated. It is also evaluated by comparing an ideal case of no-scintillation and worst case, quantitatively.

3.3.1.1 Simulation configuration

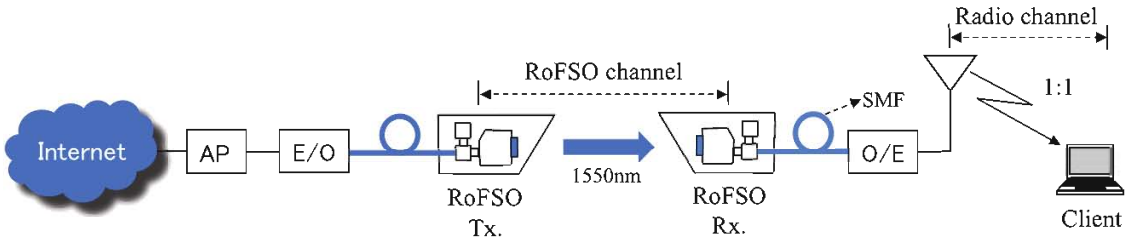

Fig. 3.4: Simulation configuration.

Fig. 5.1 shows a simulation configuration for application of RoFSO downlink to be used for throughput performance evaluations of IEEE 802.11a signal transmission. RF signals transmitted from a WLAN access point (AP) are converted into optical signals by the intensity modulation (IM) in the LD. The optical signals are transmitted through RoF link, and emitted to the RoFSO receiver (Rx) from the RoFSO transmitter (Tx). Optical signals that have experienced optical scintillation in the RoFSO channel are received at the RoFSO Rx, the optical signals are converted into the RF signals by the direct detection (DD) in the PD. Then, the RF signals are radiated from a remote antenna, and they are received in the client terminal.

As shown in table 3.1 and Fig. 3.5, two cases of path length between the remote antenna and client are considered in radio channel, path lengths of 25.8 m (case (a)) and 14.5 m (case (b)). They are corresponding to the pathloss of 75 dB and 70 dB at 5.2 GHz for free space propagation channel, respectively. Free space radio channels are considered as pathloss model and a download service such

Table. 3.1: Simulation parameters of radio channel (1)

Parameters	Setup
Pathloss model	Free Space
Path length	Case (a) : 25.8 [m] (pathloss=75 dB) Case (b) : 14.5 [m] (pathloss=70 dB)
Antenna model	Omni-directional • Antenna gain : 0.0 [dB] • Antenna height : 1.5 [m]
Fading & Shadowing	None
Radio standard	IEEE 802.11a • RF carrier frequency : 5.2 [GHz] • Transmission power : +10 [dBm] • Adaptive modulation
Application	CBR (Constant Bit Rate) • Data rate : 29.44 [Mbps]

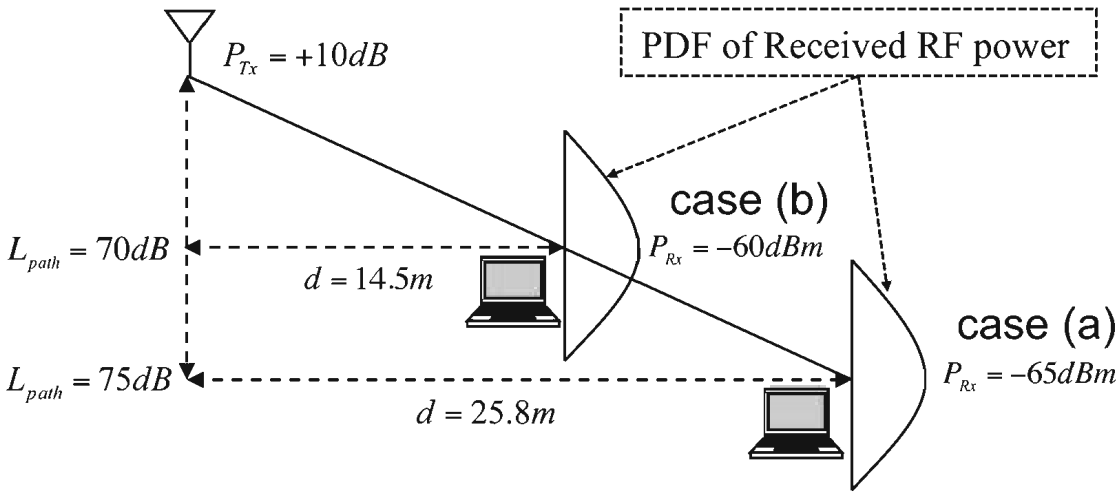

Fig. 3.5: Two cases of path length in radio channel.

Table. 3.2: Simulation parameters of RoFSO channel

Parameters	Setup
Link distance	1 [km]
Weather conditions	Clear sunny day in summer • θ>30 [°C] • R = 0 [mm/h]
Time zone	Daytime

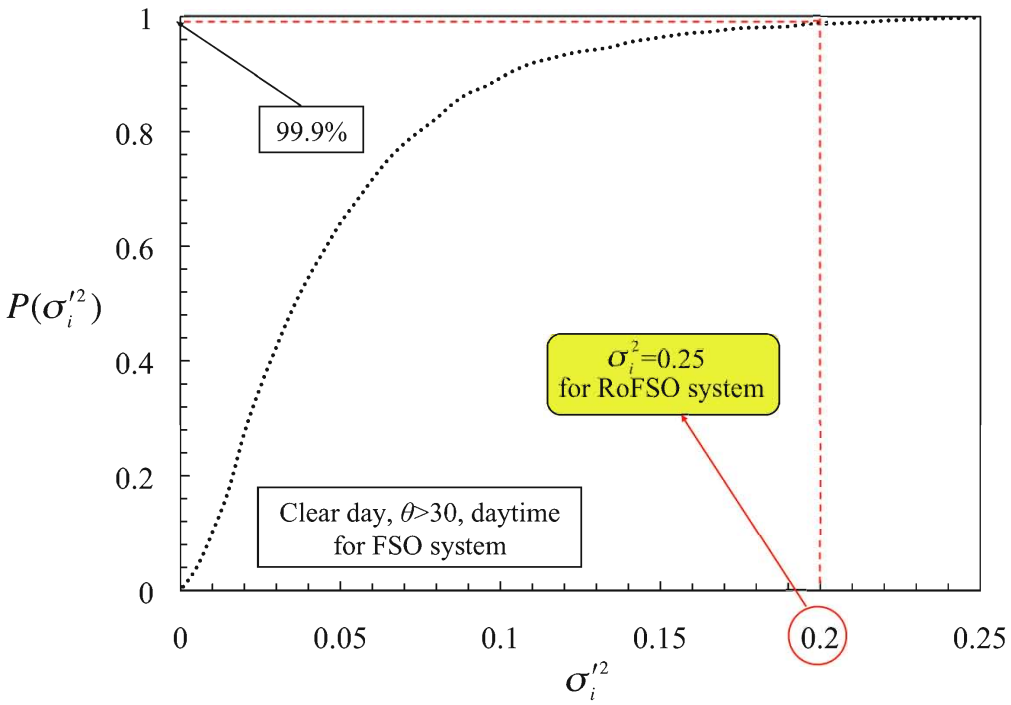

Fig. 3.6: Cumulative distribution function of the scintillation index for FSO system, $P(\sigma_i'^2)$, under the combined conditions of θ > 30, daytime, clear day.

as constant bit rate (CBR) is considered as applications. Fading, shadowing effect and interference in the radio channel are not considered in the simulation. IEEE 802.11a is considered as radio standard

with RF carrier frequency of 5.2 GHz, RF transmission power of +10 dBm from the remote antenna and the adaptive modulation are assumed.

Conditions of RoFSO channel assumed in the simulation are summarized in table 3.2. We assumed 1km optical signal transmission over RoFSO link under the RoFSO channel condition of $\theta > 30$, $R = 0$, daytime of clear sunny day in summer. Fig. 3.6 shows the cumulative distribution function (CDF) of $\sigma_i'^2$ for FSO system, $P(\sigma_i'^2)$, under the combined conditions of $\theta > 30$, daytime, clear day. We focus on this condition because it is the worst condition from the perspective of strength of optical scintillation, as shown in Fig. 2.14, and especially point of $P(\sigma_i'^2) = 99.9$ % at which $\sigma_i'^2 = 0.2$. It should be noted that $\sigma_i'^2$ of 0.2 is corresponding to σ_i^2 of 0.25 from Eq. (2.10).

3.3.1.2 Numerical results

Atmospheric turbulence results in fluctuations in the received optical intensity in a RoFSO channel. The fluctuations in the received optical intensity causes power fluctuation in a RF signal after the direct detection at the PD. The RF signal is radiated from a remote antenna at receiver side of the RoFSO downlink. That is, width and speed of power fluctuation in the transmitted RF signal are directly related to optical scintillation in RoFSO channel.

Fig. 3.7 shows the average fade duration (AFD) T_y of received optical intensity versus threshold level of optical intensity for the case of $\sigma_i^2 = 0.25$, which is to be used to examine behavior of fluctuations in transmitted RF signal power. The AFD is defined as the average period of time for which the received optical intensity is below a certain threshold level. It is given by the following equation,

$$T_y(I_{th};\sigma_i^2,f_c,N) = \frac{P[y(t) \le I_{th}]}{N_y(I_{th};\sigma_i^2,f_c,N)} \tag{3.6}$$

where, I_{th} is a threshold level, and $P[y(t) \le I_{th}]$ is the probability that the optical scintillation $y(t)$ is less than I_{th}. N_y is the level crossing rate (LCR) defined as the expected rate that received optical intensity crosses I_{th} in a positive-going or negative-going direction. In Fig. 3.7, it is found that for $I_{th} = 0$ dB, $T_y = 3.8$ ms at $f_c = 200$ Hz, and $T_y = 66.9$ ms at $f_c = 10$ Hz.

Fig. 3.8 illustrates images of fluctuations in the transmitted RF signal powers for the cases of $f_c = 200$ Hz and $f_c = 10$ Hz, when it is presumed that the transmitted RF signal power sinusoidally fluctuates. From the results of AFD shown in Fig. 3.7, it is found in Fig. 3.8 that half-period of transmitted RF signal power for the case of $f_c = 200$ Hz is 3.8 ms, and that for the case of $f_c = 10$ Hz is 66.9 ms. When UDP payload length of 1472 octets and 54 Mbps-mode (64-QAM) data rate are assumed, one data frame period of 802.11a is approximately 400 μm [83]. From this approximation, it is found that a half-period of transmitted RF signal is much longer than one data frame period of

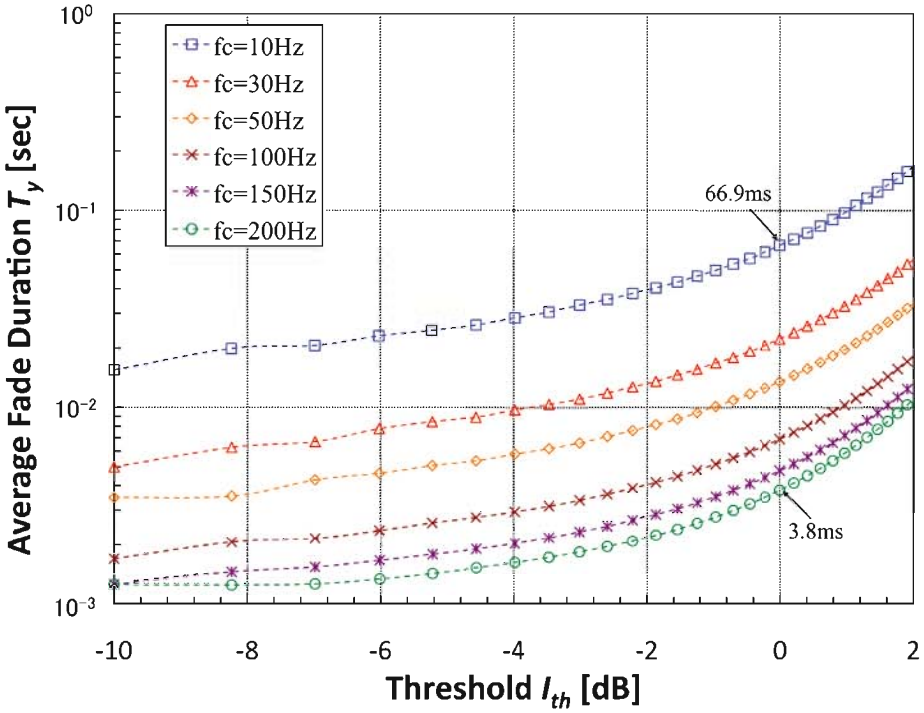

Fig. 3.7: Average fade duration (AFD) of received optical intensity versus threshold level of optical intensity for the case of $\sigma_i^2 = 0.25$.

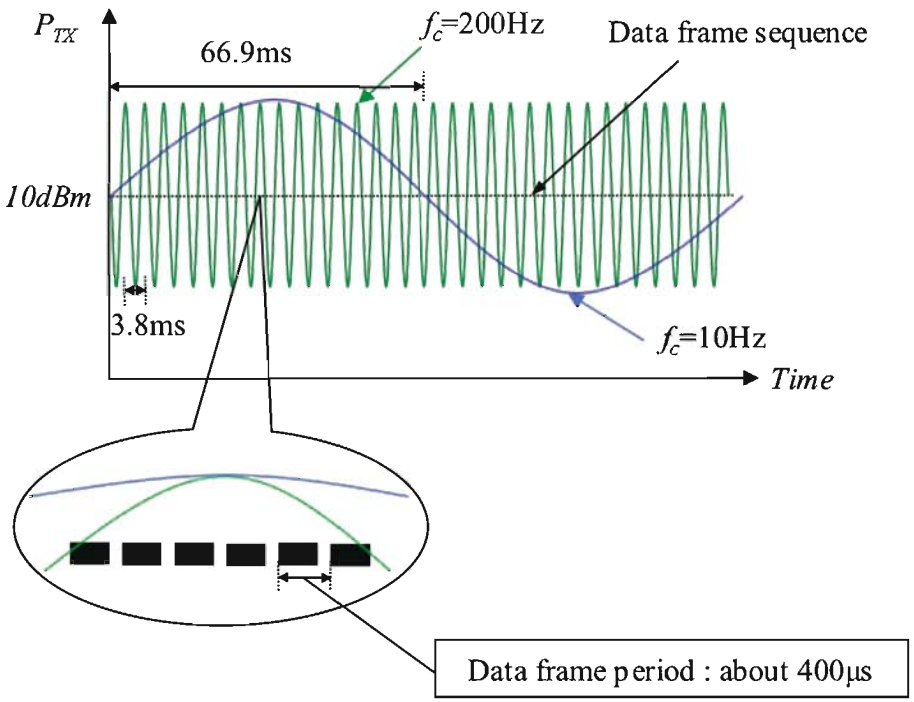

Fig. 3.8: Images of fluctuations in transmitted RF signal powers for the cases of f_c = 200 Hz and f_c = 10 Hz.

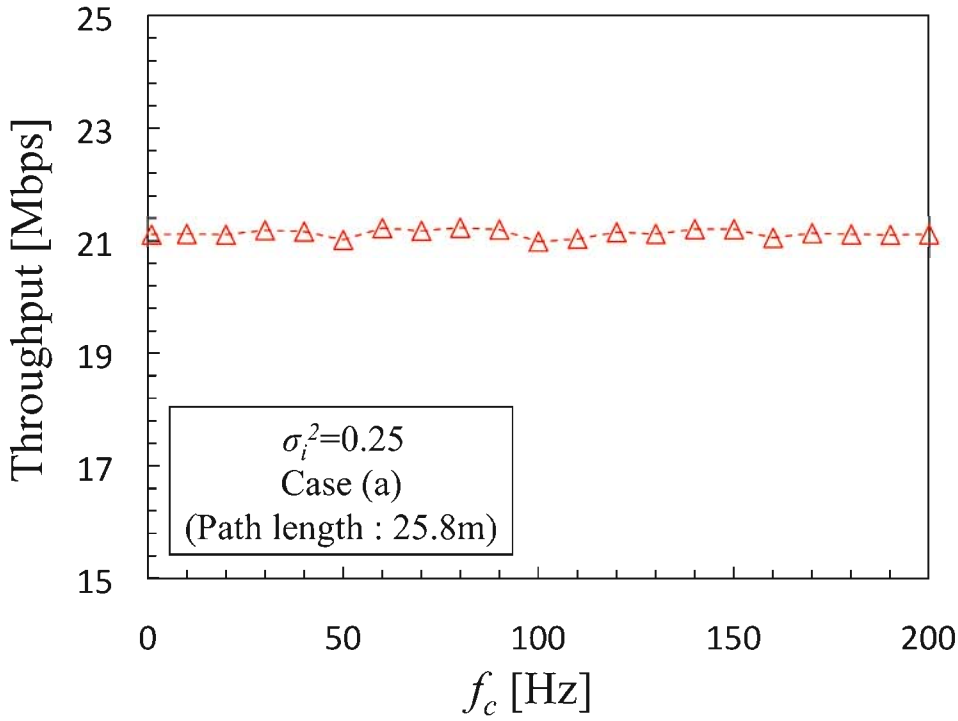

Fig. 3.9: Throughput performance versus f_c for case (a) and $\sigma_i^2 = 0.25$.

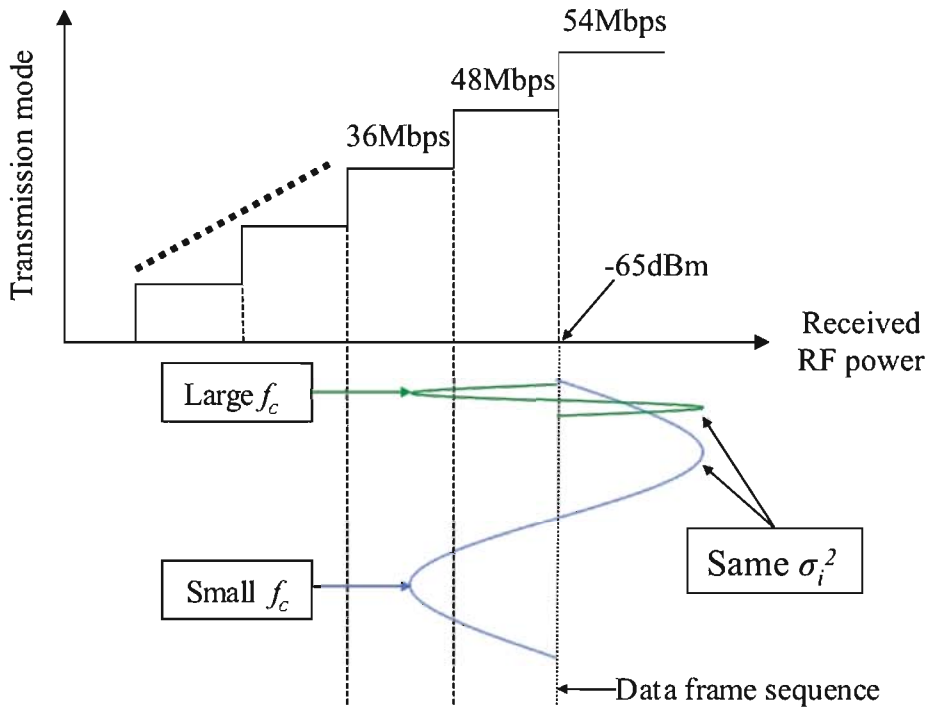

Fig. 3.10: Images of fluctuations in received RF signal powers for case (a), for large f_c and small f_c, but a same σ_i^2.

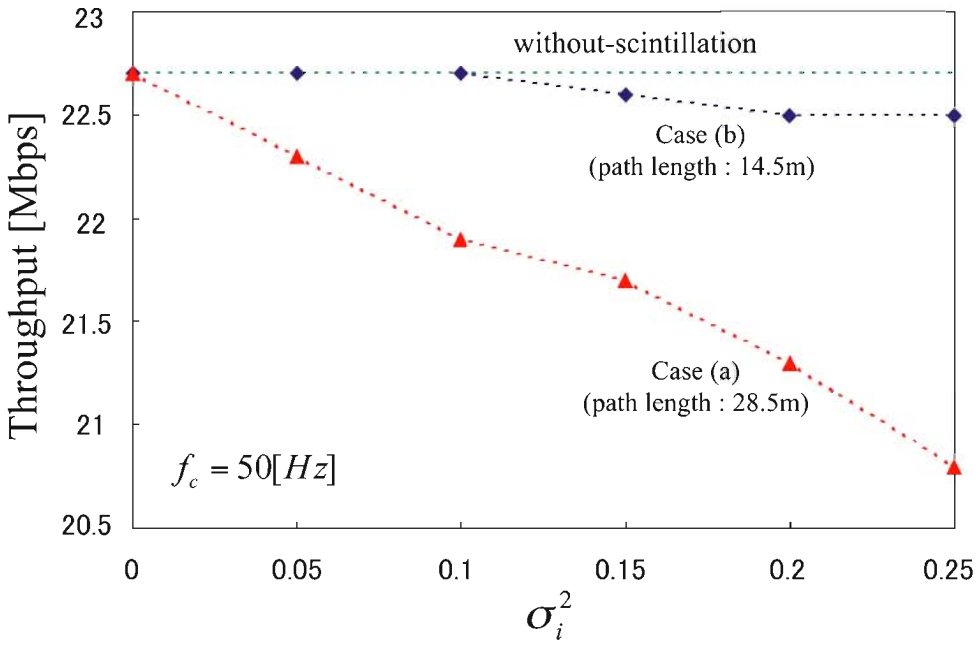

Fig. 3.11: Throughput performance versus σ_i^2 for cases (a) and (b) (f_c = 50 Hz).

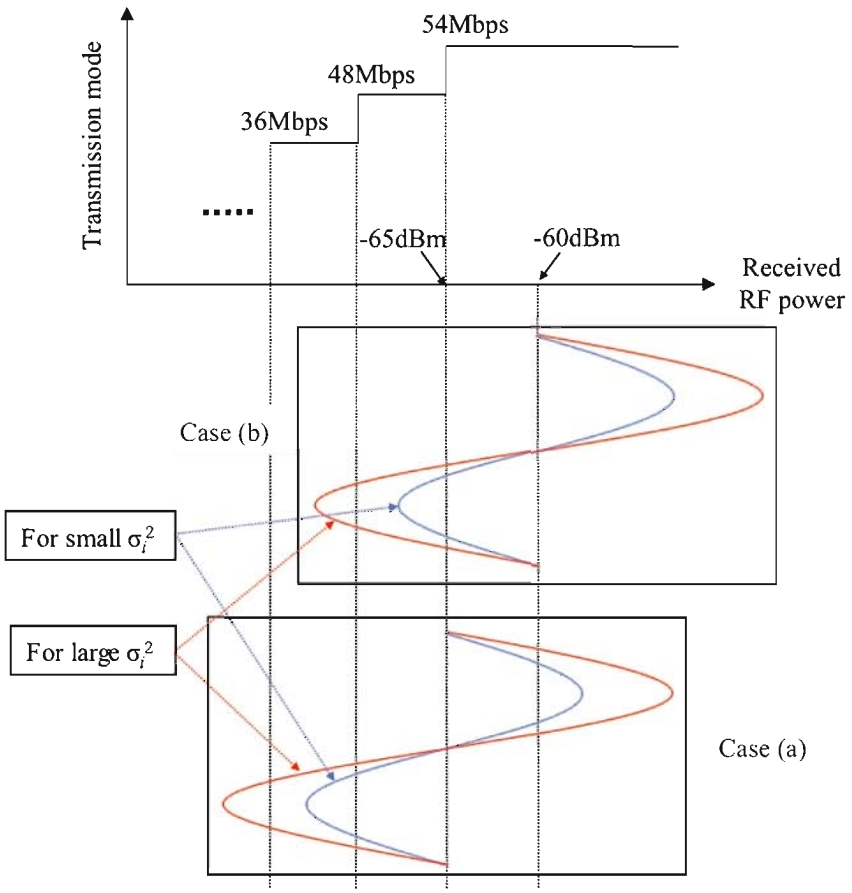

Fig. 3.12: Images of fluctuations in received RF signal powers for cases (a) and (b), for large σ_i^2 and small σ_i^2, but a same f_c.

802.11a. Therefore, it can be concluded that optical scintillation speed is slow enough to disregard the amplitude variation within data frame length of 802.11a for both cases of large f_c and small f_c.

Fig. 3.9 shows a result of throughput performance versus f_c for σ_i^2 = 0.25 and case (a). It should be noted that the leftmost plotted symbol is not corresponding to f_c of 0 Hz in the graph, but f_c of 1 Hz. Fig. 3.10 illustrates images of fluctuations in received RF signal powers for case (a), for large f_c and small f_c, but a same σ_i^2. From the above discussion, it is found that for same σ_i^2, probability that received RF power is within a certain receive sensitivity level are same regardless of f_c, as illustrated in Fig. 3.10. In other word, for same σ_i^2, average throughputs during one period both for cases of large f_c and small f_c are almost same. Therefore, it is observed that throughput performance is almost constant as about 21.0 Mbps, regardless of f_c, in Fig. 3.9.

Fig. 3.11 shows a result of throughput performance versus σ_i^2 for f_c = 50 Hz for following the two cases of radio path lengths. It should be noted that in Fig. 3.11, σ_i^2 of 0 denotes an ideal case that there is no optical scintillation in RoFSO channel. For case (a), it is observed that throughput decreases as σ_i^2 increases almost linearly. In other word, degradation in throughput performance due to scintillation is enhanced in proportion to σ_i^2. On the average, degradation of 0.38 Mbps is occurred per σ_i^2 increase of 0.05. On the other hand, when compared with case (a), throughput is almost constant as about 21.0 Mbps regardless of σ_i^2 for case (b).

Optical scintillation in RoFSO channel causes fluctuation in transmitted RF signal power for downlink, and thus received RF signal power also fluctuates. Fig. 3.12 illustrates images of fluctuations in received RF signal powers for large σ_i^2 and small σ_i^2, but a same f_c. A width of fluctuation in received RF signal power is directly related to a width of optical scintillation. As illustrated in Fig. 3.12, a width of fluctuation in the received RF signal power increases as σ_i^2 increases, and then more received RF signal powers may be distributed below a certain receive sensitivity level. Consequently, degradation in throughput performance is enhanced. Average received RF signal power for case (a) is less than that for case (b) by 5 dB, therefore, case (a) is more sensitive to σ_i^2.

In Fig. 3.11, it is found that path length for the case (b) is short enough that the optical scintillation almost cannot affect the throughput performance in the given range of σ_i^2. It is also found that when compared with the ideal case of without scintillation, throughput performance is degraded by mere 2.1 Mbps when σ_i^2 = 0.25 for radio path length of 25.8 m. As will be described in Sec. 3.3.2, degradation due to scintillation is small when compared with other effects such as shadowing for indoor radio propagation environment. As shown in Fig. 3.12, however, for longer radio path length, that is, for smaller received RF signal power, degradation in throughput performance due to scintillation is more enhanced even for small σ_i^2.

3.3.2 A case of combining shadowing and scintillation

In this section, a case of combining shadowing with scintillation is considered. Two indoor radio propagation environments are assumed, corridor and small room. Throughput performance is quantitatively evaluated for each radio environment. Effect of optical scintillation on throughput performance is compared with that of shadowing.

3.3.2.1 Simulation configuration

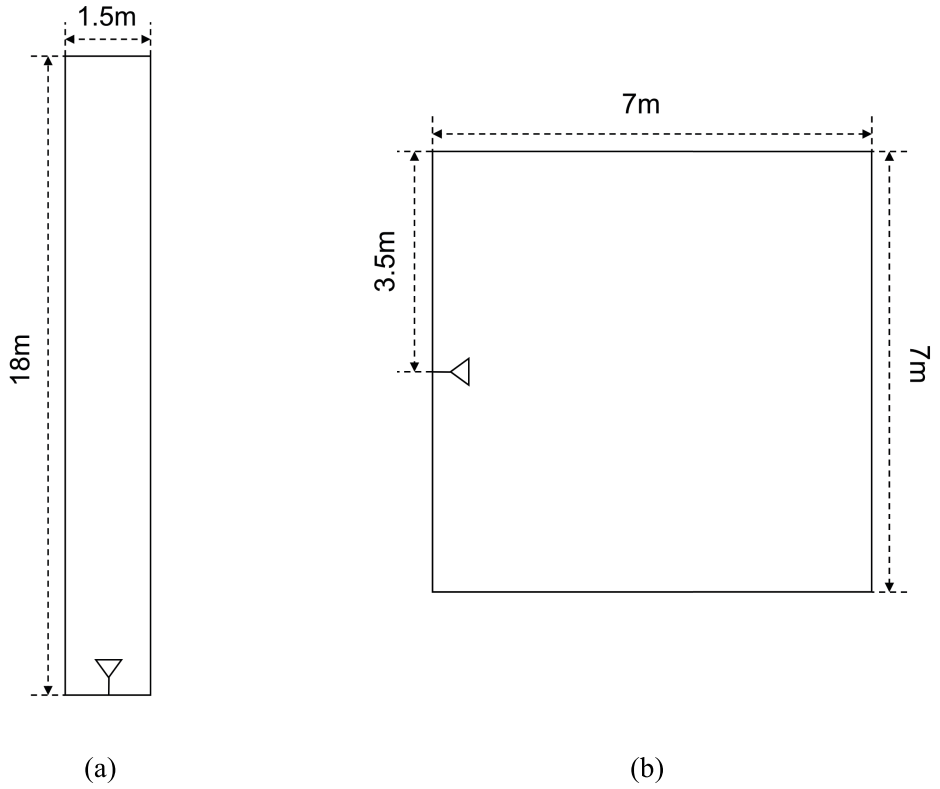

Fig. 3.13: Two kinds of indoor radio propagation environments, (a) corridor and (b) small room.

Fig. 13.3 (a) and (b) illustrates two kinds of indoor radio propagation environments considered in the simulation, corridor (18 m × 1.5 m) and small room (7 m × 7 m) such as an office, respectively. The receiver is randomly located 10 times in range of each area, and their average throughput is calculated. In the simulation, bodyworn terminal is considered as the receiver.

As shown in Table 3.3, two cases of shadowing model, the lognormal distribution with its standard deviation of 5.4 dB for corridor and 15.7 dB for an office are assumed [84]. Moreover, in the both cases, four cases are considered; (1) an ideal case that there are no shadowing in radio channel and no scintillation in RoFSO channel, (2) a case that there are shadowing in radio channel, but no scintillation in RoFSO channel, (3) a case that there are scintillation in RoFSO channel, but no shadowing in radio channel, and (4) a case of combining shadowing with scintillation, that is, there are shadowing in radio channel, and scintillation in the RoFSO channel, for each radio environment are

Table 3.3: Simulation parameters of radio channel (2)

Parameters	Setup
Pathloss model	Free Space
Shadowing model	Lognormal • σ_{sh} = 5.4 [dB] (Corridor) • σ_{sh} = 15.7 [dB] (Small room)
Antenna model	Omni-directional • Antenna gain : 0.0 [dB] • Antenna height : 1.5 [m]
Fading	None
Radio standard	IEEE 802.11a • RF carrier frequency : 5.2 [GHz] • Transmission power : +10 [dBm] • Adaptive modulation
Application	CBR (Constant Bit Rate) • Data rate : 29.44 [Mbps]

considered. In the simulation, the worst case from perspective of strength of scintillation, that is, σ_i^2 = 0.25 is assumed.

From the results given in Sec. 3.3.1, it was found that f_c is slow enough to disregard the amplitude variation for symbol length of IEEE 802.11a, it is not considered in the simulation.

The total variance of fluctuation in the received RF signal power can be estimated by adding variance of fluctuation in received RF signal power due to scintillation to variance of shadowing, σ_{sh}^2. σ_i^2 is the variance of fluctuation in received optical intensity. Using the characteristic function [60] of Gamma random variable, variance of fluctuation in the received RF signal power due to scintillation, σ_{sc}^2, can be derived as following equation,

$$\sigma_{sc}^2 = 6\sigma_i^6 + 10\sigma_i^4 + \sigma_i^2. \tag{3.7}$$

And, the total standard deviation of fluctuation in the received RF signal power caused by combining shadowing plus scintillation, σ, is represented as the sum of them in dB unit, that is,

$$\sigma = \sigma_{sh} + \sigma_{sc} \text{ [dB]}. \tag{3.8}$$

The other parameters are identical with those in Sec. 3.3.2.

3.3.2.2 Numerical results

Results of average throughputs for four cases in each radio environment are shown in Table 3.4. In the corridor, degradation in throughput performance of 53.8 % occurs for the worst case (4) when compared with an ideal case (1). σ_i^2 = 0.25 is corresponding to σ_{sc} = 5.7 dB in Eq. (3.7), and it is almost same with σ_{sh} = 5.4 dB. Since the PDF of fluctuation in received optical intensity is Gamma distribution, the PDF of transmitted RF signal power of squared optical intensity is also Gamma distribution [34]. In fact, the two distributions, lognormal distribution and Gamma distribution, are fairly similar [85]. Therefore, degradation in throughput performance for case (2) is almost equivalent to that for case (3) as 10.1 %, as shown in Table 3.4. It can be concluded that degradation in throughput performance due to scintillation with σ_i^2 = 0.25 is almost same with that due to shadowing in corridor environment. When compared with case (2), degradation in throughput performance due to scintillation of 48.5 % occurs for case (4).

Table 3.4: Average throughputs at the receiver for four cases in corridor and small room

Throughput [Mbps]	Case (1)	Case (2)	Case (3)	Case (4)
Corridor	22.7	20.4	20.3	10.5
Small room	22.7	7.2	22.7	1.2

In the small room like an office, degradation in throughput performance of 94.7 % occurs for the worst in case (4) when compared with case (1). There is no degradation for case (3), while degradation of 68.3 % occurs for case (2). From this result, it is found that a radio path length between the remote antenna and the client randomly located within the small room is short enough to be almost not affected by optical scintillation. When compared with case (2), degradation in throughput performance due to scintillation of 83.3 % occurs for case (4), even though there is no degradation for case (3).

From the results, it can be concluded that degradation in throughput performance due to scintillation is less than that due to shadowing. However, degradation due to shadowing is more enhanced, when it occurs simultaneously with scintillation. Especially, it is found that the degradation due to scintillation is more enhanced when shadowing with a large variation width occurring simultaneously. That is, it also depends on radio propagation environment.

3.4 Concluding remarks

We have proposed a new statistical model of time correlated optical scintillation, which can express not only the PDF, but also the time correlation characteristic of optical scintillation. The proposed model enables us to generate a time correlated Gamma random process, which has PSD and PDF estimated from a given RoFSO channel condition, such as time zone, θ, and R.

Using the proposed model, we have evaluated an effect of optical scintillation on throughput performance of IEEE 802.11a signal transmitted over RoFSO link, taking both strength and speed of optical scintillation. From the results, it is newly found followings:

(1) Speed of optical scintillation is slow enough to disregard the amplitude variation within data frame length of 802.11a even for the case of large f_c.
- For a case of same σ_i^2, probability that received RF power is within a certain receive sensitivity level are same regardless of f_c.
- For a case of same σ_i^2, average throughputs during one period both for cases of large f_c and small f_c are almost same.

(2) Radio path length of 14.5 m (received RF signal power of -60 dBm) is short (large) enough to be almost not affected by σ_i^2.
- When compared with the ideal case of without scintillation, throughput performance is degraded by mere 2.1 Mbps when σ_i^2 = 0.25 for radio path length of 25.8 m (received RF signal power of -65 dBm).
- However, for longer radio path length, that is, for smaller received RF signal power, degradation in throughput performance due to scintillation is more enhanced even for small σ_i^2.

(3) In the indoor radio environments of corridor and small room like office, degradation in throughput performance due to optical scintillation is less than that due to shadowing.
- However, degradation due to shadowing is more enhanced, when it occurs simultaneously with scintillation.
- Degradation due to scintillation is more enhanced when shadowing with a large variation width occurs simultaneously.

Chapter 4

WDM optical power allocation method for RoFSO system

4.1 Introduction

Analog FSO systems have a possibility of the reduction of the cost of transceiver equipment as compared with a digital implementation [86, 87]. The RoFSO system, which is one of analog FSO systems, can transmit different types of wireless service signals transparently between an optical fiber and a free space with keeping their radio signal formats. Followings are important points in designing a RoFSO system.

(1) Each transmitted radio signal has its inherent frequency, bandwidth, modulation format, receiver sensitivity, and in the case of OFDM signal, total number of multicarriers.

(2) Each transmitted radio signal has its own radio regulation in the transmission power, the spectral spurious, the spectral mask, adjacent channel leakage ratio (ACLR), and so on. These regulations must be satisfied when the radio signal is radiated from a remote station of RoFSO downlink. Different regulations for different radio signals demand different required transmission qualities for RoFSO link.

(3) RoFSO system has to keep the regulation on Eye-Safety [88]. Class 3A in the regulation corresponding to RoFSO system operated at 1.5 μm WDM band allows the laser emission power of up to 500 mW [88, 89].

When RoFSO system is designed without consideration of these constraints, it is likely that some of RF signals transmitted over RoFSO link cannot achieve their own required qualities, and others have some surplus qualities. To properly guarantee requirements for each heterogeneous radio signal, the effective design method of RoFSO link has to be established. However, such methods have not been found as far as we know.

In this chapter, we propose a WDM optical power allocation method to independently guarantee the

required quality of each RF signal under the limitation of total optical transmission power to keep Eye-Safety regulation Class 3A. Because RoFSO using WDM can transmit any kind of RF signals without their mutual interferences, the proposed method can optimize each optical modulation index (OMI) for each WDM channel.

4.2 WDM optical power allocation for fixed OMIs

In this section, WDM optical allocation method for given OMIs of heterogeneous radio signals, that is, for fixed OMIs, is proposed. The validity of the proposed method is shown, by comparing with the conventional case that WDM optical power is equally allocated.

Regarding a method for the optimum OMIs, it will be discussed in Sec. 4.4.

4.2.1 CNDR of WDM RoFSO link

Fig. 4.1 shows the basic configuration of WDM RoFSO link. In the optical Tx antenna side, RF signals transmitted over RoFSO link are intensity modulated (IM) in the laser diodes (LDs), optical signals from LDs are multiplexed in the WDM multiplexer (MUX), then total optical power is amplified by the Eye-Safety limitation power in the booster erbium-doped optical fiber amplifier (EDFA) and radiated to free space. In the optical Rx antenna side, received optical signal attenuated by propagation loss are amplified in the post EDFA and demultiplexed in the WDM demultiplexer (DEMUX), and then the optical signals are converted to RF signals by direct detection (DD) in the photodiode (PD).

As for the generated noises in the link, there are the thermal noise N_{th}, the optical shot noise N_{shot}, the relative intensity noise (RIN) from the laser diode (LD) N_{RIN}, and the sums of amplified spontaneous emission (ASE)-signal noise N_{ASEB} and ASE-ASE noise from the optical amplifiers N_{ASEP}. For kth radio signal, where k = 1, 2, …, K, each noise power is given by the following equations [3].

$$N_{th} = 4K_B T B_{RF,k} F_{RF} G_{RF}, \tag{4.1}$$

$$N_{shot,k} = 2e(\alpha_{PD} P_{r,k}) B_{RF,k} R_L G_{RF}, \tag{4.2}$$

$$N_{RIN,k} = (RIN)(\alpha_{PD} P_{r,k})^2 B_{RF,k} R_L G_{RF}, \tag{4.3}$$

$$N_{ASEB,k} = \left\{4\alpha_{PD}(\alpha_{PD} P_{r,k}) N_{spB} + 2(\alpha_{PD} N_{spB})^2 (B_o - f_k)\right\} B_{RF,k} R_L G_{RF}, \tag{4.4}$$

$$N_{ASEP,k} = \left\{4\alpha_{PD}(\alpha_{PD} P_{r,k}) N_{spP} + 2(\alpha_{PD} N_{spP})^2 (B_o - f_k)\right\} B_{RF,k} R_L G_{RF}, \tag{4.5}$$

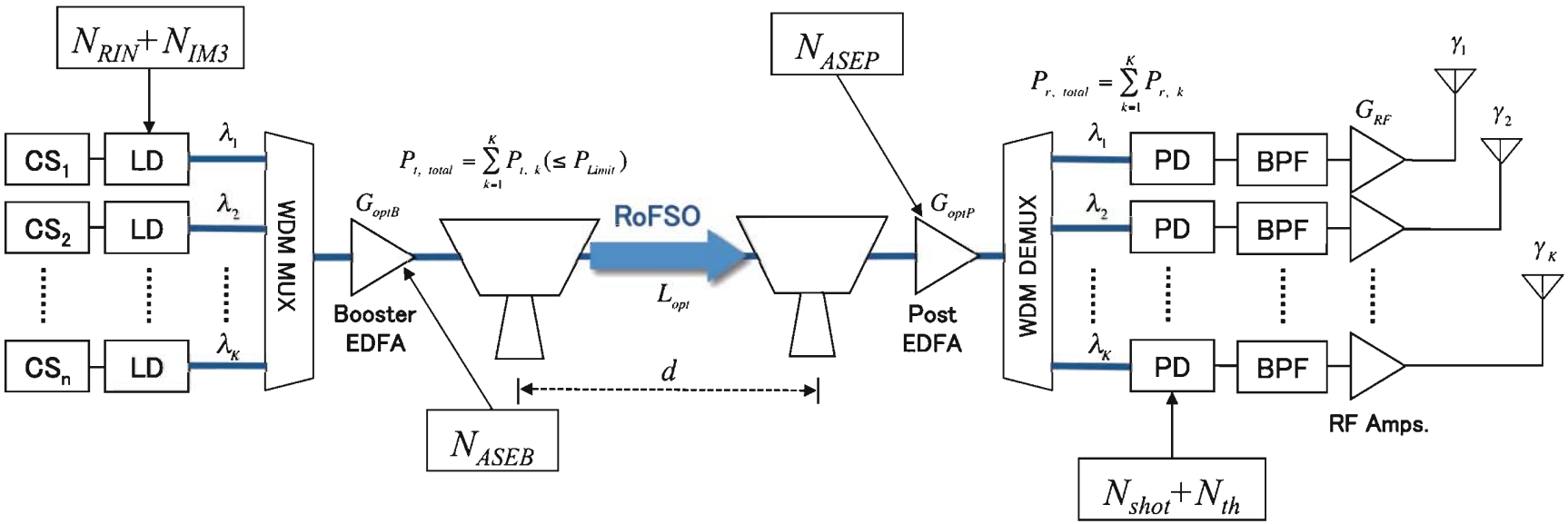

Fig. 4.1: Configuration of WDM RoFSO downlink.

where the subscript k (k = 1, 2,…, K) denotes kth RF signal. The subscripts "B" and "P" respectively denote the generated beat noises from the Booster EDFA and Post EDFA. In Eqs. (4.1) ~ (4.5), K_B, T, $B_{RF,k}$, F_{RF}, G_{RF}, e, α_{PD}, R_L, $P_{r,k}$, RIN, L_{opt}, G_{optP}, and B_o denote the Boltzmann's constant, the equivalent noise temperature, the bandwidth of kth RF signal, the noise figure (NF) of the RF Pre-Amplifier at the RoFSO receiver side, gain of the RF Pre-Amplifier at the RoFSO receiver side, the electric charge, the responsibility of the PD, the load resistance, the power of received optical signal for kth RF signal, the power spectral density (PSD) level of relative intensity noise, the optical transmission loss, and the bandwidth of the optical filter, respectively.

N_{spB} and N_{spP} are the power densities of the ASE beat noises given by

$$N_{spB} = \eta_{spB}(G_{optB} - 1)hvL_{opt}G_{optP}, \tag{4.6}$$

$$N_{spP} = \eta_{spP}(G_{optP} - 1)hv, \tag{4.7}$$

where η_{spB} and η_{spP} respectively denote the ASE coefficients of the Booster EDFA and Post EDFA, h is the Plank's constant, and v is the optical frequency. Since in general, shot noise power of ASE light is smaller than other noise power in one digit or more, it is not considered in this analysis. Shot noise of amplified optical signal is considered as noise generated from the PD.

When the LD is directly intensity modulated by multicarrier signal, the intermodulation distortion (IMD) is caused due to nonlinearity of the LD, and it may result in degradation in quality of radio signal at the RoFSO receiver side. For the sake of simplicity, we assume all the tones to be modulated with the same OMI m_k. Then, the third order intermodulation distortion (IMD3) which falls into n_kth subcarrier frequency among equally spaced N_k subcarriers is described as [3],

$$N_{IM3,k} = \frac{1}{2}\left(\frac{3}{4}a_3 m_k^3 D_2(N_k, n_k) + \frac{3}{2}a_3 m_k^3 D_3(N_k, n_k)\right)^2 \left(\alpha_{PD}P_{r,k}\right)^2 R_L G_{RF} N_k, \tag{4.8}$$

where a_3 is the third-order nonlinear coefficient of the LD. $D_2(N_k, n_k)$ and $D_3(N_k, n_k)$ represent the numbers of two-tone type and three-tone type intermodulation distortion products that influence the n_kth subcarrier given by [3]

$$D_2(N_k, n_k) = \frac{1}{2}(N_k - 2 - \frac{1}{2}(1-(-1)^{N_k})(-1)^{N_k}), \tag{4.9}$$

$$D_3(N_k, n_k) = \frac{n_k}{2}(N_k - n_k + 1) + \frac{1}{4}((N_k - 3)^2 - 5) - \frac{1}{8}(1-(-1)^{N_k})(-1)^{N_k+n_k}. \tag{4.10}$$

The received carrier power is represented as

$$C_k = \frac{1}{2}m_k^2(\alpha_{PD}P_{r,k})^2 R_L G_{RF} N_k. \tag{4.11}$$

The received carrier to noise-plus-distortion ratio (CNDR) is defined by

$$\gamma_k = \frac{C_k}{N_{RIN,\,k} + N_{shot,\,k} + N_{th} + N_{ASEB,\,k} + N_{ASEP,\,k} + N_{IM3,\,k}}. \tag{4.12}$$

4.2.2 WDM optical power allocation ratio for fixed OMIs

WDM optical power allocation ratio for fixed OMI is derived for effectively guaranteeing quality of each wireless service signal transmitted over RoFSO downlink, under total optical transmission power limitation.

Eq. (4.12) can be rewritten as a function of the received optical signal power $P_{r,\,k}$ as the following representation,

$$\gamma_k' = \frac{AP_{r,\,k}^2}{BP_{r,\,k}^2 + CP_{r,\,k} + D}, \tag{4.13}$$

where,

$$A = \frac{C_k}{P_{r,\,k}^2} = \frac{1}{2} m_k^2 \alpha_{PD}^2 R_L G_{RF} N_k, \tag{4.14}$$

$$\begin{aligned} B &= \frac{N_{RIN,\,k} + N_{IM3,\,k}}{P_{r,\,k}^2} \\ &= \alpha_{PD}^2 R_L G_{RF} \left\{ (RIN) B_{RF,\,k} + \frac{N_k}{2} \left(\frac{3}{4} a_3 m_k^3 D_2(N_k, n_k) + \frac{3}{2} a_3 m_k^3 D_3(N_k, n_k) \right)^2 \right\}, \end{aligned} \tag{4.15}$$

$$C = 2\alpha_{PD} B_{RF,\,k} R_L G_{RF} \left\{ e + 2\alpha_{PD} (N_{spB} + N_{spP}) \right\}, \tag{4.16}$$

$$D = N_{th} + 2\alpha_{PD}^2 (B_o - f_c) B_{RF,\,k} R_L G_{RF} (N_{spB}^2 + N_{spP}^2). \tag{4.17}$$

By substituting the required CNDR for kth radio signal $\gamma_{k,\,req}$, the required received optical signal power to achieve $\gamma_{k,\,req}$ is derived as,

$$P_{r,\,k,\,req} = -\frac{1}{2} \frac{C\gamma_{k\,req} \pm \sqrt{C^2 \gamma_{k\,req}^2 - 4D\gamma_{k\,req} (B\gamma_{k\,req} - A)}}{B\gamma_{k\,req} - A}. \tag{4.18}$$

Since in general, $B\gamma_{k\,req} - A < 0$, $C > 0$, and $D > 0$,

$$C\gamma_{k\,req} < \sqrt{C^2 \gamma_{k\,req}^2 - 4D\gamma_{k\,req} (B\gamma_{k\,req} - A)}. \tag{4.19}$$

Therefore, the solution of Eq (4.18) satisfying $P_{r,\,k} > 0$ is obtained as,

$$P_{r,\,k,\,req} = -\frac{1}{2} \frac{C\gamma_{k\,req} + \sqrt{C^2 \gamma_{k\,req}^2 - 4D\gamma_{k\,req} (B\gamma_{k\,req} - A)}}{B\gamma_{k\,req} - A}. \tag{4.20}$$

Eq. (20) represents the minimum received optical signal power that is required to achieve a given CNDR requirement $\gamma_{k,\,req}$ for kth radio signal for a specific L_{opt}.

For a case of K types of radio signals transmission over RoFSO link, the total required received optical signal power to achieve each required CNDR of every radio signals $\gamma_{k,\,req}$ (k = 1, 2,…, K), $P_{r,\,total,\,req}$, is derived as the sum of each required received optical signal power to achieve the given CNDR requirement on each radio signal, $P_{r,\,k,\,req}$, and obtained by

$$P_{r,\,total,\,req} = \sum_{k=1}^{K} P_{r,\,k,\,req} = P_{r,\,1,\,req} + P_{r,\,2,\,req} + \cdots + P_{r,\,K,\,req}. \tag{4.21}$$

From Eq. (21), the ratio of each required received optical signal power to total required received optical signal power is derived by

$$r_k = \frac{P_{r,\,k,\,req}}{P_{r,\,total,\,req}},\ \ k = 1,2,...,K. \tag{4.22}$$

Since the ratio between transmitted optical signal power $P_{t,\,k}$ and received optical signal power $P_{r,\,k}$ stays constant from the relation of $P_{r,\,k} = L_{opt} G_{optP} P_{t,\,k}$, Eq. (21) represents the WDM optical power allocation ratio, which maximizes tolerable optical transmission loss for K types of radio signals transmission over RoFSO link under total optical transmission power limitation. Each required WDM optical transmission power allocated by the ratio given in Eq. (4.22) is calculated by

$$P_{t,\,k,\,req} = r_k P_{t,\,total,\,req},\ \ k = 1,2,...,K. \tag{4.23}$$

In Eq. (4.23), $P_{t,\,total,\,req}$ is total required transmitted optical signal power, which is derived as the sum of each required transmitted optical signal power $P_{t,\,k,\,req}$ (k = 1, 2,…, K) in the same manner with Eq. (4.22).

Under a total optical transmission power limitation P_{Limit}, total required transmitted optical signal power to achieve required CNDR of every radio signals for $L_{opt} = L_{opt,\,Limit}$ can be expressed as,

$$P_{t,\,total,\,req}(L_{opt}) = \sum_{k=1}^{K} P_{t,\,k,\,req}(L_{opt}) = P_{Limit}, \tag{4.24}$$

where $L_{opt,\,Limit}$ is the maximum tolerable optical transmission loss. From Eq. (4.23), $L_{opt,\,Limit}$ can be derived as a function of $P_{t,\,k,\,req}$ by the following equation,

$$\begin{aligned} L_{opt,\,Limit} &= P^{-1}_{t,\,k,\,req}(r_k P_{Limit}) \\ &= -\frac{1}{2}\frac{\kappa P_{t,\,k,\,req} \pm \sqrt{(\kappa P_{t,\,k,\,req})^2 - 4\psi(\rho P^2_{t,\,k,\,req} + \xi P_{t,\,k,\,req} + \zeta)}}{\rho P^2_{t,\,k,\,req} + \xi P_{t,\,k,\,req} + \zeta}, \end{aligned} \tag{4.25}$$

where,

$$\rho = \alpha^2_{PD} G^2_{optP} R_L G_{RF} \left[\left\{ (RIN) B_{RF,\,k} + \frac{N_k}{2}\left(\frac{3}{4} a_3 m_k^3 D_2(N_k, n_k) + \frac{3}{2} a_3 m_k^3 D_3(N_k, n_k) \right)^2 \right\} \gamma_{k,\,req} - \frac{N_k}{2} m_k^2 \right], \tag{4.26}$$

$$\xi = 4\alpha^2_{PD} \gamma_{k,\,req} G^2_{optP} B_{RF,\,k} R_L G_{RF} \eta_{spB} (G_{optB} - 1) h\nu, \tag{4.27}$$

$$\zeta = 2\alpha_{PD}^2 \gamma_{k,\,req} G_{optP}^2 B_{RF,\,k} R_L G_{RF} (B_o - f_c)\left\{\eta_{spB}(G_{optB} - 1)h\nu\right\}^2, \tag{4.28}$$

$$\kappa = 2\alpha_{PD} G_{optP} \gamma_{k,\,req} B_{RF,\,k} R_L G_{RF} (e + 2\alpha_{PD} N_{spP}), \tag{4.29}$$

$$\psi = \gamma_{k,\,req}\left\{N_{th} + 2(\alpha_{PD} N_{spP})^2 (B_o - f_c) B_{RF,\,k} R_L G_{RF}\right\}. \tag{4.30}$$

Since in general, $\rho P_{t,\,k,\,req}^2 + \xi P_{t,\,k,\,req} + \zeta < 0$, $\kappa > 0$, and $\psi > 0$,

$$\kappa P_{t,\,k,\,req} < \sqrt{(\kappa P_{t,\,k,\,req})^2 - 4\psi(\rho P_{t,\,k,\,req}^2 + \xi P_{t,\,k,\,req} + \zeta)}. \tag{4.31}$$

Therefore, the maximum tolerable optical transmission loss satisfying $L_{opt,\,Limit} > 0$ is obtained as,

$$L_{opt,\,Limit} = -\frac{1}{2}\frac{\kappa P_{t,\,k,\,req} + \sqrt{(\kappa P_{t,\,k,\,req})^2 - 4\psi(\rho P_{t,\,k,\,req}^2 + \xi P_{t,\,k,\,req} + \zeta)}}{\rho P_{t,\,k,\,req}^2 + \xi P_{t,\,k,\,req} + \zeta}, \text{ (for any } k\text{).} \tag{4.32}$$

We propose the WDM optical power allocation (WOPA) method that allocating optical power to each WDM channel with the ratio given in Eq. (4.23). In the thesis, the proposed method is referred as WOPA with fixed OMIs.

4.2.3 Application to RoFSO downlink

4.2.3.1 System parameters and required CNDR

We assume four types of wireless service signals transmission over RoFSO link under the total optical transmission power limitation from Class 3A in Eye Safety regulations, that is, P_{Limit} = 500 mW. Assumed wireless services are digital television (DTV), 3rd generation (3G) cellular, WLAN IEEE 802.11g, and 802.11a, which were used in a long-term experiment of RoFSO transmission as shown in Fig. 2.15. Parameters used in calculation are summarized in Table 4.1 and 4.2. In Table 4.1, OMIs are assumed as values obtained in a long-term experiment of RoFSO transmission as shown in Fig. 2.15, at which overmodulation due to peak power of multicarrier signal was not generated.

In designing RoFSO downlink, it is most important to satisfy the regulation on quality of radio signal, such as the spectral mask and ACLR, is radiated from a remote station of RoFSO receiver side. At a receiving terminal, each wireless service signal transmitted through a radio channel has to achieve its required carrier-to-noise ratio (CNR) determined by required bit error rate (BER) and so forth. As shown in Table 4.1, when compared with required CNR at a receiving terminal, required CNDR for radio signal radiated from a remote station of RoFSO is much larger. In the thesis, we set each required CNDR as a value of CNDR guaranteeing regulation of a wireless service signal.

For DTV, the regulation on spectral mask is most strictly limit the received CNDR of RoFSO link, which is restricted by -20 dBc at offset frequency of ±2.86 MHz, -27 dBc at offset frequency of

Table 4.1: RoFSO link parameters used in numerical calculations (fixed OMIs)

Wireless services			DTV		3G WCDMA	WLAN(11g)	WLAN(11a)
			Full Segment (12+1 Segs.)	One Segment (1 Seg.)			
Carrier Frequency [GHz]		f_c	473.142857×10^{-3}		2.1	2.4	5.2
Number of Carriers (OFDM)		N	5617(ISDB-T Mode 3)		-	52	52
Signal Bandwidth [MHz]		B_{RF}	6		5 (after SS*)	16.6	16.6
Optical Wavelength [nm]		λ	1551.72		1552.72	1553.33	1554.13
ITU-T WDM Channel No.			32		31	30	29
Optical Modulation Index (OMI) [dB]		m_{total}	-5.1		-2.9	-1.58	-1.58
Optical Gain of Booster EDFA [dB]		G_{optB}	10 (Common)				
Optical Gain of Post EDFA [dB]		G_{optP}	10 (Common)				
Receiver RF Pre-Amp. Gain [dB]		G_{RF}	20 (Common)				
Noise Figure of RF Amp. [dB]		F_{RF}	5 (Common)				
Required CNDR [dB]	γ_{req}	Case I*	40		45	40	40
		Case II*	45		50	45	45

*SS : Spread spectrum
*Case I: Required CNDR set for satisfying each radio regulation on the average
*Case II: Required CNDR set for satisfying each radio regulation with a probability of 99.7% under the worst case of σ_i^2=0.1395

Table 4.2: Common parameters and physical constants

Plank's Constant	h	6.626×10^{-34}
Speed of Light [m/s]	c	3×10^{8}
Electric Charge	e	1.6×10^{-16}
Boltzmann's Constant	K_B	1.381×10^{-23}
Eye-Safety Power Limitation [W]	P_{Limit}	0.5
RIN [dB/Hz]	RIN	-140
Load Resistance [Ohm]	R_L	50
PD Responsibility [A/W]	α_{PD}	0.8
ASE Coefficient	η_{sp}	1.99053585
Optical Filter Bandwidth [GHz]	B_o	100
Equivalent Noise Temperature [K]	T	300
3rd Order Nonlinear Coefficient of LD	a_3	1×10^{-5}

±3.00 MHz, and -40 dBc at the offset frequencies of ±4.36 MHz [90]. In this thesis, under an assumption that power of RF signal transmitted from a remote station of RoFSO downlink is 0.25 W, γ_{req} is set on the basis of the regulation on spectral mask. In general, IMD3 is the maximum at the center subchannel within a signal bandwidth, and it decreases as offset frequency from the center frequency increases, while level of noise power is constant within a signal bandwidth. That is, if the received CNDR regulated in the signal bandwidth is above the ratio of out-of-band spurious emission to carrier power that is normalized in the regulation on spectral mask, the regulation on spectral mask is satisfied. Therefore, for satisfying the most restrict regulation of the regulations of spectral mask, γ_{req} for DTV is set as 40 dB.

For 3G cellular systems, the regulation on ACLR is most strictly limit the received CNDR of RoFSO link, which is restricted by -45 dBc at the offset frequencies of ±5 MHz, and -50 dBc at the offset frequencies of ±10 MHz [91]. In general, out-of-band emission power at offset frequency of ±10 MHz can be easily suppressed by a bandpass filter, but it is difficult to suppress a leakage power at the offset frequencies of ±5 MHz. From that perspective, for satisfying the regulation on ACLR at the

offset frequencies of ±5 MHz, γ_{req} for the WCDMA signal is set as 45 dB.

For WLAN 802.11g, the regulation on spectral mask is most strictly limit the received CNDR of RoFSO link, which is restricted by -20 dBc at the offset frequencies of ±11 MHz, -28 dBc at the offset frequencies of ±20 MHz, and -40 dBc at the offset frequencies of ±30 MHz [92]. Therefore, in the same manner with DTV, for satisfying the regulations of spectral mask, γ_{req} for 802.11g is set as 40 dB.

For WLAN 802.11a, the regulation on ACLR is most strictly limit the received CNDR of RoFSO link, which is restricted by -25 dBc within the band of ±9 MHz at the offset frequency of ±20 MHz, and -40 dBc within the band of ±9 MHz at the offset frequencies of ±40 MHz, for the system with bandwidth of 20 MHz [93]. Therefore, for satisfying the regulation on ACLR, γ_{req} for 802.11a is set as 40 dB.

Each required received CNDR γ_{req} for the four types of wireless service is summarized in Case I in Table 4.1. It should be noted that the setting of Case I satisfies each regulation on the average. However, since one or more regulations may be not satisfied instantly when the received optical signal power is reduced due to optical scintillation, it is necessary to design some degree of margin.

As described in Sec. 2.3, for the case of $R = 0$ and daytime, the scintillation index increases as θ increases, and then it is up to 0.1395 the maximum when $\theta \geq 30$. When the tracking gain of 6 dB [94] and the normalized Gamma distribution as a statistical model of optical scintillation are taken into consideration, by adding a margin of 2.5 dB to required received optical signal power, the probability that the regulations are not satisfied due to optical scintillation can be kept below 0.3 % for the scintillation index of 0.1395.

The margin of 2.5 dB in the received optical signal power corresponds to the margin of 5 dB in the received CNDR after optical detection. In Case II, therefore, the margin of 5 dB is added to the required received CNDR γ_{req} set in Case I in order to suppress the probability that the regulations are not satisfied below 0.3 %, even though reduction in the received optical signal power occurs due to optical scintillation.

4.2.3.2 Tolerable optical transmission loss and achievable RoFSO link distance

Under the condition that the total optical transmission power is limited by Class 3A in Eye Safety regulations, that is, P_{Limit} = 500 mW, the case that optical power is allocated to each WDM wavelength by the WOPA with fixed OMIs, and the that optical power is equally allocated to each WDM wavelength, are compared in terms of the tolerable optical transmission loss $L_{opt,\ Limit}$ and the achievable RoFSO link distance d_{Limit}. In the thesis, the conventional method of equal allocation (EA) of WDM optical power is referred as EA.

Fig. 4.2 (a) and (b) show the optical transmission loss L_{opt} versus each received CNDR of DTV, WCDMA, 802.11g, and 802.11a for the case of WOPA with fixed OMIs, for required CNDR settings of Case I and Case II in Table 4.1, respectively. The results for the case of EA with fixed OMIs are also plotted in Fig. 4.2 (a) and (b).

In Fig. 4.2 (a), it is found that for the case of EA with fixed OMIs, each required CNDR can be achieved at $L_{opt} \leq 33.3$ dB for DTV, $L_{opt} \leq 33.6$ dB for 3G, $L_{opt} \leq 36.4$ dB for 802.11g and 802.11a. Therefore, DTV dominates the tolerable optical transmission loss in RoFSO link, that is, $L_{opt,\,Limit}$ = 33.3 dB. On the other hand, when WDM optical transmission power is allocated by WDM optical power allocation ratio for required CNDR settings of Case I obtained from Eq. (4.22), $r_{DTV}:r_{3G}:r_{11g}:r_{11a}$ = 0.341:0.319:0.170:0.170, each required CNDR for every wireless services can be achieved at $L_{opt} \leq$ 34.7 dB regardless of wireless service type. For required CNDR settings of Case I, therefore, the improvement in the tolerable optical transmission loss $L_{opt,\,Limit}$ of 1.4 dB is achieved by WOPA with fixed OMIs when compared with the case of EA with fixed OMIs.

In Fig. 4.2 (b), it is found that for the case of EA with fixed OMIs, each required CNDR can be achieved at $L_{opt} \leq$ 26.9dB for DTV, $L_{opt} \leq$ 27.7dB for 3G, $L_{opt} \leq$ 31.3dB for 802.11g and 802.11a. Therefore, DTV dominates the tolerable optical transmission loss in RoFSO link, that is, $L_{opt,\,Limit}$ = 26.9 dB. On the other hand, when WDM optical transmission power is allocated by WDM optical power allocation ratio for required CNDR settings of Case II obtained from Eq. (4.22), $r_{DTV}:r_{3G}:r_{11g}:r_{11a}$ = 0.382:0.330:0.144:0.144, each required CNDR for every wireless services can be achieved at $L_{opt} \leq$ 29.0 dB regardless of wireless service type. For required CNDR settings of Case II, therefore, the improvement in the tolerable optical transmission loss $L_{opt,\,Limit}$ of 2.1 dB is achieved by WOPA with fixed OMIs when compared with the case of EA with fixed OMIs.

Next, using Eq. (2.20) the approximate expression of optical transmission loss, the two methods are compared in terms of the achievable RoFSO link distance.

Fig. 4.3 (a) and (b) show the optical propagation distance, that is, RoFSO link distance d versus each received CNDR of DTV, WCDMA, 802.11g, and 802.11a for the case of WDM optical power allocated by WOPA with fixed OMIs, for required CNDR settings of Case I and Case II, respectively. The results for the case of EA with fixed OMIs are also plotted in Fig. 4.3 (a) and (b).

In Fig. 4.3 (a), it is found that for the case of EA with fixed OMIs, each required CNDR can be achieved at $d \leq 2.47$ km for DTV, $d \leq 2.52$ km for 3G, $d \leq 2.80$ km for 802.11g and 802.11a. Therefore, DTV dominates the achievable RoFSO link distance, that is, d_{Limit} = 2.47 km. On the other hand, when WDM optical transmission power is allocated by WOPA with fixed OMIs, each required CNDR for every wireless services can be achieved at $d \leq 2.68$ km regardless of wireless service type. For required CNDR settings of Case I, therefore, the improvement in the achievable RoFSO link distance d of 0.21 km is achieved by WOPA with fixed OMIs when compared with the case of EA

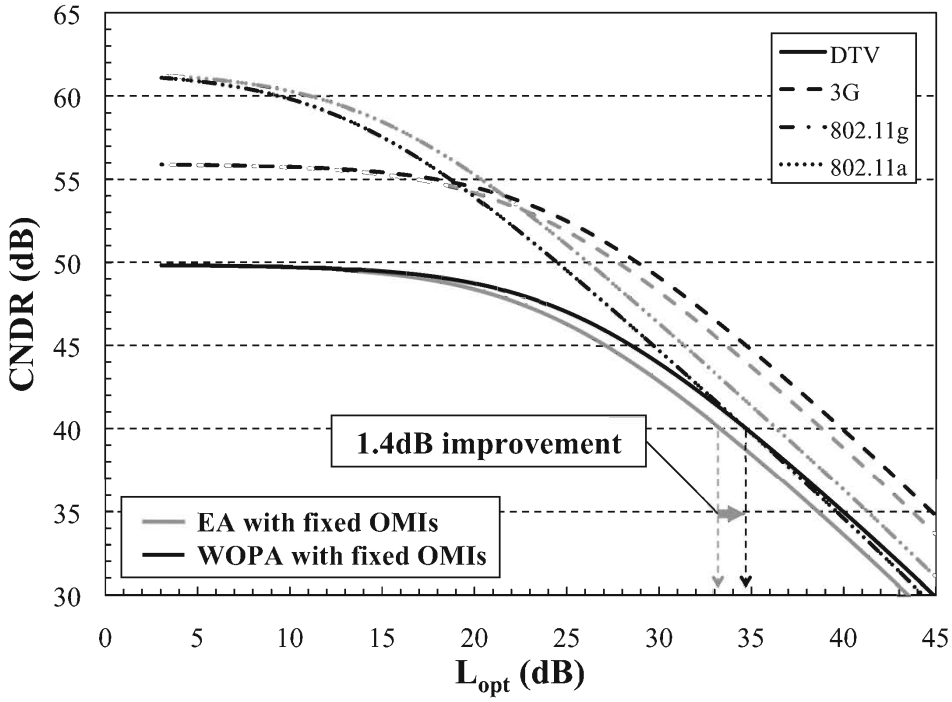

(a)

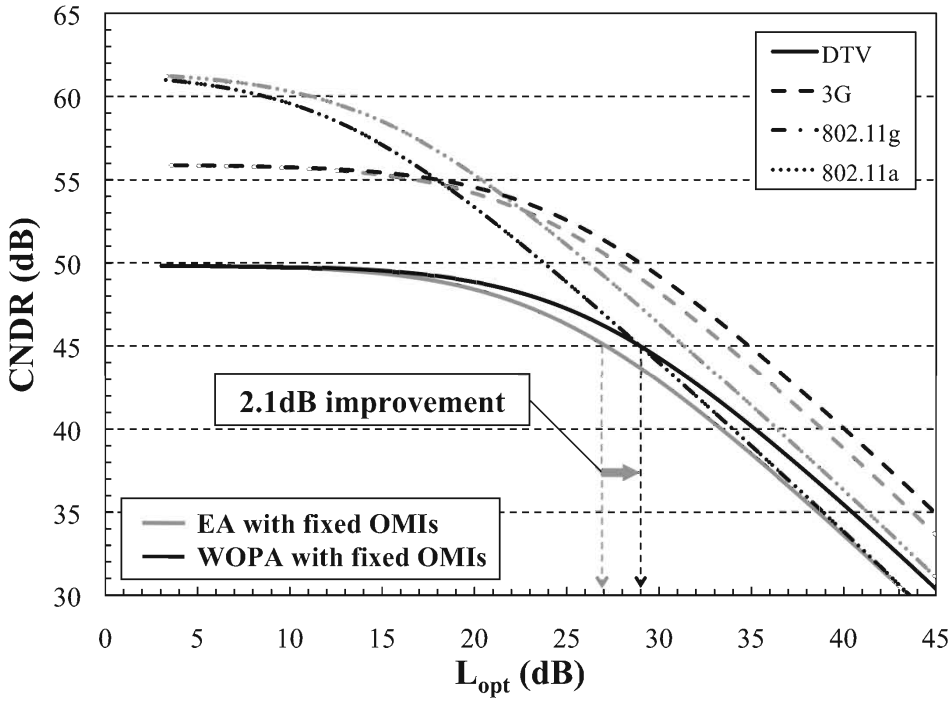

(b)

Fig. 4.2: Optical transmission loss L_{opt} versus CNDR characteristics for EA with fixed OMIs and WOPA with fixed OMIs for (a) Case I and (b) Case II.

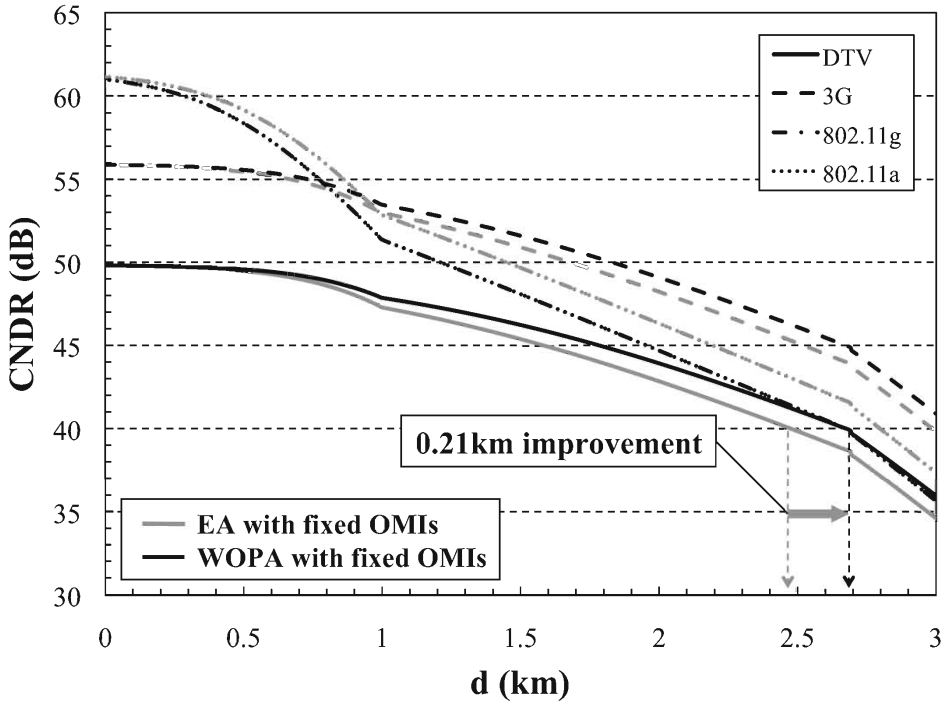

(a)

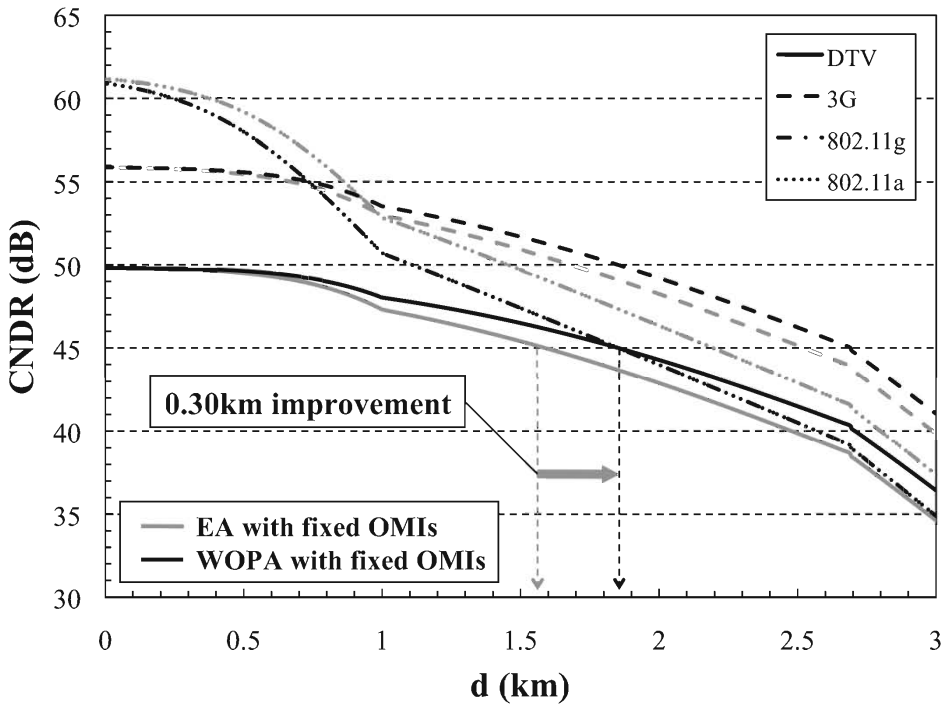

(b)

Fig. 4.3: RoFSO link distance *d* versus CNDR characteristics for EA with fixed OMIs and WOPA with fixed OMIs for (a) Case I and (b) Case II.

with fixed OMIs.

In Fig. 4.3 (b), it is found that for the case of EA with fixed OMIs, each required CNDR can be achieved at $d \leq 1.57$ km for DTV, $d \leq 1.68$ km for 3G, $d \leq 2.19$ km for 802.11g and 802.11a. Therefore, DTV dominates the achievable RoFSO link distance, that is, $d_{Limit} = 1.57$ km. On the other hand, when WDM optical transmission power is allocated by WOPA with fixed OMIs, each required CNDR for every wireless services can be achieved at $d \leq 1.87$ km regardless of wireless service type. For required CNDR settings of Case II, therefore, the improvement in the achievable RoFSO link distance d of 0.30 km is achieved by WOPA with fixed OMIs when compared with the case of EA with fixed OMIs.

Improvement in the number of transmittable wireless service signals also can be achieved by WOPA with fixed OMIs for a specific RoFSO link distance. For example, for required CNDR settings of Case II, when WDM optical power is equally allocated to each wireless service, DTV cannot be transmitted over a RoFSO link with $d > 1.57$ km, thus, the transmittable wireless services are restricted by three types of wireless services, 3G, 802.11g, and 802.11a. Moreover, In a RoFSO link with $d > 1.68$ km, DTV and 3G cannot be transmitted over the link, thus, the transmittable wireless services are seriously restricted by only two types of wireless services, 802.11g and 802.11a. On the other hand, all wireless services are transmittable in a RoFSO $d \leq 1.87$ km when the WOPA with fixed OMIs is adopted in the link design.

4.3 WDM optical power allocation for optimum OMIs

In this section, WDM optical allocation method for optimum OMIs of heterogeneous radio signals is proposed. The validity of the proposed method is shown, by comparing with the case that WDM optical power is equally allocated for optimum OMIs, in the same manner with Sec. 4.3.

4.3.1 WDM optical power allocation ratio for optimum OMIs

WDM optical power allocation ratio for optimum OMI is derived for effectively guaranteeing quality of each wireless service signal transmitted over RoFSO downlink, under total optical transmission power limitation.

The optimum OMI per subcarrier $m_{k,\,opt}$ for kth wireless service signal which results in maximum received CNDR can be derived by $d\gamma_k / dm_k = 0$ as

$$m_{k,\,opt} = \left\{ \frac{N_{RIN,\,k} + N_{shot,\,k} + N_{th} + N_{ASEB,\,k} + N_{ASEP,\,k}}{\left(\frac{3}{4}a_3 D_2(N_k, n_k) + \frac{3}{2}a_3 D_2(N_k, n_k)\right)^2 (\alpha_{PD} P_{r,\,k})^2 R_L G_{RF} N_k} \right\}^{1/6}. \tag{4.33}$$

When $m_k = m_{k,\,opt}$, the CNDR at output of RoFSO link for *k*th wireless service signal can be represented as

$$\begin{aligned} \gamma_k\big|_{m_k = m_{k,\,opt}} &= \left. \frac{C_k}{N_{RIN,\,k} + N_{shot,\,k} + N_{th} + N_{ASEB,\,k} + N_{ASEP,\,k} + N_{IM3,\,k}} \right|_{m_k = m_{k,\,opt}} \\ &= \frac{C_k\big|_{m_k = m_{k,\,opt}}}{N_{RIN,\,k} + N_{shot,\,k} + N_{th} + N_{ASEB,\,k} + N_{ASEP,\,k} + N_{IM3,\,k}\big|_{m_k = m_{k,\,opt}}}, \end{aligned} \tag{4.34}$$

where

$$\begin{aligned} C_k\big|_{m_k = m_{k,\,opt}} &= \frac{1}{2} m_{k,\,opt}^2 (\alpha_{PD} P_{r,\,k})^2 R_L G_{RF} N_k \\ &= \frac{1}{2} \frac{(N_{RIN,\,k} + N_{shot,\,k} + N_{th} + N_{ASEB,\,k} + N_{ASEP,\,k})^{1/3}}{\left(\frac{3}{4}a_3 D_2(N_k, n_k) + \frac{3}{2}a_3 D_3(N_k, n_k)\right)^{2/3}} (\alpha_{PD} P_{r,\,k})^{4/3} (R_L G_{RF} N_k)^{2/3}, \end{aligned} \tag{4.35}$$

$$\begin{aligned} N_{IM3,\,k}\big|_{m_k = m_{k,\,opt}} &= \frac{1}{2}\left(\frac{3}{4}a_3 m_{k,\,opt}^3 D_2(N_k, n_k) + \frac{3}{2}a_3 m_{k,\,opt}^3 D_3(N_k, n_k)\right)^2 (\alpha_{PD} P_{r,\,k})^2 R_L G_{RF} N_k \\ &= \frac{1}{2}(N_{RIN,\,k} + N_{shot,\,k} + N_{th} + N_{ASEB,\,k} + N_{ASEP,\,k}) \end{aligned}. \tag{4.36}$$

From Eq. (4.36), it is found that $N_{IM3,\,k}$ is one half of total noise power when $m_k = m_{k,\,opt}$.

By substituting Eqs. (4.35) and (4.36) into Eq. (4.34), the CNDR at $m_k = m_{k,\,opt}$ can be derived as follow equation,

$$\begin{aligned} \gamma_k\big|_{m_k = m_{k,\,opt}} &= \frac{1}{3\left\{\frac{3}{4}a_3 D_2(N_k, n_k) + \frac{3}{2}a_3 D_3(N_k, n_k)\right\}^{2/3}} \\ &\cdot \frac{(R_L G_{RF} N_k)^{2/3} (\alpha_{PD} P_{r,\,k})^{4/3}}{(N_{RIN,\,k} + N_{shot,\,k} + N_{th} + N_{ASEB,\,k} + N_{ASEP,\,k})^{2/3}} \end{aligned}. \tag{4.37}$$

Eq. (4.37) represents the maximum CNDR for any received optical signal power $P_{r,\,k} = P_{t,\,k} L_{opt} G_{optP}$. It can be rewritten as a function of $P_{r,\,k}$ as following representation,

$$\gamma_k' = \frac{A P_{r,\,k}^2}{B P_{r,\,k}^2 + C P_{r,\,k} + D}, \tag{4.38}$$

where *A*, *B*, *C*, and *D* are newly given by

$$A = \alpha_{PD}^2 R_L G_{RF} N_k, \tag{4.39}$$

$$B = (RIN)\alpha_{PD}^2 R_L G_{RF} B_{RF}, \tag{4.40}$$

$$C = 2\alpha_{PD} B_{RF} R_L G_{RF} \left\{ e + 2\alpha_{PD}(N_{spB} + N_{spP}) \right\}, \tag{4.41}$$

$$D = N_{th} + 2\alpha_{PD}^2 (B_o - f_c) B_{RF} R_L G_{RF} (N_{spB}^2 + N_{spP}^2), \tag{4.42}$$

$$\gamma_k' = 3\sqrt{3}\left\{ \frac{3}{4} a_3 D_2(N_k, n_k) + \frac{3}{2} a_3 D_3(N_k, n_k) \right\} \gamma_k^{3/2} \Big|_{m_k = m_{k,\,opt}}. \tag{4.43}$$

It should be noted that A, B, C, and D used in Eqs. (4.38)~(4.42) are different with them given in Eqs. (4.38)~(4.42).

By substituting $\gamma_k \big|_{m_k = m_{k,\,opt}} = \gamma_{k,\,req}$, where $\gamma_{k,\,req}$ is the required CDNR of kth wireless service, the required received optical signal power to achieve $\gamma_{k,\,req}$ is derived as

$$P_{r,\,k,\,req} \Big|_{m_k = m_{k,\,opt}} = \frac{C\gamma_{k,\,req}' \pm \sqrt{C^2 (\gamma_{k,\,req}')^2 - 4D\gamma_{k,\,req}' (B\gamma_{k,\,req}' - A)}}{-2(B\gamma_{k,\,req}' - A)}, \tag{4.44}$$

where

$$\gamma_{k,\,req}' = 3\sqrt{3}\left\{ \frac{3}{4} a_3 D_2(N_k, n_k) + \frac{3}{2} a_3 D_3(N_k, n_k) \right\} \gamma_{k,\,req}^{3/2}. \tag{4.45}$$

In general, $B\gamma_{k,\,req}' - A < 0$, $C > 0$, and $D > 0$, thus the solution of Eq. (4.44) which satisfies $P_{r,\,k} > 0$ is obtained as

$$P_{r,\,k,\,req} \Big|_{m_k = m_{k,\,opt}} = \frac{C\gamma_{k,\,req}' + \sqrt{C^2 (\gamma_{k,\,req}')^2 - 4D\gamma_{k,\,req}' (B\gamma_{k,\,req}' - A)}}{-2(B\gamma_{k,\,req}' - A)}. \tag{4.46}$$

Eq. (26) represents the minimum received optical signal power required to achieve the given CNDR requirement at the output of RoFSO link for kth wireless service signal for a specific L_{opt}. In other word, various combinations of $P_{r,\,k}$ and m_k exist which achieve the required CNDR, and the value of $P_{r,\,k}$ derived by Eq. (4.46) is the smallest among them because it is the value at $m_k = m_{k,\,opt}$.

Therefore, under total optical transmission limitation P_{Limit}, the minimum total optical transmission power to achieve each required CNDR of every wireless services for $L_{opt} = L_{opt,\,Limit}$ can be expressed as

$$P_{t,\,total,\,req} = \sum_{k=1}^{K} P_{t,\,k,\,req} = \sum_{k=1}^{K} \frac{P_{r,\,k,\,req} \Big|_{m_k = m_{k,\,opt}}}{L_{opt,\,Limit} G_{optP}} = P_{Limit}, \tag{4.47}$$

where $L_{opt,\,Limit}$ is the maximum tolerable L_{opt} for guaranteeing each required CNDR of every wireless services with combinations of the OMI and optical transmission power. When $L_{opt} > L_{opt,\,Limit}$, it

becomes that $P_{r,k} < P_{r,k,req}\big|_{m_k=m_{k,opt}}$, thus, it is impossible to achieve the required CNDR with any OMI for that received optical power level. Since the ratio between $P_{r,k}$ and $P_{t,k}$ stays constant, at that time the ratio of WDM optical transmission power can be derived by

$$r_k = \frac{P_{r,k,req}\big|_{m_k=m_{k,opt}}}{P_{r,total,req}}. \tag{4.48}$$

Therefore, WDM optical transmission power allocated per a wavelength by the ratio given in Eq. (4.48) is given by

$$P_{t,k,req} = r_k P_{Limit}, \quad k = 1,2,...,K \tag{4.49}$$

From Eq. (4.47), $L_{opt,Limit}$ can be derived by

$$L_{opt,Limit} = \frac{1}{P_{Limit} G_{optP}} \sum_{k=1}^{K} P_{r,k,req}\big|_{m_k=m_{k,opt}} (L_{opt,Limit}). \tag{4.50}$$

For optimum OMI, we propose the WDM optical power allocation (WOPA) method that allocating optical power to each WDM channel with the ratio given in Eq. (4.48). In the thesis, the proposed method is referred as WOPA with optimum OMIs.

4.3.2 Application to RoFSO downlink

4.3.2.1 System parameters and required CNDR

Fixed OMIs are adopted to design RoFSO downlink in Sec. 4.2.3, which are obtained from a long-term experiment of RoFSO transmission as shown in Fig. 2.15. On the other hand, in this section, the optimum OMI $m_{k,opt}$ for each wireless service signal is assumed as shown in Table 4.3, which can be obtained from Eq. (4.33). The optimum OMI $m_{k,opt}$ is a function of received optical signal power $P_{r,k}$, as shown in Eq. (4.33). Because $P_{r,k} = P_{t,k} L_{opt} G_{optP}$, $m_{k,opt}$ is also a function of the optical transmission loss L_{opt}, that is, RoFSO link distance d. Therefore, $m_{k,opt}$ changes depending on L_{opt} or d. It should be noted that the results that will be presented in Sec. 4.4.2.2 is based on the optimum OMI for every $P_{r,k}$, not a constant optimum value for a specific L_{opt} or d.

The other parameters including required CNDR summarized in Table 4.3 are equal with those in Table 4.1.

4.3.2.2 Tolerable optical transmission loss and achievable RoFSO link distance

Under the condition that the total optical transmission power is limited by Class 3A in Eye Safety regulations, that is, P_{Limit} = 500 mW, the case that optical power is allocated to each WDM wavelength by WOPA with optimum OMIs, and the case of EA with optimum OMIs, are compared in the same

Table 4.3: RoFSO link parameters used in numerical calculations (Optimum OMIs)

Wireless services			DTV		3G WCDMA	WLAN(11g)	WLAN(11a)
			Full Segment (12+1 Segs.)	One Segment (1 Seg.)			
Carrier Frequency [GHz]	f_c		473.142857×10^{-3}		2.1	2.4	5.2
Number of Carriers (OFDM)	N		5617(ISDB-T Mode 3)		-	52	52
Signal Bandwidth [MHz]	B_{RF}		6		5(after SS*)	16.6	16.6
Optical Wavelength [nm]	λ		1551.72		1552.72	1553.33	1554.13
ITU-T WDM Channel No.			32		31	30	29
Optical Modulation Index (OMI)	m_{opt}		Optimum OMI value for each type of wireless services				
Optical Gain of Booster EDFA [dB]	G_{optB}		10 (Common)				
Optical Gain of Post EDFA [dB]	G_{optP}		10 (Common)				
Receiver RF Pre-Amp. Gain [dB]	G_{RF}		20 (Common)				
Noise Figure of RF Amp. [dB]	F_{RF}		5 (Common)				
Required CNDR [dB]	γ_{req}	Case I*	40		45	40	40
		Case II*	45		50	45	45

*SS: Spread spectrum
*Case I: Required CNDR set for satisfying each radio regulation on the average
*Case II: Required CNDR set for satisfying each radio regulation with a probability of 99.7% under the worst case of σ_i^2=0.1395

manner with Sec. 4.2.3.2.

Fig. 4.4 (a) and (b) show the optical transmission loss L_{opt} versus each received CNDR of DTV, WCDMA, 802.11g, and 802.11a for the case of WDM optical power allocated by WOPA with optimum OMIs, for required CNDR settings of Case I and Case II, respectively. The results for the case of the EA with optimum OMIs are also plotted in Fig. 4.4 (a) and (b).

In Fig. 4.4 (a), it is found that for the case of the EA with optimum OMIs, each required CNDR can be achieved at $L_{opt} \leq 34.8$ dB for DTV, $L_{opt} \leq 35.5$ dB for 3G, $L_{opt} \leq 49.8$ dB for802.11g and 802.11a. Therefore, DTV dominates the tolerable optical transmission loss in RoFSO link, that is, $L_{opt,\,Limit} = 34.8$ dB. On the other hand, when WDM optical transmission power is allocated by WDM optical power allocation ratio for required CNDR settings of Case I obtained from Eq. (4.48), $r_{DTV} : r_{3G} : r_{11g} : r_{11a} = 0.527:0.439:0.017:0.017$, each required CNDR for every wireless services can be achieved at $L_{opt} \leq 38.1$ dB regardless of wireless service type. For required CNDR settings of Case I, therefore, the improvement in the tolerable optical transmission loss $L_{opt,\,Limit}$ of 3.3 dB is achieved by WOPA with optimum OMIs when compared with the case of EA with optimum OMIs.

In Fig. 4.4 (b), it is found that for the case of EA with optimum OMIs, each required CNDR can be achieved at $L_{opt} \leq 27.0$ dB for DTV, $L_{opt} \leq 27.9$ dB for 3G, $L_{opt} \leq 43.2$ dB for 802.11g and 802.11a. Therefore, DTV dominates the tolerable optical transmission loss in RoFSO link, that is, $L_{opt,\,Limit} = 27.0$ dB. On the other hand, when WDM optical transmission power is allocated by WDM optical power allocation ratio for required CNDR settings of Case II obtained from Eq. (4.48), $r_{DTV} : r_{3G} : r_{11g} : r_{11a} = 0.534:0.440:0.013:0.013$, each required CNDR for every wireless services can be achieved at $L_{opt} \leq 30.5$ dB regardless of wireless service type. For required CNDR settings of Case II, therefore, the improvement in the tolerable optical transmission loss $L_{opt,\,Limit}$ of 3.5 dB is achieved by WOPA with optimum OMIs when compared with the case of EA with optimum OMIs.

Next, Using Eq. (2.20) the approximate expression of optical transmission loss, the two methods are compared in terms of the achievable RoFSO link distance.

Fig. 4.5 (a) and (b) show the optical propagation distance, that is, RoFSO link distance d versus each received CNDR of DTV, WCDMA, 802.11g, and 802.11a for the case of WDM optical power allocated by WOPA with optimum OMIs, for required CNDR settings of Case I and Case II, respectively. The results for the case of EA with optimum OMIs are also plotted in Fig. 4.5 (a) and (b).

In Fig. 4.5 (a), it is found that for the case of EA with optimum OMIs, each required CNDR can be achieved at $d \leq 2.68$ km for DTV, $d \leq 2.73$ km for 3G, $d \leq 3.83$ km for 802.11g and 802.11a. Therefore, DTV dominates the achievable RoFSO link distance, that is, $d_{Limit} = 2.68$ km. On the other hand, when WDM optical transmission power is allocated by WOPA with optimum OMIs, each required CNDR for every wireless services can be achieved at $d \leq 2.92$ km regardless of wireless service type. For required CNDR settings of Case I, therefore, the improvement in the achievable

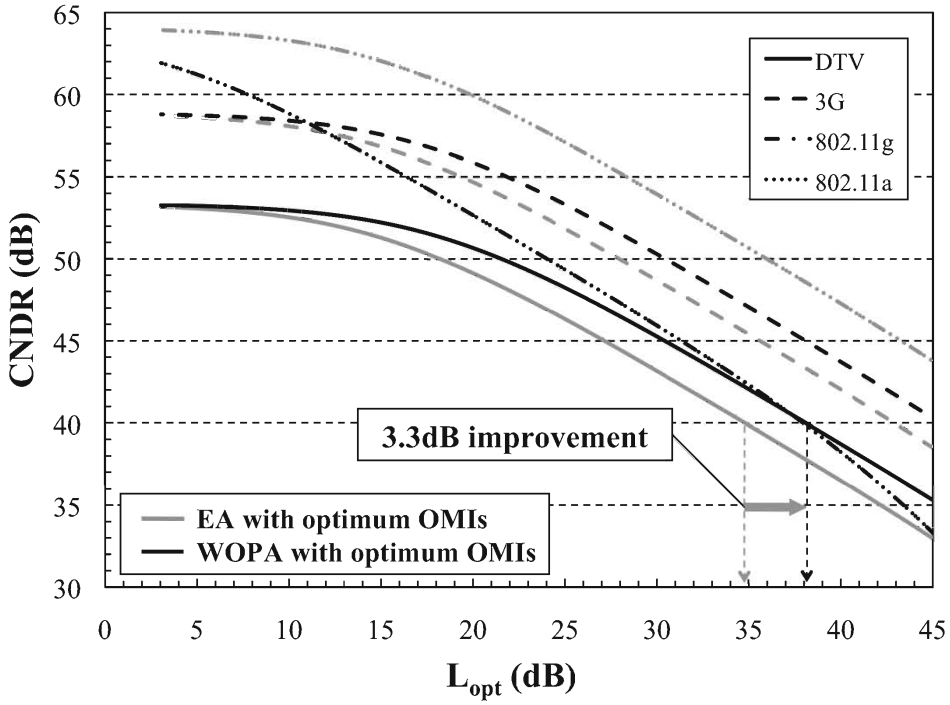

(a)

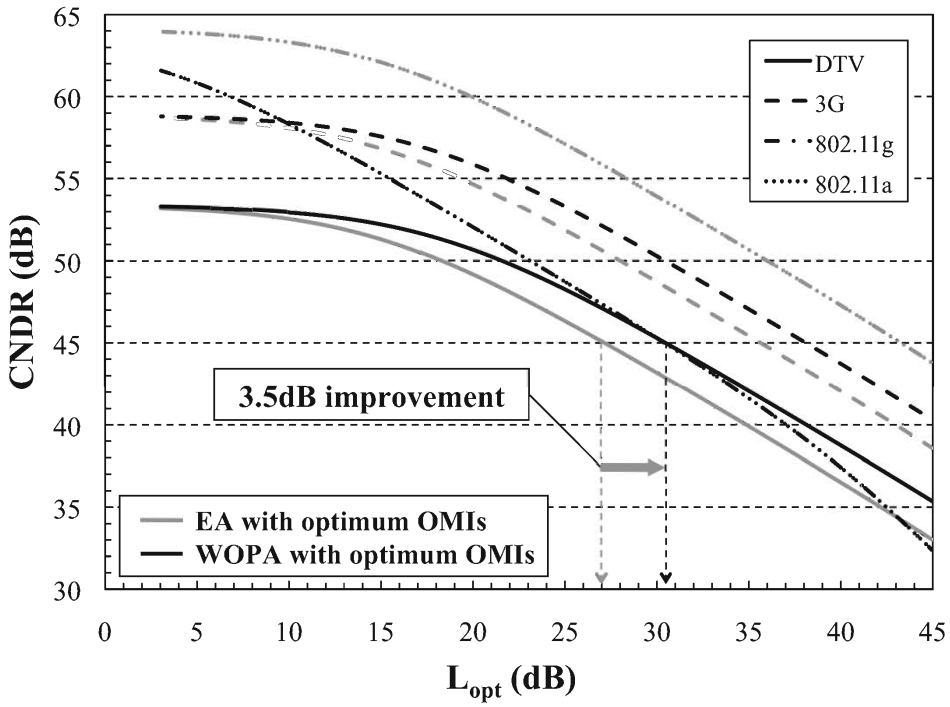

(b)

Fig. 4.4: Optical transmission loss L_{opt} versus CNDR characteristics for EA with optimum OMIs and WOPA with optimum OMIs for (a) Case I and (b) Case II.

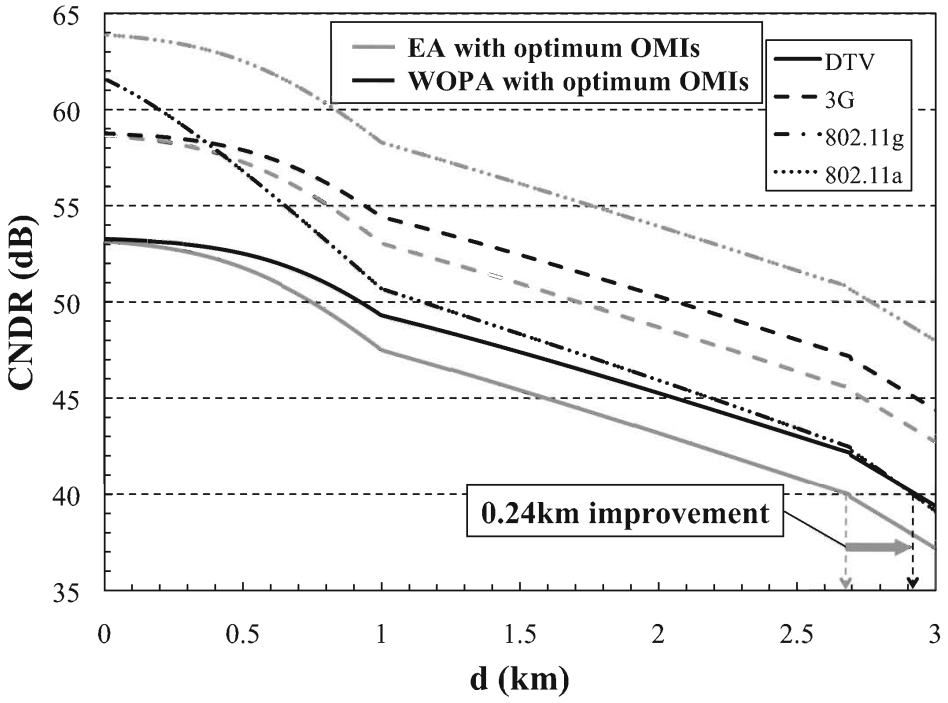

(a)

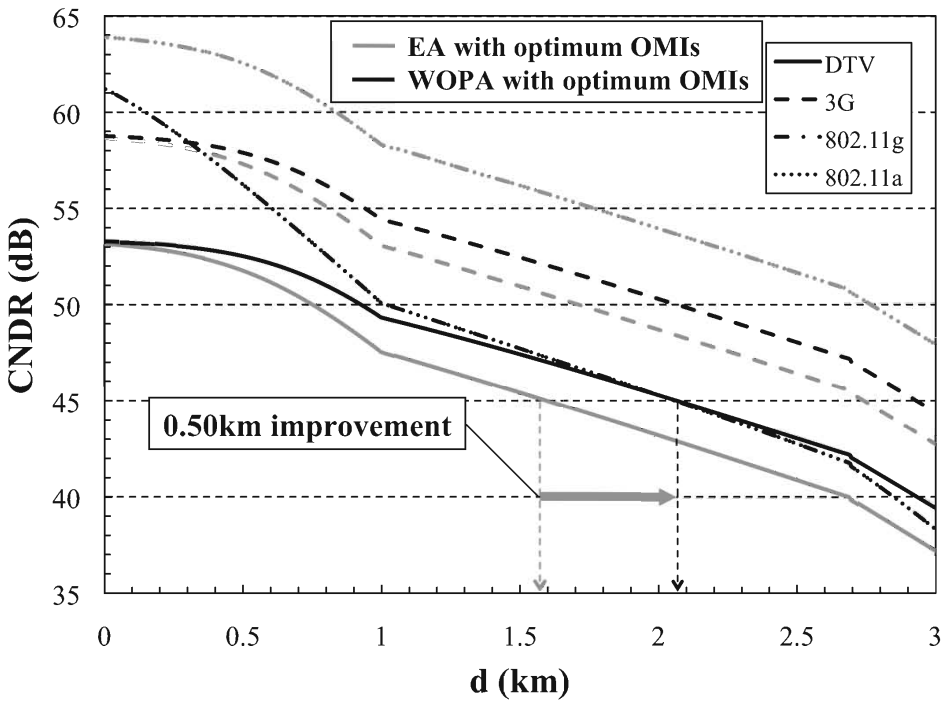

(b)

Fig. 4.5: RoFSO link distance *d* versus CNDR characteristics for EA with optimum OMIs and WOPA with optimum OMIs for (a) Case I and (b) Case II.

RoFSO link distance d_{Limit} of 0.24 km is achieved by WOPA with optimum OMIs when compared with the case of EA with optimum OMIs.

In Fig. 4.5 (b), it is found that for the case of EA with optimum OMIs, each required CNDR can be achieved at $d \leq 1.57$ km for DTV, $d \leq 1.71$ km for 3G, $d \leq 3.32$ km for 802.11g and 802.11a. Therefore, DTV dominates the achievable RoFSO link distance, that is, $d_{Limit} = 1.57$ km. On the other hand, when WDM optical transmission power is allocated by WOPA with optimum OMIs, each required CNDR for every wireless services can be achieved at $d \leq 2.07$ km regardless of wireless service type. For required CNDR settings of Case II, therefore, the improvement in the achievable RoFSO link distance d_{Limit} of 0.50 km is achieved by WOPA with optimum OMIs when compared with the case of EA with optimum OMIs.

In the same manner with Sec. 4.2.3.2, improvement in the number of transmittable wireless service signals also can be achieved by WOPA with optimum OMIs for a specific RoFSO link distance. For example, for required CNDR settings of Case II, when WDM optical power is equally allocated to each wireless service with the optimum OMI, DTV cannot be transmitted over a RoFSO link with $d >$ 1.57 km, thus, the transmittable wireless services are restricted by three types of wireless services, 3G, 802.11g, and 802.11a. Moreover, In a RoFSO link with $d > 1.71$ km, DTV and 3G cannot be transmitted over the link, thus, the transmittable wireless services are seriously restricted by only two types of wireless services, 802.11g and 802.11a. On the other hand, all wireless services are transmittable in a RoFSO $d \leq 2.07$ km when the WOPA with optimum OMIs is adopted in the link design.

4.4 Concluding remarks

As an optimal design method of RoFSO system, we have proposed WDM optical power allocation method under total transmission power limitation by Eye-Safety regulation, to effectively guarantee each requirement of radio signal at a remote station of RoFSO downlink. For conventional WDM optical allocation methods of EA with fixed OMIs and EA with optimum OMIs, WOPA with fixed OMI and WOPA with optimum OMI have been respectively proposed, and those four types of WDM optical allocation methods were examined with some discussion.

For Case I in which each required CNDR of radio signals was set as a value of CNDR guaranteeing the most severe regulation on quality of radio signal on the average, EA with fixed OMIs and EA with optimum OMIs achieve the tolerable optical transmission losses, $L_{opt,\ Limit}$ of 33.3 dB and 34.8 dB, respectively. On the other hand, WOPA with fixed OMIs and WOPA with optimum OMIs improve $L_{opt,\ Limit}$ up to of 34.7 dB and 38.1 dB, respectively. In terms of the achievable RoFSO link distance

d_{Limit}, while EA with fixed OMIs and EA with optimum OMIs respectively achieve d_{Limit} of 2.47 km and 2.68 km, WOPA with fixed OMIs and WOPA with optimum OMIs respectively improve d_{Limit} up to of 2.68 km and 2.92 km.

For Case II in which each required CNDR of wireless service signals was set as a value of CNDR keeping the probability that the regulations are not satisfied due to optical scintillation below 0.3 %, even though $\theta \geq 30$, daytime in a clear sunny day, EA with fixed OMIs and EA with optimum OMIs achieve $L_{opt,\ Limit}$ of 26.9 dB and 27.0 dB, respectively. On the other hand, WOPA with fixed OMIs and WOPA with optimum OMIs improve $L_{opt,\ Limit}$ up to of 29.0 dB and 30.5 dB, respectively. In terms of the achievable RoFSO link distance d_{Limit}, while EA with fixed OMIs and EA with optimum OMIs achieve d_{Limit} of 1.57 km, WOPA with fixed OMIs and WOPA with optimum OMIs respectively improve d_{Limit} up to of 1.87 km and 2.07 km.

It can be concluded that the best performance of RoFSO link can be achieved by WOPA with optimum OMIs among the four types of WDM optical allocation methods, and we can realize longer RoFSO link using WOPA with optimum OMIs.

Chapter 5

Conclusions

This thesis contributed to design and performance evaluation of RoFSO communication system for radio signal transmission. Firstly, RoFSO channel models on the power spectral density (PSD) of optical scintillation, the scintillation index, and the optical transmission loss were proposed for design and performance evaluation of RoFSO system. Dependencies of the PSD and the scintillation index of optical scintillation on the channel conditions like time zone, temperature, and rainfall intensity were investigated based on a long-term experimental data. Based on the proposed optical transmission loss, a RoFSO link margin was estimated as a simple function of link distance. Secondly, the two-dimensional statistical model of optical scintillation was proposed. Using the model, the effect of optical scintillation on the throughput performance of WLAN signal was evaluated and discussed in free space radio channel. Moreover, the evaluations under the radio communication environments like office and corridor were also conducted, and effects of optical scintillation in RoFSO channel and shadowing in radio channel were discussed. Thirdly, as an optimal design method of RoFSO system, WDM optical power allocation method was proposed, under total transmission power limitation by Eye-safety regulation. A ratio of WDM optical power allocation for effectively guaranteeing each regulation on radio signal quality at a remote station of RoFSO downlink was theoretically derived. Validity of the proposed method was shown through the comparison with the conventional method of the equal WDM optical power allocation.

The significant results obtained in this work can be summarized as follows:

(1) Through the investigation on dependencies of the cutoff frequency, the spectral slope, and the scintillation index, it was newly found that in general, optical scintillation with higher fluctuation speed occurs in a rainy day than a clear sunny day, higher the temperature θ, slower the optical scintillation is at night in a clear day, the spectral slope is approximately f^{-2} regardless of time zone, temperature, and rainfall intensity, strength of optical scintillation decreases as temperature increases at night in a clear day, while at daytime, strength of optical scintillation increases as temperature increases on the whole.

(2) Through the analysis of optical transmission loss in RoFSO system, it was newly found that for a RoFSO system with link distance of around 1km, sufficient margin for scintillation loss taking very strong turbulence into consideration should be designed, and it is enough for the atmospheric attenuation loss, while for a RoFSO system with relatively long link distance *d* of more than 2km, it is enough to consider margin design for atmospheric attenuation loss.

(3) Through the evaluation of effect of optical scintillation, it was newly found that for same strength of optical scintillation, average throughputs of 802.11a during one period are same even for optical scintillation with rapid fluctuation speed, and degradation in throughput performance due to scintillation is considerably depending on a radio path length, or received RF signal power.

(4) By comparing the effects of optical scintillation in RoFSO channel and shadowing in radio channel, it was newly found that under radio communication environments like office and corridor, degradation due to scintillation is less than that due to shadowing, but degradation due to shadowing is enhanced, when it occurs simultaneously with scintillation, moreover, degradation due to scintillation more enhanced when shadowing with a large variation width occurs simultaneously.

(5) It was clarified that the proposed WDM optical power allocation method with optimum OMIs can improve the tolerable optical transmission loss and the achievable RoFSO link distance, compared with the conventional method of the equal WDM power allocation. Using the proposed model, we can realize a longer RoFSO link.

The radio on free space optical system will become more and more important key technology for infrastructure of future wireless communication system in which the flexibility and universality to various kinds of wireless services are significant. The RoFSO systems treated in the thesis will become one of the promising candidates for extending broadband wireless environment easily, rapidly, and cost effectively. The author wishes that the results presented in the thesis contribute toward the technological development of future radio on free space optical communication networks.

Bibliography

[1] S. Komaki, “Proposal of radio highway network for future multimedia personal wireless communication,” in Proc. IEEE ICPWC 94, pp. 204-208, Aug. 1994.

[2] K. Tsukamoto, S. Komaki, and M. Matsumoto, “Development project of radio on free space optics,” Proc. SPIE, Broadband Access Communication Technologies II, Vol. 6776, pp. 677606_1-8, Jan. 2007.

[3] H. Al-Raweshidy and Shozo Komaki, Radio over fiber technologies for mobile communications networks, 1st Ed., Artech House, Norwood, MA, 2002.

[4] W. S. C. Chang, RF photonic technology in optical fiber links, 1st Ed., Cambridge Univ. Press, Cambridge, UK, 2002.

[5] C. H. Cox III, Analog optical links: theory and practice, 1st Ed., Cambridge Univ. Press, Massachusetts, 2004.

[6] S. Hunziker and W. Baechtold, “Cellular remote antenna feeding: optical fiber or coaxial cable?,” Electronics Letters, Vol. 34, No. 11, pp. 1038-1040, 1988.

[7] H. Willebrand and B. Ghuman, Free space optics: enabling optical connectivity in today’s networks, Sams Publishing, Indianapolis, IN, 2002.

[8] V. W. S. Chan, “Free-space optical communications,” J. Lightwave Technol., Vol. 24, No. 12, pp. 4750-4762, 2006.

[9] O. Bouchet, H. Sizun, C. Boisrobert, F. de Fornel, and P. N. Favennec, Free-space optics: propagation and communication, Wiley-ISTE, London, UK, 2006.

[10] D. Kedar and S. Arnon, “Urban optical wireless communication networks: the main challenges and possible solutions,” IEEE Commun. Mag., Vol. 42, No. 5, pp. S2-S7, May 2004.

[11] Report ITU-R F.2106, “Fixed service applications using free-space optical links,” ITU-R, Geneva, Swiss, 2007.

[12] A. K. Majumdar and J. C. Ricklin, Free-space laser communications: principles and advances, Springer, New York, NY, 2008.

[13] I. I. Kim, M. Mitchel, and E. Korevaar, "Measurement of scintillation for free-space laser communication at 785nm and 1550nm," Proc. SPIE, Optical Wireless Communications II, Vol. 3850, pp. 49-62, Sept. 1999.

[14] I. I. Kim, R. Stieger, J. A. Koontz, C. Moursund, M. Barclay, P. Adhikari, J. Schuster, E. Korevaar, R. Ruigrok, and C. Decusatis, "Wireless optical transmission of fast ethernet, FDDI, ATM, and ESCON protocol data using the TerraLink laser communication system," Opt. Eng., Vol. 37, No. 12, pp. 3143-3155, Dec. 1988.

[15] H. H. Refai, J. J. Sluss, Jr., H. H. Refai, and M. Atiquzzaman, "Transporting RF signals over free-space optical links," Proc. SPIE, Vol. 5712, pp. 46-54, 2005.

[16] H. H. Refai and J. J. Sluss, "Interconnection of IS-95 CDMA microcells using free space optical link," Proc. WOCN, Muscat, Oman, pp. 78-81, 2004.

[17] H. H. Refai, J. J. Sluss, and Jr. H. H. Refai, "The use of free-space optical links for CATV applications," Proc. SPIE, Vol. 5825, pp. 408-415, 2005.

[18] K. Tsukamoto, K. Nakaduka, M. Kamei, T. Higashino, S. Komaki, K. Wakamori, Y. Aburakawa, T. Nakamura, K. Takahashi, T. Suzuki, K. Kazaura, K. Omae, M. Matsumoto, S. Kuwano, and H. Watanabe, "Development of DWDM radio on free space optic link system for ubiquitous wireless," Technical Digest of AP-MWP, pp. 295-296, 2007.

[19] K. Tsukamoto, A. Hashimoto, Y. Aburakawa, and M. Matsumoto, "The case for free space -Exploring the prospect of free-space optical links for backhaul applications-," IEEE Microw. Mag., Vol. 10, No. 5, pp. 84-92, 2009.

[20] K. Kazaura, K. Wakamori, M. Matsumoto, T. Higashino, K. Tsukamoto, and S. Komaki, "RoFSO: A universal platform for convergence of fiber and free space optical communication networks," IEEE Commun. Mag., Vol. 48, No. 2, pp. 130-137, 2010.

[21] I. I. Kim and E. J. Korevaar, "Availability of free-space optics (FSO) and hybrid FSO/RF systems," Proc. SPIE, Vol, 4530, pp. 84-95, Nov. 2001.

[22] L. C. Andrews and R. L. Phillips, Laser beam propagation through random media, 2nd Ed., SPIE Press, Bellingham, WA, 2005.

[23] A. Prokes, "Atmospheric effects on availability of free space optics systems," Opt. Eng. Vol. 48, No. 6, pp. 066001_1-10, June 2009.

[24] S. Bloom, E. Korevaar, J. Schuster, and H. Willebrand, "Understanding the performance of free-space optics," J. Optical Networking, Vol. 2, No. 6, pp. 178-200, 2003.

[25] Kyung-Hwan Kim, T. Higashino, K. Tsukamoto, S. Komaki, K. Kazaura, and M. Matsumoto, "Spectral model of optical scintillation for terrestrial free-space optical communication link

design," Opt. Eng., vol. 50, no. 3, pp. 035005.1-11, March 2011.

[26] Kyung-Hwan Kim, T. Higashino, K. Tsukamoto, and S. Komaki, "Optical fading analysis considering spectrum of optical scintillation in terrestrial free-space optical channel," Proc. IEEE International Conference on Space Optical Systems and Applications, pp. 58-66, Santa Monica, CA, USA, May 2011.

[27] Kyung-Hwan Kim, H. Onodera, T. Higashino, T. Nakamura, Y. Aburakawa, K. Tsukamoto, S. Komaki, K. Wakamori, T. Suzuki, K. Kazaura, A. M. Shah, K. Takahashi, K. Ohmae, T. Satou, M. Matsumoto, "RoFSO link analysis using statistical model of time-correlated optical intensity fluctuation," Technical Report of IEICE, pp.13-18, Kyoto, Japan, May 2008.

[28] Kyung-Hwan Kim, H. Onodera, T. Higashino, T. Nakamura, Y. Aburakawa, K. Tsukamoto, S. Komaki, K. Wakamori, T. Suzuki, K. Kazaura, A. M. Shah, K. Takahashi, K. Ohmae, T. Satou, M. Matsumoto, "Development of Radio on Free Space Optics System for Ubiquitous Wireless Services-(2) Estimation of scintillation variance and its fluctuation speed according to weather condition" IEICE Society Conference, C-14-11, p. 242, Tokyo, Japan, Sep. 2008.

[29] Kyung-Hwan Kim, T. Higashino, K. Tsukamoto, S. Komaki, K. Wakamori, and M. Matsumoto, "Optical power allocation method and new optical transmission loss model for WDM radio on free space optics system," IEICE Trans. Electron., Vol. J94-C, No. 12, pp. 496-509 , Dec. 2011.

[30] Kyung-Hwan Kim, H. Onodera, T. Higashino, K. Tsukamoto, S. Komaki, Y. Aburakawa, T. Nakamura, K. Takahashi, T. Suzuki, K. Kazaura, A. M. Shah, K. Ohmae, M. Matsumoto and K. Wakamori, "A new statistical model of scintillation in RoFSO link and performance evaluation of WLAN system," Technical Digest of IEEE International Topical Meeting on Microwave Photonics, pp.193-196, Gold Coast, Australia, Sep. 2008.

[31] Kyung-Hwan Kim, T. Higashino, T. Nakamura, Y. Aburakawa, K. Tsukamoto, S. Komaki, K. Wakamori, T. Suzuki, K. Kazaura, A. M. Shah, K. Takahashi, K. Ohmae, M. Matsumoto, "Throughput performance of IEEE 802.11a over RoFSO link," Proc. Asia-Pacific Microwave Photonics Conference, pp. APMP46.1-4, Beijing, China, April 2009.

[32] Kyung-Hwan Kim, H. Onodera, T. Higashino, T. Nakamura, Y. Aburakawa, K. Tsukamoto, S. Komaki, K. Wakamori, T. Suzuki, K. Kazaura, A. M. Shah, K. Takahashi, K. Ohmae, T. Satou, M. Matsumoto, "Development of Radio on Free Space Optics System for Ubiquitous Wireless Services-(2) Time correlated optical intensity fluctuation model for RoFSO link evaluation", IEICE General Conference, C-14-1, p.320, Kyushu, Japan, March 2008.

[33] Kyung-Hwan Kim, T. Higashino, T. Nakamura, Y. Aburakawa, K. Tsukamoto, S. Komaki, K. Wakamori, T. Suzuki, K. Kazaura, A. M. Shah, K. Takahashi, K. Ohmae, T. Satou, and M. Matsumoto, "Performance evaluation of WLAN signal transmission by using a new statistical

model of RoFSO channel," Proc. International Conference on Space Optical Systems and Applications, pp. 199-205, Tokyo, Japan, Feb. 2009.

[34] Kyung-Hwan Kim, H. Onodera, T. Higashino, T. Nakamura, Y. Aburakawa, K. Tsukamoto, S. Komaki, K. Wakamori, T. Suzuki, K. Kazaura, A. M. Shah, K. Takahashi, K. Ohmae, T. Satou, M. Matsumoto, "Development of Radio on Free Space Optics System for Ubiquitous Wireless Services-(4) A new analytical approach for scintillation model," IEICE Society Conference, C-14-10, p. 239, Tottori, Japan, Sep. 2007.

[35] Kyung-Hwan Kim, T. Higashino, K. Tsukamoto, and S. Komaki, "WDM optical power allocation method for adaptive Radio on Free Space Optics system design," Technical Digest of IEEE International Topical Meeting on Microwave Photonics, pp. 361-364, Singapore, Singapore, Oct. 2011.

[36] Kyung-Hwan Kim, T. Nagata, T. Higashino, K. Tsukamoto, S. Komaki, K. Kazaura, and M. Matsumoto, "Radio on free space optics technology and its system design for heterogeneous radio networks," The Japan Society for Aeronautical and Space Sciences, pp. 2107-2110, Kyoto, Japan, Sep. 2009.

[37] P. T. Dat, A. M. Shah, K. Kazaura, K. Wakamori, T. Suzuki, K. Takahashi, M. Matsumoto, Y. Aburakawa, T. Nakamura, T. Higashino, K. Tsukamoto, and S. Komaki, "A study on transmission of RF signals over a turbulent free space optical link," Technical Digest of IEEE International Topical Meeting on Microwave Photonics, 173-176, 2008.

[38] A. Bekkali, P. T. Dat, K. Kazaura, K. Wakamori, M. Matsumoto, T. Higashino, K. Tsukamoto, and S. Komaki, "Performance evaluation of an advanced DWDM RoFSO system for transmitting multiple RF signals," IEICE Trans. Fundamentals, Vol. E92-A, No. 11, pp. 2697-2705, 2009.

[39] K. Tsukamoto, T. Higashino, T. Nakamura, K. Takahashi, Y. Aburakawa, S. Komaki, K. Wakamori, T. Suzuki, K. Kazaura, A. M. Shah, K. Omae, and M. Matsumoto, "Development of radio on free space optics system for ubiquitous wireless," Proc. PIERS, Vol. 4, pp. 427-431, 2008.

[40] Y. Arimoto, M. Presi, V. Guarino, A. D'Errico, G. Contestabile, M. Matsumoto, and E. Ciaramella, "320 Gbit/s (8 × 40 Gbit/s) double-pass terrestrial free-space optical link transparently connected to optical fibre line," Proc. ECOC, pp. 1-2, 2008.

[41] E. Ciaramella, Y. Arimoto, G. Contestabile, M. Presi, A. D'Errico, V. Guarino, and M. Matsumoto, "1.28 terabits/s (32×40 Gbit/s) WDM transmission system for free space optical communications," IEEE J. Sel. Area. Comm., Vol. 27, No. 9, pp. 1639-1645, 2009.

[42] K. Kazaura, K. Omae, T. Suzuki, M. Matsumoto, E. Mutafungwa, T. Murakami, K. Takahashi, H. Matsumoto, K. Wakamori, and Y. Arimoto, "Performance evaluation of next generation free-space optical communication system," IEICE Trans. Electron., Vol. E90-C, No. 2, pp. 381-388, 2007.

[43] K. Kazaura, K. Omae, Suzuki, M. Matsumoto, E. Mutafungwa, T. O. Korhonen, T. Murakami, K. Takahashi, H. Matsumoto, K. Wakamori, and Y. Arimoto, "Enhancing performance of next generation FSO communication systems using soft computing-based predictions," Opt. Express, Vol. 14, No. 12, pp. 4958-4968, 2006.

[44] R. S. Lawrence and J. W. Strohbehn, "A survey of clear-air propagation effects relevant to optical communications," Proc. IEEE, Vol. 58, pp. 1523-1545, 1970.

[45] V. I. Tatarskii, Wave propagation in a turbulent medium, English transl., McGraw-Hill, NY, 1961.

[46] V. I. Tatarskii, The effects of the turbulent atmosphere on wave propagation, English transl., US. Dept. of Commerce, NTIS, Springfield, VA, 1971.

[47] S. F. Clifford, "Temporal-frequency spectra for a spherical wave propagating through atmospheric turbulence," J. Opt. Soc. Am., Vol. 61, No. 10, pp. 1285-1292, 1971.

[48] E. Ryznar, "Dependency of optical scintillation frequency on wind speed," Appl. Opt., Vol. 4, No. 11, pp. 1416-1418, 1965.

[49] A. Ishimaru, "Temporal frequency spectra of multifrequency waves in turbulent atmosphere," IEEE Trans. AP. Vol. AP-20, No. 1, pp. 10-19, 1972.

[50] A. Ishimaru, Wave propagation and scattering in random media, Vol. 2, IEEE Press, New York, 1977.

[51] V. Thiermann and A. Kohnle, "A simple model for the structure constant of temperature fluctuations in the lower atmosphere," J. Phys., Vol. 21, pp. S37-S40, 1988.

[52] D. L. Hutt, "Modeling and measurements of atmospheric optical turbulence over land," Opt. Eng., Vol. 38, No. 8, pp. 1288-1295, 1999.

[53] S. N. Bendersky, N. Kopeika, and N. Blaunstein, "Atmospheric optical turbulence over land in middle east coastal environments: prediction modeling and measurements," Appl. Opt., Vol. 43, pp. 4070-4079, 2004.

[54] D. Sadot and N. S. Kopeika, "Forecasting optical turbulence strength on basis of macroscale meteorology and aerosols: models and validation," Opt. Eng., Vol. 31, pp. 200-212, 1992.

[55] P. T. Dat, A. Bekkali, K. Kazaura, K. Wakamori, and M. Matsumoto, "A universal platform for

ubiquitous wireless communications using radio over FSO system," J. Lightwave Technol., Vol. 28, No. 16, pp. 2258-2267, 2010.

[56] L. Wasiczko and C. Davis, "Aperture averaging of optical scintillation in the atmosphere: experimental results," Proc. SPIE, Vol. 5793, pp. 197-207, 2005.

[57] P. T. Dat, C. B. Naila, P. Liu, K. Wakamori, M. Matsumoto, and K. Tsukamoto, "Next generation free space optics system for ubiquitous communications," Proc. PIERS, pp. 75-80, March 2011.

[58] M. Nakagami, "The m-distribution – A general formula of intensity distribution of rapid fading," Statistical Methods in Radio Wave Propagation, W. Hoffman(Ed), Perfamon Press, pp.3-36, 1960.

[59] R. L. Phillips and L. C. Andrews, "Universal statistical model for irradiance fluctuations in a turbulent medium," J. Opt. Soc. Am., Vol. 72, No. 7, pp. 864-870, 1982.

[60] A. Papoulis, Probability random variables and stochastic processes, McGraw-Hill, New York, 1991.

[61] C. F. Bohren and D. Huffman, Absorption and scattering of light by small particles, Wiley, Hoboken, NJ, 1983.

[62] B. Flecker, M. Gebhart, E. Leitgeb, M. S. Sheikh, and C. Chlestil, "Results of attenuation-measurements for optical wireless channels under dense fog conditions regarding different wavelength," Proc. SPIE, Vol. 6303, 63030P, 2006.

[63] M. Naboulsi, H. Sizun, and F. de Fornel, "Fog attenuation prediction for optical and infrared waves," Opt. Eng., Vol. 43, No. 2, pp. 319-329, 2004.

[64] S. S. Muhammad, P. Kohldorfer, and E. Leigeb, "Channel modeling for terrestrial free space optical links," Proc. ICTON, Vol. 1, pp. 407-410, July 2005.

[65] L. C. Andrews and R. L. Phillips, Laser beam propagation through random media, 2nd Ed., SPIE Press, 2005.

[66] L. C. Andrews, R. L. Phillips, C. Y. Hopen, and M. A. Al-Habash, "Theory of optical scintillation," J. Opt. Soc. Am. A, Vol. 16, No. 6, pp. 1417-1429, July 1999.

[67] J. H. Churnside, "Aperture averaging of optical scintillations in the turbulent atmosphere," Appl. Opt., Vol. 30, No. 15, pp. 1982-1994, May 1991.

[68] J. H. Churnside, "Aperture-averaging factor for optical propagation through the turbulent atmosphere," NOAA Technical Memorandum ERL WPL-188, Nov. 1990. (available from the National Technical Information Service, http://www.nits.gov)

[69] L. M. Wasiczko, Techniques to mitigate the effects of atmospheric turbulence on free space optical communication links, Ph.D Dissertation, University of Maryland, College Park, 2004.

[70] H. Yuksel, S. Milner, and C. C. Davis, "Aperture averaging for optimizing receiver design and system performance of free-space optical communication links," J. Optical Networking, Vol. 4, pp. 462-475, Aug. 2005.

[71] D. Giggenbach and H. Henninger, "Fading-loss assessment in atmospheric free-space optical communication links with on-off keying," Opt. Eng., Vol. 47, No. 4, pp. 046001.1-6, April 2008.

[72] ITU-T G.694.1, "Spectral grids for WDM applications: DWDM frequency grid," May 2002.

[73] K. Takahashi, T. Higashino, T. Nakamura, Y. Aburakawa, K. Tsukamoto, S. Komaki, K. Wakamori, T. Suzuki, K. Kazaura, A. M. Shah, K. Omae, M. Matsumoto, and Y. Miyamoto, "Design and evaluation of optical antenna module suitable for radio on free space optics link system for ubiquitous wireless," Proc. SPIE, Vol. 6877, 68770H, 2008.

[74] K. Tsukamoto, H. Onodera, Kyung-Hwan Kim, T. Nakamura, T. Higashino, Y. Aburakawa, S. Komaki, K. Wakamori, K. Takahashi, T. Suzuki, K. Kazaura, A. M. Shah, K. Omae, M. Matsumoto, and T. Satou, "Link design of radio on free space optics system for heterogeneous wireless services," Technical Digest of IEEE International Topical Meeting on Microwave Photonics, pp. 232-235, 2008.

[75] M. Matsumoto, K. Kazaura, K. Wakamori, T. Higashino, K. Tsukamoto, and S. Komaki, "Experimental investigation on a radio on free space optical system suitable for provision of ubiquitous wireless services," 27th Progress in Electromagnetics Research Symposium, pp. 750-755, March 2010.

[76] Infrared Communication System Association (ICSA), http://www.icsa.gr.jp/

[77] I. I. Bruce, B. McArthur, and E. Korevaar, "Comparison of laser beam propagation at 785nm and 1550nm in fog and haze for optical wireless communications," Proc. SPIE, Vol. 4214, pp. 26-37, 2000.

[78] A. C. Motlagh, V. Ahmadi, Z. Ghassemlooy, and K. Abedi, "The effect of atmospheric turbulence on the performance of the free space optical communication," 6th International Symposium on Communication Systems, Networks and Digital Signal Processing, pp. 540-543, July 2008.

[79] G. Xu, X. Zhang, J. Wei, and X. Fu, "Influence of atmospheric turbulence on FSO link performance," Proc. SPIE, Vol. 5281, pp. 816-823, 2004.

[80] B. Saleh, Photoelectron Statistics, Springer-Verlag, NY, 1978.

[81] M. Al-Habash, L. Andrews and R. Phillips, "Mathematical model for the irradiance probability

density function of a laser beam propagating through turbulent media," Opt. Eng., Vol. 40, No. 8, pp. 1554-1562, Aug. 2001.

[82] Qualnet, http://www.qualnet.com

[83] M. Morikura and S. Kubota, 802.11 high-speed wireless LAN textbook, 3rd Ed., Impress R&D, 2008.

[84] K. I. Ziri-Castro, W. G. Scanlo, and N. E. Evans, "Indoor radio channel characterization and modeling for a 5.2 GHz bodyworn receiver," IEEE Ant. and Wire. Prop. Letter, Vol. 3, pp. 219-222, 2004.

[85] M. Fatima Vaz and M. A. Fortes, "Grain size distribution: the lognormal and the gamma distribution functions," Pergamon Journals, Scripta Metallurgica, Vol. 22, pp. 35-40, 1988.

[86] F. Bulcholtz, C. I. Moore, H. R. Burris, C. S. Mc.Dermitt, R. Mahon, M. R. Syite, J. V. Michalowicz, G. C. Gilbreath, and W. S. Rabinovich, "Free-space analog optical links: systems, performance and statistical properties," OSA Technical Digest Series, Applications of Lasers for Sensing and Free Space Communications, pp. LSMC4, 2010.

[87] Hakki H. Refai, J. J. Sluss, Hazem H. Refai, and M. Atiquzzaman, "Comparative study of the performance of analog fiber optic links versus free-space optical links," Opt. Eng., Vol. 45, No. 2, pp. 025003.1-10, Feb. 2006.

[88] IEC60825-1, Ed. 1.2, 2000.

[89] J. Alwan, "Eye safety and wireless optical networks (WONs)," site: www.freespaceoptic.com/WhitePapers/WP_laser_eye_safety.pdf, last visited: 25 Nov. 2011.

[90] ARIB STD-B31, "Transmission system for digital terrestrial television broadcasting," Version 1.7, 2007.

[91] 3GPP TS 25.104, "3rd generation partnership project; Technical specification group radio access networks; UTRA (BS) FDD; radio transmission and reception (Release 1999)," Version 3.5.0, 2000.

[92] http://standard.ieee.org/getieee802/download/802.11g-2003.pdf

[93] ARIB STD-T71, "Broadband mobile access communication system (CSMA)," Version 5.0, 2007.

[94] P. T. Dat, A. Bekkali, K. Kazaura, K. Wakamori, T. Suzuki, M. Matsumoto, T. Higashino, K. Tsukamoto, and S. Komaki, "Performance evaluation of an advanced DWDM RoFSO system for heterogeneous wireless," Global Telecommunications Conference, pp. 1-6, Dec. 2009.

List of publications by the author

A. Journals

[1] Kyung-Hwan Kim, T. Higashino, K. Tsukamoto, S. Komaki, K. Kazaura, and M. Matsumoto, "Spectral model of optical scintillation for terrestrial free-space optical communication link design," Opt. Eng., Vol. 50, No. 3, pp. 035005.1-11, March 2011.

[2] Kyung-Hwan Kim, T. Higashino, K. Tsukamoto, S. Komaki, K. Wakamori, and M. Matsumoto, "Optical power allocation method and new optical transmission loss model for WDM radio on free space optics system," IEICE Trans. Electron., Vol. J94-C, No. 12, pp. 496-509 , Dec. 2011.

B. International conferences

[1] Kyung-Hwan Kim, H. Onodera, T. Higashino, K. Tsukamoto, S. Komaki, Y. Aburakawa, T. Nakamura, K. Takahashi, T. Suzuki, K. Kazaura, A. M. Shah, K. Ohmae, M. Matsumoto and K. Wakamori, "A new statistical model of scintillation in RoFSO link and performance evaluation of WLAN system," Technical Digest of IEEE International Topical Meeting on Microwave Photonics, pp.193-196, Gold Coast, Australia, Sep. 2008.

[2] Kyung-Hwan Kim, H. Onodera, T. Higashino, T. Nakamura, Y. Aburakawa, K. Tsukamoto, S. Komaki, K. Wakamori, T. Suzuki, K. Kazaura, A. M. Shah, K. Takahashi, K. Ohmae, T. Satou, and M. Matsumoto, "RoFSO channel modeling considering time correlation of scintillation and its application to performance evaluation of WLAN signal transmission," Proc. SPIE Photonics West, vol. 7234, pp. 7234OL.1-10, San Jose, CA, USA, Jan. 2009.

[3] Kyung-Hwan Kim, T. Higashino, T. Nakamura, Y. Aburakawa, K. Tsukamoto, S. Komaki, K. Wakamori, T. Suzuki, K. Kazaura, A. M. Shah, K. Takahashi, K. Ohmae, T. Satou, and M. Matsumoto, "Performance evaluation of WLAN signal transmission by using a new statistical model of RoFSO channel," Proc. International Conference on Space Optical Systems and Applications, pp. 199-205, Tokyo, Japan, Feb. 2009.

[4] Kyung-Hwan Kim, T. Higashino, T. Nakamura, Y. Aburakawa, K. Tsukamoto, S. Komaki, K.

Wakamori, T. Suzuki, K. Kazaura, A. M. Shah, K. Takahashi, K. Ohmae, M. Matsumoto, "Throughput performance of IEEE 802.11a over RoFSO link," Proc. Asia-Pacific Microwave Photonics Conference, pp. APMP46.1-4, Beijing, China, April 2009.

[5] Kyung-Hwan Kim, T. Higashino, K. Tsukamoto, and S. Komaki, "Scintillation impact on RF signal transmission of WLAN over RoFSO link," Proc. International Meeting for Future of Electron Devices, Kansai, pp.124-125, Osaka, Japan, May 2009.

[6] Kyung-Hwan Kim, T. Higashino, K. Tsukamoto, and S. Komaki, "Experimental investigation on ISDB-T signal transmission over RoFSO link with optical scintillation," Proc. 2nd Global COE International Symposium Electronic Devices Innovation, pp.117-118, Osaka, Japan, Dec. 2009.

[7] Kyung-Hwan Kim, T. Higashino, K. Tsukamoto, S. Komaki, K. Kazaura, and M. Matsumoto, "Statistical analysis on the optical fading in free space optical channel for RoFSO link design," Proc. of SPIE Photonics West, vol. 7620, pp. 7620OL.1-10, San Francisco, CA, USA, Jan. 2010.

[8] Kyung-Hwan Kim. Kim, T. Higashino, K. Tsukamoto, and S. Komaki, "Optical scintillation prediction method to improve RoFSO link performance," Proc. Asia-Pacific Microwave Photonics Conference, pp. TB1.1-4, Hung Hom, Hong Kong, April 2010.

[9] Kyung-Hwan Kim, T. Higashino, K. Tsukamoto, and S. Komaki, "Investigation on cut-off frequency of optical scintillation," Proc. Student Conference on Innovative Electronic Topics, p. 78, Osaka, Japan, July 2010.

[10] Kyung-Hwan Kim, T. Higashino, K. Tsukamoto, and S. Komaki, "Optical fading analysis considering spectrum of optical scintillation in terrestrial free-space optical channel," Proc. IEEE International Conference on Space Optical Systems and Applications, pp. 58-66, Santa Monica, CA, USA, May 2011.

[11] Kyung-Hwan Kim, T. Higashino, K. Tsukamoto, and S. Komaki, "WDM optical power allocation method for adaptive Radio on Free Space Optics system design," Technical Digest of IEEE International Topical Meeting on Microwave Photonics, pp. 361-364, Singapore, Singapore, Oct. 2011.

C. Domestic conferences

[1] Kyung-Hwan Kim, H. Onodera, T. Higashino, T. Nakamura, Y. Aburakawa, K. Tsukamoto, S. Komaki, K. Wakamori, T. Suzuki, K. Kazaura, A. M. Shah, K. Takahashi, K. Ohmae, T. Satou, M. Matsumoto, "Development of Radio on Free Space Optics System for Ubiquitous Wireless Services-(4) A new analytical approach for scintillation model," IEICE Society Conference, C-14-10, p. 239, Tottori, Japan, Sep. 2007.

[2] Kyung-Hwan Kim, H. Onodera, T. Higashino, T. Nakamura, Y. Aburakawa, K. Tsukamoto, S. Komaki, K. Wakamori, T. Suzuki, K. Kazaura, A. M. Shah, K. Takahashi, K. Ohmae, T. Satou, M. Matsumoto, "Development of Radio on Free Space Optics System for Ubiquitous Wireless Services-(2) Time correlated optical intensity fluctuation model for RoFSO link evaluation", IEICE General Conference, C-14-1, p.320, Kyushu, Japan, March 2008.

[3] Kyung-Hwan Kim, H. Onodera, T. Higashino, T. Nakamura, Y. Aburakawa, K. Tsukamoto, S. Komaki, K. Wakamori, T. Suzuki, K. Kazaura, A. M. Shah, K. Takahashi, K. Ohmae, T. Satou, M. Matsumoto, "RoFSO link analysis using statistical model of time-correlated optical intensity fluctuation," Technical Report of IEICE, pp.13-18, Kyoto, Japan, May 2008.

[4] Kyung-Hwan Kim, H. Onodera, T. Higashino, T. Nakamura, Y. Aburakawa, K. Tsukamoto, S. Komaki, K. Wakamori, T. Suzuki, K. Kazaura, A. M. Shah, K. Takahashi, K. Ohmae, T. Satou, M. Matsumoto, "Development of Radio on Free Space Optics System for Ubiquitous Wireless Services-(2) Estimation of scintillation variance and its fluctuation speed according to weather condition" IEICE Society Conference, C-14-11, p. 242, Tokyo, Japan, Sep. 2008.

[5] Kyung-Hwan Kim, T. Higashino, T. Nakamura, Y. Aburakawa, K. Tsukamoto, S. Komaki, K. Wakamori, T. Suzuki, K. Kazaura, A. M. Shah, K. Takahashi, K. Ohmae, T. Satou, and M. Matsumoto, "Development of Radio on Free Space Optics System for Ubiquitous Wireless Services-(2) Evaluation of performance degradation due to scintillation in IEEE 802.11a," IEICE General Conference, C-14-2, p.285, Ehime, Japan, March 2009.

[6] Kyung-Hwan Kim, T. Nagata, T. Higashino, K. Tsukamoto, S. Komaki, K. Kazaura, and M. Matsumoto, "Radio on free space optics technology and its system design for heterogeneous radio networks," The Japan Society for Aeronautical and Space Sciences, pp. 2107-2110, Kyoto, Japan, Sep. 2009.

[7] Kyung-Hwan Kim, T. Higashino, K. Tsukamoto, and S. Komaki, "Analysis method on scintillation based on MSE for free space optical link design," Kansai-section Joint Convention of Institutes of Electrical Engineering, G8-20, p. G221, Osaka, Japan, Nov. 2009.